UNIVERSITÀ DEGLI STUDI DI TRIESTE

XXIX CICLO DEL DOTTORATO DI RICERCA IN BIOMEDICINA MOLECOLARE

A new covalent PIN1 inhibitor selectively targets cancer cells by a dual mechanism of action

Settore scientifico-disciplinare: **BIO/13**

DOTTORANDA
ELENA CAMPANER

COORDINATORE
PROF. SSA GERMANA MERONI

SUPERVISORE DI TESI
PROF. GIANNINO DEL SAL

ANNO ACCADEMICO 2015/2016

UNIVERSITÀ DEGLI STUDI DI TRIESTE

XXIX CICLO DEL DOTTORATO DI RICERCA IN BIOMEDICINA MOLECOLARE

A new covalent PIN1 inhibitor selectively targets cancer cells by a dual mechanism of action

Settore scientifico-disciplinare: **BIO/13**

DOTTORANDA
ELENA CAMPANER

COORDINATORE
PROF. SSA GERMANA MERONI

SUPERVISORE DI TESI
PROF. GIANNINO DEL SAL

ANNO ACCADEMICO 2015/2016

This thesis is dedicated to my parents
who have always supported me throughout my studies.

Table of contents

Abstract

In the last decades targeted drugs have improved cancer treatment, but revealed to be ineffective mainly in the treatment of solid tumors, largely because of tumor heterogeneity, activation of redundant pathways, and drug resistance. A common and central signal transduction mechanism in many oncogenic pathways is the phosphorylation of proteins at serine or threonine residues followed by proline (S/T-P). Importantly, the phospho-S/T-P motifs of these proteins are recognized by the peptidyl-prolyl *cis/trans* isomerase (PPIase) PIN1, which catalyzes the *cis-trans* or *trans-cis* conformational change around the S-P or T-P bond. Among PPIases, PIN1 is the only enzyme able to efficiently bind proteins containing phosphorylated S/T-P motifs. As a consequence, the phosphorylation dependent prolyl-isomerase PIN1 acts as a critical modifier of multiple signaling pathways. It is overexpressed in the majority of cancers and its activity strongly contributes to tumor initiation and progression. Conversely, inactivation of PIN1 function curbs tumor growth and cancer stem cell expansion, restores chemosensitivity and blocks metastatic spread, thus providing the rationale for a therapeutic strategy based on PIN1 inhibition. Notwithstanding, potent PIN1 inhibitors are still missing from the arsenal of anti-cancer drugs. By a mechanism-based screening we have identified a novel covalent PIN1 inhibitor, KPT-6566, able to selectively inhibit PIN1 among other prolyl-isomerases, and target it for degradation. We demonstrate that KPT-6566 covalently binds to the catalytic site of PIN1. This interaction results in the release of a quinine-mimicking drug that generates reactive oxygen species and DNA damage inducing cell death specifically in cancer cells. Accordingly, KPT-6566 treatment impairs PIN1-dependent cancer phenotypes *in vitro* and growth of lung metastasis *in vivo*.

Introduction

Anticancer drug resistance

Despite remarkable advancements achieved in drug discovery for cancer treatment, anticancer drug development is still one of the major challenge for cancer research. There is in fact a high demand of new and improved therapeutic approaches to efficiently inhibit key target and to overcome cancer's drug resistance to both cytotoxic and molecularly targeted drugs[1,2]. Traditional cytotoxic chemotherapies for example are not effective for all types of cancer and, more importantly, they can cause toxicity by affecting normal proliferating cells. In addition, these chemotherapeutics can also give rise to second malignancies[3]. By virtue of advances in the understanding of the molecular landscape of cancer cells, cancer specific vulnerabilities have been identified and defined as oncogene addiction and non-oncogene addiction of cancer cells. As a consequence, targeted drugs have been developed to specifically hit cellular targets that are genetically altered in cancer and that are essential for proliferation, survival and dissemination of tumor cells (oncogene addiction)[3]. In addition, recent drug development has been focused on targeting cellular machineries that are essential to support oncogenesis (non-oncogene addiction)[3,4]. However, albeit initial positive responses to targeted therapy, also in this case acquisition of drug resistance often leads to tumor relapse. Major mechanisms of resistance include mutation of the target, activation of redundant pathways and activation of survival/detoxifying mechanisms[3]. To cope with cancer cells resistance, recent rational regimens combine two or more molecularly targeted drugs. However, the effectiveness of such combinations needs to be evaluated in long-term studies[1,3].

Altogether these observations suggest that the sole targeting of mutant or overexpressed oncoproteins is unlikely to represent a successful cancer therapy, especially for solid tumors that are characterized by the presence of a spectrum of gene mutations[3]. Cancer cells within a tumor are in fact heterogeneous, and there is increasing evidence that intratumoral heterogeneity contributes to therapy failure and disease progression. Phenotypic and functional heterogeneity can arise from genetic or epigenetic changes in cancer cells or from extrinsic factors that depend on the microenvironment[5]. Moreover, some types of tumors are characterized by a hierarchical organization in which a subpopulation of tumorigenic cancer stem cells (CSCs) gives rise to a differentiated progeny and sustains not only the long-term clonal maintenance of the tumors but also the metastatic potential[6]. Importantly, only few therapies are evolved to hit CSCs. Differentiation therapies, in fact, specifically target cancer stem cells and force them to differentiate, as for example the use of retinoic acid in the treatment of acute promyelocytic leukaemia (APL) and neuroblastoma[7].

Therefore, the major goal of anticancer drug development remains the identification of novel cancer-specific targets whose inhibition, could make cancer cells more vulnerable and less prone to develop resistance[8]. A promising strategy towards this end is the identification of central common signaling mechanisms in both cancer cells and CSCs, in order to block them with specific inhibitors[9].

Prolyl-isomerization is a common signal transduction mechanism

The phosphorylation of proteins at serine or threonine residues followed by proline (S/T-P, proline-directed phosphorylation) represents a common and central signal transduction mechanism in many cellular pathways. This post-translational modification (PTM) is executed by a repertoire of proline-directed kinases, such as Cyclin-dependent kinases (CDKs) and Mitogen Activated Protein kinases (MAPK) or Glycogen synthase kinase 3 beta (GSK3beta), that fulfill key roles in controlling signal transduction and integrate various stimuli to elicit specific cellular responses[10].

Due to the proline moiety, S/T-P motifs can adopt either a *cis* or a *trans* conformation and the spontaneous conversion between these isomers occurs at a very slow rate. As a consequence, prolines containing proteins can exist in different conformations that are often endowed with different functions. A class of enzymes, called peptidyl prolyl *cis/trans* isomerases, are necessary to catalyze the *cis-trans* or *trans-cis* conversion of S/T-P motifs in a biologically useful timeframe, suggesting that their availability and activity represents an additional layer of control over protein structure and function. Indeed, along several signal transduction pathways, peptidyl prolyl *cis-trans* isomerases have been shown to finely regulate conformational changes in both protein kinases and their substrates, which is particularly important because different enzymes, including some kinases, phosphatases and F-box proteins, are conformation specific[10].

It is worth noting that phosphorylation of the S/T-P motifs further decreases the rate of the *cis/trans* conversion and renders the peptide bonds inaccessible to all known peptidyl-prolyl *cis/trans* isomerase (PPIase) except to one particular isomerase called PIN1. PIN1, or NIMA-interacting 1, is unique among all PPIases, since it specifically recognizes phosphorylated S-P or T-P motifs (pS/T-P) in many cellular proteins and is involved in a plethora of cellular functions, both in physiologic conditions and disease. Intriguingly, PIN1 plays critical but opposed roles in the pathogenesis of Alzheimer's disease (AD) and human cancers. Impairment of PIN1 levels or activity has indeed been correlated with neurodegenerative diseases and premature ageing, while, on the contrary, upregulation and aberrant function of PIN1 is observed in many cancer cells where it promotes proliferation and survival[10–12].

In human cancers, prolyl-isomerization by PIN1 has emerged as a central post-phosphorylation signal transduction mechanism. Indeed, numerous oncogenes and tumor suppressors either are directly regulated by and/or trigger signaling pathways involving phosphorylation of S/T-P and their isomerization by PIN1[10]. PIN1 is overexpressed in the majority of human cancers and its levels correlate with poor clinical prognosis. Genetic ablation of *Pin1* reduces tumor growth and metastasis in several oncogene-induced mouse models of tumorigenesis, indicating that PIN1 has relevant roles both in tumor development and progression. In addition, PIN1 drives the expansion and tumorigenesis of CSCs in breast cancers and in leukemia. It seems therefore that PIN1 inhibition might have the desirable ability to simultaneously block multiple cancer-driving pathways in cancer and in CSCs[9,13] and for these reasons several attempts to find PIN1 inhibitors have been done since the discovery of human PIN1 more than two decades ago[14]. However, still many open questions regarding for example its precise mechanism of action, its regulation in cancer, its different impact on the fate of proteins, still pose challenges for the discovery of drugs targeting this enzyme in cancer[15,16].

PIN1 structure and function

PPIases consist of three conserved families: cyclophilins, FK506-binding proteins (FKBPs) and parvulins. Members of the cyclophilin and FKBP families are commonly referred to as immunophilins because they mediate the effects of immunosuppressive drugs cyclosporin A (CsA), FK506 and rapamycin. These drugs bind in the respective active sites of the immunophilins and block their PPIase catalytic activity[17]. The parvulin family comprises highly conserved proteins that neither display sequence similarity to either cyclophilins or FKBPs nor exhibit binding to any immunosuppressive drugs.

The parvulin PIN1 is the only PPIase able to specifically recognize phospho-S/T-P motifs and to catalyze their *cis-trans* or *trans-cis* conformational change around the S-P or T-P bond[10]. This specific function among PPIases is guaranteed by a peculiar structure. PIN1 is a 163 amino acids protein, structurally divided into two domains that are connected by a flexible linker: the N-terminal WW domain mediates protein-protein interaction, while the C-terminal PPIase domain catalyzes peptidyl-prolyl isomerization of the substrates (Figure 1)[14].

The N-terminal WW domain is a small structural motif composed by 39 amino acids and consists of a triple stranded antiparallel β-sheet that forms a deep hydrophobic concave surface that comprises one wall of the hydrophobic cavity. The WW domain is present in many functionally and evolutionarily diverged proteins, but, among PPIases, it is present exclusively in PIN1, conferring its specificity for phospho-S/T-P containing substrate. The C-terminal PPIase domain forms the

opposing wall of the interdomain hydrophobic cavity. Here, a conserved residue of the active site, C113, is crucial for efficient catalysis in PIN1, while a conserved cluster, consisting of K63, R68 and R69, is responsible for the high preference of substrates presenting a phospho-serine, phospho-threonine or a negative charged residue amino acid preceding the proline[18].

PIN1 is a conserved gene during evolution, in fact it is present from yeast to humans[14]. It is essential in some organisms such as *S. cerevisiae*, *A .nidulans* and *C. albicans*, but not in others such as fission yeast and mice, although *PIN1*-knockout animals do have some phenotypic alterations[19–23]. Furthermore, a gene that is highly related to *PIN1*, *PIN1L*, and its corresponding mRNA have been identified, but no protein expression was detected and its function is still unknown[10].

PIN1 mediated conformational change can have profound effects on phosphorylation-dependent signaling by regulating the activities of a spectrum of target proteins. Common consequences of such modifications include: altered protein stability, different subcellular localization, occurrence of other post-translational modifications and changes in protein-protein interactions. As a consequence, PIN1 acts as a fine modulator of diverse cellular processes such as proliferation, apoptosis, stem cell self-renewal, and differentiation, and thus its deregulation can have a major impact on disease development and progression, especially in cancer[24].

PIN1 is overexpressed in human cancers

PIN1 is a ubiquitously expressed protein. In normal tissue, its expression generally correlates with cell proliferation and its levels decrease with ageing. By contrast, protein expression analyses revealed that 38 out of 60 different tumor types, including breast, prostate, lung, ovary, and liver tumors, display PIN1 overexpression in more than 10% of the cases compared to the corresponding normal tissues[25]. In addition, PIN1 expression correlates with cancer prognosis. PIN1 overexpression is in fact associated with disease progression, recurrence and metastasis dissemination in prostate, breast and other types of cancers[13]. Still open questions regard how PIN1 overexpression relates with cancer progression. Dissecting various mechanisms of PIN1 function and understanding the action of PIN1 on single substrates will pave the way to novel possible therapeutic interventions.

Regulation of PIN1 expression and activity in cancer

PIN1 is not annotated as a cancer gene, since it is not mutated in the majority of cancers, according to different cancer databases, or it is mutated at very low frequency in some tumour types[16]. However, PIN1 is aberrantly activated in human cancers by various mechanisms. *PIN1* promoter is

a direct target of E2F transcription factors (E2F1, E2F2, E2F3) and different oncogenic signaling pathways, such as those downstream of activated ErbB2/HER2 or HRAS, promote *PIN1* transcription via E2F[26]. Moreover, two members of the NOTCH receptor family (NOTCH1 and NOTCH4) directly induce *PIN1* transcription[27,28] (Figure 2). Interestingly, *PIN1* is one of the most strongly repressed genes by the tumor suppressor BRCA1. In addition, *PIN1* promoter activity is decreased by two different single-nucleotide polymorphisms (SNPs). In particular, the rs2233678 SNP reduces PIN1 expression and the risk of cancer incidence in Asian and Caucasian populations[29]. Moreover, *PIN1* mRNA levels are found to be down-modulated by members of the miR-200 family of small non coding RNAs in breast and prostate cancers[30,31].

Activity and protein levels of PIN1 are also regulated by post-translational modifications (Figure 2). In particular, its phosphorylation status is deeply modulated during cell cycle progression. PIN1 can be phosphorylated on S16 by protein kinase A (PKA) and Aurora kinase A (AURKA), and this phosphorylation abolishes PIN1 ability of binding substrates as well as its sub-cellular localization[9,32]. Moreover, polo-like kinase 1 (PLK1) phosphorylates S65 in the catalytic domain of PIN1. This phosphorylation increases its stability by inhibiting its ubiquitylation and subsequent proteasome-mediated degradation, an event particularly relevant during mitosis[33]. The tumor suppressor death-associated protein kinase 1 (DAPK1) phosphorylates PIN1 at S71 inhibiting its isomerase activity and its nuclear localization, thus abolishing its oncogenic functions[34]. Interestingly, DAPK1 expression is often lost in human cancers[35]. On the contrary, mixed-lineage kinase 3 (MLK3), a MAP3K family member, was shown to phosphorylate PIN1 on S138 and to increase its catalytic activity and nuclear translocation[36]. Finally, sumoylations that occur on K6 and K63 inhibits PIN1 activity and oncogenic function, while desumoylation of these residues by SENP1 increases PIN1 protein stability[37]. Recently, different groups demonstrated that oxidation of PIN1 at the residue C113 reduces its catalytic activity *in vitro*. PIN1 was found oxidized in brains form AD patients indicating that such modification can indeed occur *in vivo*. The significance of such modification in cancer is unknown[38,39].

PIN1 amplifies oncogenic signaling

Prolyl *cis-trans* isomerization plays a critical role in determining the timing and duration of several activated signaling pathways involved in cell proliferation, apoptosis and several other processes, and, depending on the cellular context, its deregulation may contribute to cancer development and progression. PIN1 overexpression and/or hyperactivation have been shown to disrupt the balance between oncogene and tumor suppressor activation, leading to oncogenesis. Indeed, PIN1 was

shown to simultaneously potentiate the activity of many oncogenes and to inhibit the growth-suppressing functions of tumor suppressors (Figure 3)[9].

Notably, PIN1 controls protein turnover of many substrates by either favouring or blocking their recognition by several E3 ubiquitin-ligases. The conformation of S/T-P motifs in fact affects the recognition and interaction with the SKP1-CUL1-F-box (SCF) E3 ligase complex and thus proteasomal degradation. Moreover, PIN1 controls the ability of many transcription factors to interact with their partners on gene promoters and instructs transcription complexes towards a specific gene expression profile[40].

Several lines of evidence document the critical role of phosphorylation-specific prolyl-isomerization in amplifying oncogenic pathways at multiple levels. One such example is the HER2-RAS-RAF-ERK signaling pathway. PIN1 in fact was shown to increase HER2 expression and protein stability, to increase c-JUN stability and transcriptional activity towards *CCND1* and also to promote Cyclin D1 protein stability. Moreover PIN1 promotes the inactivation of pRB, the major inhibitor of E2Fs, thus producing a positive feed-forward loop between PIN1 and this oncogenic pathway[9]. Accordingly, PIN1 was shown to be essential for breast tumorigenesis induced by oncogenic HER2 or HRAS *in vivo*[41].

PIN1 regulates a large number of transcription factors and transcription regulators responsive to growth signals. For example PIN1 promotes the WNT pathway by preventing the interaction of β-catenin with adenomatous polyposis coli (APC). Consequently, PIN1 increases the transcription of β-catenin target genes, thereby enhancing Cyclin D1 and c-MYC expression[42]. PIN1 also activates NF-κB by antagonizing its interaction with the NF-κB inhibitor IκBα, which increases its tumorigenic activity via the nuclear accumulation of NF-κB and its transcriptional activity[43]. PIN1 increases also the activation of NOTCH signaling by promoting NOTCH1 cleavage by the γ-secretase in the cellular membrane, leading to an increased release of the active NOTCH1 intracellular domain (N1-ICD) in the nucleus[27]. Here, it also increases N1-ICD stability preventing its FBXW7-mediated degradation and prolonging in this way duration of transcription at target genes. N1-ICD in turn directly induces PIN1 transcription in a positive feedback loop that promotes not only breast tumorigenesis, but also self-renewal of breast CSCs and metastasis in mouse xenograft experiments. Indeed, a strong correlation between PIN1 overexpression and NOTCH1 activation is found in breast cancers, as well as with survival of breast cancer patients with highly activated NOTCH1[27,28]. Similarly, PIN1 increases NOTCH3 protein processing to stabilize the cleaved product, enhancing NOTCH3-dependent invasiveness in T cell acute lymphoblastic leukaemia[44]. PIN1 was also shown to activate AP1 transcription factor by promoting ERK1/2 and JNK activities on c-JUN and c-FOS and by directly interacting with both proteins to increase

neoplastic transformation and expansion of breast CSCs[45–47]. A growing body of evidence supports the idea that PIN1 might coordinate hormone action with growth factor signaling in cancer. For example, PIN1 activates Estrogen receptor α (ERα) by promoting the up-regulation of transcription and protein levels[48,49]. In addition, PIN1 cooperates with steroid receptor co-activator 3 (SRC3) to enhance oestrogen-dependent transactivation[50].

On the contrary, PIN1 negatively affects tumor suppressive transcription factors and co-regulators such as promyelocytic leukaemia protein (PML), forkhead box transcription factors (FOXOs), runt-related transcription factor 3 (RUNX3), Retinoblastoma protein (pRB), and SMAD2/3[13]. Interestingly, although PIN1 destabilizes tumor suppressors PML and retinoic acid receptor α (RARα), it stabilizes the fusion oncoprotein PML-RARα[51]. Indeed, an important challenge is to understand why or how PIN1 is producing strikingly opposite effects on oncogenes and tumor suppressors. This is probably due to different functions of *cis* and *trans* isomers, thus conformation specific antibodies against PIN1 substrates would clarify this apparent contrast[9,16].

Different from what stated above, it was previously demonstrated that PIN1 function is required for the activation of growth arrest and apoptosis of *TP53* (encoding the p53 protein) and its family members p63 and p73, following oncogenic or genotoxic stress signals[12].

In human tumors the majority of mutations in the *TP53* gene are missense and allow for expression of full length mutant p53 proteins unable to recognize wild-type p53 response elements on DNA but often endowed with new oncogenic functions (gain of function, GOF) due to their ability to form aberrant complexes with proteins promoting metastasis and cancer chemoresistance[52]. Interestingly, PIN1-mediated prolyl-isomerization of mutant p53 increases the ability of mutant p53 to engage with transcription factors thus leading to a reprogramming of gene expression including repression of tumor suppressor genes, as well as activation of genes promoting invasion and metastasis[53]. These data indicate that, depending on the *TP53* status, PIN1 activity can lead to opposite outcomes. Indeed, in cancers, where p53 is likely inactivated or mutated, PIN1 acts as a tumor promoter rather than a tumor suppressor. In support of this view, PIN1 ablation prevents the development of malignant tumors in *Trp53* knockout mice and in mice expressing an oncogenic p53 mutant protein[53,54].

Altogether, these data indicate that PIN1 dysregulation may have a major impact on cancer development and progression by disrupting the existing balance between oncogenic and tumor-suppressive pathways.

PIN1 promotes cancer development

The early steps of cancer development are characterized by uncontrolled proliferation and apoptosis evasion[55]. PIN1 was discovered as an important regulator of mitosis both in yeast and in higher eukaryotes[24]. Further studies revealed a role for PIN1 in all phases of the cell cycle. In fact, during cell cycle progression there is a precise timing and sequence of activation and inactivation of Cyclin/CDK complexes which are known to be phosphorylated on S/T-P motifs and, indeed, PIN1 fits perfectly in this molecular organization[10,24]. The G1-S transition dictates entrance in the cell cycle and a key regulator of this passage is Cyclin D1, a known PIN1 substrate. During early G1 phase, pRB binds and inhibits E2Fs, which is disrupted by pRB hyperphosphorylation to activate *CCND1* transcription, triggering cell cycle progression. As an E2F target gene, PIN1 levels are elevated at the G1-S transition in normal cells, but become constitutively elevated in transformed cells. PIN1 interacts with hypophosphorylated pRB in mid-late G1 to promote its hyperphosphorylation. Furthermore, PIN1-dependent *CCND1* upregulation, further activates G1 CDKs in a positive feedback loop to promote the G1-S transition[56,57].

Once cells enter S phase, another important step regulated by PIN1 is the coordination of centrosome duplication and DNA synthesis. PIN1 is localized in the centrosomes and induces their duplication. Indeed, PIN1 overexpression was shown to disrupt the coordination between DNA synthesis and centrosome duplication during cell cycle leading to centrosome amplification, aneuploidy and tumorigenesis *in vitro* and in mouse models[58].

During the S phase, RNA polymerase II is recruited on gene promoters while it is released in M phase. Notably, PIN1 coordinates this dynamic association by directly binding the RNA polymerase II[59]. PIN1 controls also G2-M transition, acting on the early mitotic inhibitor-1 (EMI1) and, consequently, on anaphase promoting complex (APC) thus coordinating the S and M phases[60]. Mitosis is controlled by PIN1 through the regulation of Cyclin B1 via WEE1 and CDC25C[61,62]. Moreover PIN1 interacts with topoisomerase II to induce chromatin condensation[63].

Highly regulated PIN1 temporally and spatially orchestrates the activity of cell cycle regulators into a signaling cascade that proceeds in a finely organized manner. Constitutively active PIN1 in cancer cells disrupts this coordination, contributing to cell transformation[9].

In cancer, PIN1 promotes also cell survival by enhancing pro-survival pathways like PKB/AKT[64]. Moreover, PIN1 regulates cell apoptosis by directly inhibiting pro-apoptotic proteins such as B-cell lymphoma 2 (Bcl-2)-associated X protein (BAX) and death associated protein 6 (Daxx) and promoting anti-apoptotic proteins such as Bcl-2 and myeloid cell leukemia-1 (MCL-1)[40]. For example, activated ERK1/2 phosphorylates MCL-1 and this phosphorylation causes the association

between PIN1 and MCL-1, which results in MCL-1 stabilization and paclitaxel resistance. Consistently, inhibition of PIN1 sensitized breast cancer cells to paclitaxel treatment[65].

PIN1 promotes cancer progression and aggressiveness

Several reports have shown that PIN1 is also linked to cancer progression and aggressive traits. Indeed, PIN1 protein levels are higher in high-grade and more aggressive breast cancer subtypes[66]. A tissue array study showed that high PIN1 protein expression positively correlates with clinical staging and its levels function as an independent prognostic marker in prostate cancer [67]. A growing body of evidence indicates that PIN1 is involved in almost every step of the metastatic cascade. In fact, its deregulated overexpression acts on crucial steps of cell plasticity, likely through modulation of several key transcription factors that control cell shape and migratory capability. In particular, PIN1 promotes epithelial-to-mesenchymal transition (EMT) through downregulation of E-Cadherin levels in breast epithelial cells[28,31]. Another important PIN1 target involved in the metastatic process is the focal adhesion-associated non-receptor protein-tyrosine kinase (FAK). Phosphorylated FAK becomes a PIN1 target that, through the isomerization, is then dephosphorylated and can promote migration, invasion, and metastasis[68]. In addition, PIN1 plays an important role in mutant p53-driven transformation and metastasis. PIN1 supports the inhibition of the anti-metastasis factor p63 induced by mutated oncogenic forms of p53 and promotes the induction of a mutant p53 transcriptional program to increase cancer cells migration and metastasis formation *in vivo*. This transcriptional program correlates with poor prognosis in breast cancer patients and PIN1 ablation reduces the oncogenic function of mutant p53 causing a decrease in metastatic proclivity[53].

PIN1 acts as a fundamental regulator of stem cell features in the breast cancer stem cell (CSCs) compartment through increased activation of the NOTCH1 and NOCTH4 receptors and the small GTPase RAB2GAP. In fact, *in vitro* and *in vivo* functional studies have shown that PIN1 critically controls CSC self-renewal, replicative potential, frequency and drug resistance, while its ablation causes tumour shrinkage, decreased metastatic spread and synergizes with conventional therapy in eradicating CSCs[28,31,47]. PIN1 is also involved in the regulation of leukaemia stem cells (LSCs) through the stabilization of the fusion oncoprotein PML-RARα, the driver oncogene of human acute promyelocytic leukaemia (APL). Inhibition of PIN1 induces the degradation of PML-RARα that drives LSCs, and thereby treats APL[51].

PIN1 has been also linked to chemoresistance. PIN1 in fact is more expressed in breast CSCs, which are known to be intrinsically chemoresistant. Besides the role of PIN1 in mediating chemoresistance through induction and maintenance of CSCs, it can be considered a direct mediator of chemoresistance for example through MCL-1 or NOTCH1, that promotes the expression of cell

survival (e.g. *BIRC5* and *BCL-2*) and drug efflux pump genes (e.g. *ABCG2*)[28]. Similarly, PIN1 is involved in Tamoxifen resistance of ER positive tumors, by keeping high both levels and activity of ERα and by enhancing ER-independent mechanisms[69].

Targeting PIN1 for cancer treatment

Compelling data indicate that targeting PIN1 may have great benefit for cancer treatment. PIN1 inhibitors are predicted to have the ability to simultaneously block multiple cancer-driving pathways in CSCs and non-CSC tumor cells with limited toxicity[9,13]. Indeed, PIN1 knockdown inhibits breast cancer cell growth *in vivo* and *Pin1*^{-/-} mice are resistant to oncogene-driven breast tumorigenesis[41], while in normal tissues no major side effects were detected[22]. Moreover, PIN1 ablation prevents the development of malignant tumors in mice expressing oncogenic mutant p53[53]. PIN1 inhibition also sensitizes breast cancer cells to targeted- and chemo-therapies[65,70,71] and overcomes drug resistance[28]. Altogether, these data indicate that PIN1 is a promising target for cancer therapy.

In addition, PIN1 is overexpressed in the majority of human cancers and was shown to be involved in the development of many human cancers of different origin including non-small cell lung cancer, hepatitis B virus-induced hepatocellular carcinoma, T cell acute lymphoma induced by NOTCH3 and APL PML-RARα[44,51,72,73]. Moreover PIN1 overexpression correlates with worse patient survival in prostate, breast and gastric cancer[28,53,67,74]. For this reason, PIN1 may also be regarded as a exploitable biomarker for cancer diagnosis and treatment[75,76].

Given the physiological role of PIN1 in the regulation of many signaling pathways, PIN1 inhibitors could have broad-ranging effects. However, *Pin1*^{-/-} mice develop normally to adult-hood with few developmental defects. These mice exhibit a developmental delay in neuronal cell differentiation during the neonatal stage, defects in testes and in breast development due to stem cell depletion, and late skeletal, neuro- and retinal degeneration[19–22,77–80]. These age-related phenotypes could raise concerns regarding long-term side effects of PIN1 inhibitors. However, short-term cancer treatments with PIN1 inhibitors might not elicit the same side effects as those due to chronic lack of PIN1. Moreover, since drugs never inhibit their target completely *in vivo*, and given that tumors with elevated levels of PIN1 are likely to be more dependent on PIN1 activity than normal cells, there may be a therapeutic window where PIN1 inhibitors could be effective only in cancer cells. In addition, some unwanted neurodegenerative side effects might be avoided by designing inhibitors that cannot pass through the blood brain barrier[9,13].

PIN1 is considered a druggable target since it has a defined active site and substrate specificity. Indeed, a number of PIN1 inhibitors have been isolated so far (Table 1). PIN1 antagonists have been developed to either inhibit its PPIase activity or target the WW domain to prevent the binding of PIN1 to its substrates. PPIase domain inhibitors identified from enzymatic assays include Juglone, PiB and Dipentamethylene thiauram monosulfide (DTM)[15]. Epigallo-cathechin-gallate (ECGC), a green tea flavonoid, was found to inhibit both the WW and PPIase domains.

The naphtoquinone Juglone, a reactive molecule produced by walnut trees, inhibits bacterial parvulins, but its lack of activity on FKBPs or cyclophilins has been used to justify its use as a specific PIN1 inhibitor. Juglone inhibits PIN1 by forming Michael adducts with C113[81]. However, it covalently modifies active cysteines in many other enzymes and retains antiproliferative potency in $Pin1^{-/-}$ mouse embryo fibroblasts indicating that it has other cellular targets, which may include the mitotic checkpoint component BubR1 and tubulin[82]. The anti-tumour effect of Juglone was ascribed also to production of ROS, typical of Quinones, that produce oxidative stress-mediated DNA damage[83].

Library screening identified PiB, which inhibited PIN1 and Parvulin14 with similar potency. PiB is an ester-containing symmetrical compound reported to have slightly greater antiproliferative activity versus $Pin1^{+/+}$ MEFs than $Pin1$-deficient counterparts[84]. However, apart from its reported ability to inhibit PIN1 in enzymatic assays, there is little evidence that PiB actually binds to PIN1. Few studies have employed PiB, which may be explained by its insolubility in DMSO[15]. DTM was identified as a highly potent competitive inhibitor of the PIN1 PPIase domain in a screen using enzymatic assay[85]. The structural simplicity of DTM, however, raises questions regarding its specificity[15].

Epigallocatechin gallate (EGCG), a cancer chemo-preventative compound that is the major flavonoid in green tea, likely inhibits PIN1 via its binding to the WW domain[86]. However, EGCG has additional targets, including proteasome[87], and shows low potency against PIN1.

Structure-based design led to the identification of a series of peptido-mimetic inhibitors of PIN1. These inhibitors contain a core that mimics the PIN1 binding consensus of its substrates, which is needed to target the phosphate-binding pocket of the PIN1 active site. However, although these inhibitors are low nanomolar inhibitors *in vitro*, they are inactive or poorly active in cells because their structures render these inhibitors cell impermeable. Lack of cell permeability is a common problem in the pursuit of PIN1 inhibitors[15].

Very recently the team of K.P. Lu uncovered all-*trans* retinoic acid (ATRA) as a specific PIN1 inhibitor. ATRA is a known therapeutic for APL that causes down-regulation of the oncoprotein PML-RARα. Through a mechanism-based high-throughput screening ATRA was identified as a

drug able to bind and inhibit non phosphorylated-S71, thus active, PIN1. The ability of ATRA to target PIN1 has been demonstrated in clinically relevant APL animal models and in patients with APL. PIN1 acts on PML-RARα to increase its stability. Treatment with ATRA elicits myeloid differentiation, PIN1 inhibition, and degradation of PML-RARα, three processes that underlie complete remission of APL patients[51]. ATRA was also tested for its effect on breast cancer growth *in vitro* and in mouse xenografts but had only modest antitumor activity due to a short half-life, which is consistent with the findings from clinical trials that ATRA has moderate efficacy against advanced breast cancer. These results confirm that targeting PIN1 is a valid approach to treat cancer, and also underscore the importance of developing longer-acting ATRA or more potent and specific PIN1 inhibitors for cancer therapy[9,51].

Notwithstanding, PIN1 still poses challenges for the development of inhibitors. This is mainly due to its small and shallow enzymatic pocket, as well as to the requirement for a negatively charged moiety to interface with the catalytic center of PIN1. Small molecule inhibitors would perfectly fit into the PIN1 active site, however they may raise specificity concerns. Substrate mimicking drugs, like negatively charged peptidic PPIAse inhibitors, would overcome this problem but they are substantially cell impermeable because of their chemical properties[9,13,15].

Moreover, it is important to note that PIN1 catalyses a reversible reaction, meaning that reaction products are also substrates. This makes PIN1 activity difficult to measure, but several effective assays have been described, including protease coupled assays that take advantage of the ability of peptidases such as trypsin to cleave the *trans* but not the *cis* form of phospho-S-P bonds[88].

Aim

Current targeted and personalized therapeutic strategies still face significant challenges mainly because of the establishment of resistance mechanisms. The activation of redundant oncogenic pathways is a frequent mechanism of drug resistance. Moreover it has become evident that CSCs, whose activity is known to promote tumor initiation, metastasis formation, and recurrence, are intrinsically resistant to several of the available therapies. A common signaling mechanism in many of these oncogenic pathways is proline-directed phosphorylation, and further modification by the prolyl-isomerase PIN1 critically controls structure and function of such phosphorylated proteins. PIN1 is overexpressed in different types of cancers, where it promotes its development and progression. Moreover PIN1 supports breast CSCs and leukaemia SCs expansion. Accordingly, genetic ablation of PIN1 or its inhibition with experimental inhibitors have been shown to dismantle oncogenic pathway cooperation in CSCs and non-CSC tumor cells, thus providing a rationale for the development of PIN1 targeted therapies. A number of features, including its well-defined active site, its very high specificity, and its low expression in normal tissues, make PIN1 an attractive target for the design of small molecule inhibitors. Indeed, many potential PIN1 inhibitors have been isolated so far. The vast majority of them are non covalent inhibitors, of which a few promising examples of drug-like compounds have been reported. Unfortunately, none of these molecules has reached the clinical trial phase, because of unsatisfactory pharmacological characteristics, such as low potency, selectivity, solubility, cell permeability, and stability.

The work presented in this thesis aimed at identifying small molecule PIN1 inhibitors with increased biochemical efficiency based on a covalent mechanism of action. This strategy in fact could provide several pharmacological advantages for a PIN1-directed anti-cancer therapy. In fact, slowly dissociating or covalent drugs are known to induce target degradation, so that new synthesis of the target must occur to restore its function[89]. In the case of PIN1, being highly expressed and active in tumors[51], this is a desirable goal. Moreover, PIN1 inhibitors that induce its degradation would allow for monitoring treatment efficacy, thus exploiting PIN1 both as a target and as a biomarker for cancer treatment. Despite safety concerns, related to nonspecific reactivity of covalent inhibitors, the rational design of highly selective and specific covalent compounds is a possible approach to overcome this issue[90]. In the drug discovery process, structure-based virtual screening is a fast and efficient method to identify, among libraries of compounds, novel small molecules potentially able to bind to protein targets. Indeed, in order to identify covalent inhibitors that target the cysteine C113 residue of the PIN1 catalytic pocket, we took advantage of a recently

described method of virtual screening for the discovery of covalently bound ligands (CovDock-VS)[91].

This work has been performed in collaboration with Karyopharm Therapeutics Inc., which designed and performed the virtual screening.

Results

Structure- and mechanism-based screening for PIN1 inhibitors

With the intent of isolating covalent inhibitors targeting the C113 residue of the PIN1 catalytic core, we screened a drug-like collection of 200,000 commercial compounds obtained from several drug repositories (Fig. 4a). The compound pool was first filtered applying the Lipinski's rule of five criteria for enhanced drug-likeness. Then, a virtual structure-based screening was performed using the crystal structure of human PIN1 (PDB entry 2XPB)[92]. The compounds showing the higher docking scores were then subjected to another virtual screening specifically designed to identify compounds able to covalently target the active site residue C113. To this aim, a covalent docking approach using the CovDock-VS method[91] was exploited. These approaches yielded around one hundred possible PIN1 covalent binders that were tested afterwards for cytotoxicity against melanoma A375 cells using the MTT viability assay. Non-transformed 3T3 cells were used as a control to make sure hit compounds were not generally cytotoxic. Nine compounds were selected for their different toxicity in A375 and in 3T3 cells (Supplementary Table 1) and were chosen for further characterization as potential PIN1 inhibitors.

KPT-6566 inhibits PIN1 PPIase activity through covalent binding

The compounds derived from the above screening were initially tested for their capacity to inhibit the catalytic activity of recombinant human PIN1 in a trypsin-coupled peptidyl-prolyl isomerization assay (PPIase assay)[93,94]. The mutant PIN1 S67E protein was used as control of a reduced PPIase activity[95]. The results show that, out of the nine tested compounds, only KPT-6566 (**1**) robustly and significantly inhibited the PPIase activity of PIN1 (Figure 4b) and turned out to have an IC50 of 0.64 µM (Supplementary Table 2). From a chemical point of view, KPT-6566 contains a polycyclic aromatic hydrocarbon substituted with a sulfanyl-acetic acid and a *tert*-butylphenylsulfonamide moiety (Fig. 4c).

To demonstrate whether KPT-6566 covalently binds to PIN1, recombinant human PIN1 protein was analyzed by mass spectrometry following incubation with KPT-6566 or DMSO. Liquid chromatography/mass spectrometry (LC/MS) analysis revealed a 90 Da increase of PIN1 molecular weight (MW) upon treatment with KPT-6566 (Fig. 4d), indicating that a modification by addition of a sulfanyl-acetate group (-S-CH$_2$-COOH) had occurred. The +90 Da adduct was not detected when C113 was mutated to alanine (C113A, Supplementary Fig. 1a), indicating that C113 was the target of this covalent modification.

To confirm the above results, PIN1 was incubated with KPT-6566 or DMSO, and subjected to trypsin digestion. The originated peptides were then analyzed by Matrix-assisted laser desorption

ionization–time of flight (MALDI-ToF-ToF) MS and MS/MS. MS spectrum showed the presence of a peptide at 2213.9 m/z, corresponding to the S98 – K117 peptide of PIN1 bearing a +90 Da MW increase (Supplementary Fig. 1b). MS/MS fragmentation of the peptide at 2213.9 m/z performed with MALDI-ToF-ToF unambiguously confirmed the identity of the peptide and the presence of a 90 Da adduct on C113 (Supplementary Fig. 1c). These MS analyses together indicate the covalent addition of the 90 Da sulfanyl-acetate group of KPT-6566 to the sulfur atom of C113, through a disulfide bond. Accordingly, when the peptide-KPT-6566 mixture was incubated with 100 µM of the reducing agent dithiothreitol (DTT), the 90 Da adduct was not detected on the 2213.9 m/z peptide any more, confirming that the sulfur atom of the sulfanyl-acetate moiety is involved in a disulfide bridge with the -SH group of C113 (Supplementary Fig.1d).

Next, in order to assess the mode of binding of KPT-6566 to PIN1, we performed a molecular docking using Glide from the Schrödinger suite[96–98] (Supplementary Table 3). In accordance with MS results, the best docking pose (Pose 1) obtained within this analysis suggests that KPT-6566 positions itself into the catalytic pocket of human PIN1 by creating i) a hydrogen bond with the side chains of K63 and R69, the active site residues mediating phosphate binding, and ii) hydrophobic contacts with some residues involved in the recognition of the proline substrate[18]. Importantly, the electrophile sulfanyl-acetate moiety of the compound directly faces the nucleophile sulfur atom of C113 (Fig. 4e and Supplementary Fig. 1e), which might lead to a covalent complex formation as observed in the MS analyses.

Considering the covalent mechanism of action of KPT-6566, we measured its potency as k_{inact}/K_i ratio, where K_i describes the affinity of the initial non-covalent interaction and k_{inact} is the rate of the subsequent bond-forming reaction[90]. The catalytic activity of PIN1 was measured in the presence of increasing KPT-6566 concentrations at several time points after pre-incubation (Fig. 4f and Supplementary Fig. 1f). Compared to other covalent PIN1 inhibitors such as Juglone[81], KPT-6566 shows a high potency (k_{inact}/K_i = 745.4 min^{-1} ·nM^{-1}) due to a high k_{inact} (0.466 ± 0.05781 min^{-1}) despite its affinity is in a high nanomolar range (K_i = 625.2 ± 324.7 nM) (Supplementary Table 4).

Finally, to determine whether KPT-6566 selectively inhibits PIN1 and not other PPIases, we measured the impact of KPT-6566 on the PPIase activity of recombinant GST-FKBP4 and GST-PPIA, two isomerases also containing cysteine residues and belonging to the FKBP and Cyclophilin families of PPIases[99] (Supplementary Fig. 1g). Neither of these PPIases was affected by KPT-6566, while, their specific inhibitors, FK506 and Cyclosporin A (CsA) respectively, abolished their catalytic activity (Fig. 4g,h).

KPT-6566 impacts on PIN1 cellular functions

To assess whether KPT-6566 could inhibit PIN1 function, we treated immortalized fibroblasts derived from wild-type (WT, $Pin1^{+/+}$) or $Pin1$ knockout (KO, $Pin1^{-/-}$) mouse embryos (MEFs)[27,53] with increasing amounts of KPT-6566, and monitored cell proliferation. In WT MEFs KPT-6566 had a negative, dose-dependent effect on proliferation (Fig. 5a) and induced a decrease of hyperphosphorylated pRB and Cyclin D1 levels (Fig. 5b). In $Pin1$ KO MEFs, instead, KPT-6566 treatment had no effect on proliferation even at the highest dose, and the levels of both Cyclin D1 and hyperphosphorylated pRB were unaffected (Fig. 5a,b). Ectopic expression of HA-tagged PIN1 re-sensitized $Pin1$ KO MEFs to KPT-6566 and, accordingly, Cyclin D1 levels were decreased (Fig. 5c,d). In empty-vector expressing $Pin1$ KO MEFs, instead, KPT-6566 had only a slight and statistically not significant effect on proliferation and no impact on Cyclin D1.

We next tested the effects of increasing doses of KPT-6566 on an isogenic cell model constituted of i) non-transformed MCF10A mammary epithelial cells, which express lower levels of PIN1 than cancer cell lines, and in which the enzyme is mainly inactivated due to S71 phosphorylation[51], and ii) H-RasV12-transformed MCF10AT1 cells[100] which, instead, express higher levels of active PIN1 (Fig. 5e, left). Viability assays highlighted that, consistently with the levels of PIN1, KPT-6566 was four times more potent towards MCF10AT1 than toward MCF10A cells (Fig. 5e, right and Supplementary Table 5).

To test whether sensitivity to KPT-6566 represents a common trait of cancer cells with respect to normal cells, we treated cancer cell lines of different origin and normal breast epithelial cells with increasing doses of the drug and measured their viability. All tested cancer cells expressed higher levels of PIN1 (Fig. 5f) and were more sensitive to KPT-6566, even at low micromolar concentrations (Fig. 5g).

KPT-6566 impacts on levels and function of PIN1 substrates

PIN1 influences the turnover and activity of various proteins, including Cyclin D1, p65 (NF-κB), c-JUN, NOTCH1 intracellular domain (N1-ICD) and MCL-1[40]. To understand the impact of KPT-6566 as a PIN1 inhibitor, we explored the effect of its administration on these PIN1 targets in MDA-MB-231 cells. The effect of KPT-6566 treatment on the levels of these PIN1 client proteins was comparable to that observed following $PIN1$ silencing (Fig. 6a and Supplementary Fig. 2a,b). We also confirmed down-regulation of MCL-1 upon KPT-6566 treatment in lung, prostate and pancreatic cancer cell lines (Supplementary Fig. 2c).

To confirm the above observations at a functional level we tested the effect of KPT-6566 on the activation of two pathways that are controlled by PIN1, the mut-p53 and NOTCH1 pathways[28,53].

We evaluated the effect of KPT-6566 on the transcription of endogenous mut-p53 and NOTCH1 target genes. RT-qPCR analyses of MDA-MB-231 cells treated with increasing concentrations of KPT-6566 showed a dose-dependent decrease in their expression levels (Fig. 6b). This effect was comparable in extent to that observed upon *PIN1* silencing (Supplementary Fig. 2d). Altogether these data showed that, by inactivating PIN1, KPT-6566 elicits the downregulation of PIN1 client proteins and of their target genes.

KPT-6566 impairs PIN1-dependent oncogenic phenotypes

Next we tested whether KPT-6566 interferes with colony forming efficiency of transformed cells[26,101]. We first assessed the IC_{50} of KPT-6566 by dose escalation studies in MDA-MB-231 cells (Supplementary Fig. 3a). The IC_{50} for these experiments turned out to be 1.2 μM. We used this concentration to treat MDA-MB-231 cells transfected with control- or *PIN1* siRNA (Fig. 6c). Upon KPT-6566 treatment, we observed an inhibition of colony formation in MDA-MB-231 cells transfected with control siRNA. Similar inhibitory effects were obtained with another PIN1 inhibitor, PiB[84]. Instead in *PIN1* silenced cells, which *per se* show a decreased colony forming efficiency, KPT-6566 did not further affect colony number (Fig. 6c), while PiB caused additional impairment of the colony forming efficiency, indicating off-target effects of this compound[84] (Fig. 6c). The specific effect of KPT-6566 was confirmed by using another siRNA sequence (Supplementary Fig. 3b,c). Superimposable results were also obtained with the prostate cancer cell line PC3 (Supplementary Fig. 3d-f). Altogether these data suggest that KPT-6566 impairs colony formation through specific PIN1 inhibition.

Treatment of MDA-MB-231 and PC3 cancer cells with KPT-6566 strongly impaired also the migratory and invasive properties of these cells, while having only moderate effects on proliferation in the short time-frame of the experiment (Fig. 6d and Supplementary Fig. 3g).

KPT-6566 curbs self-renewal of breast cancer stem cells

We and others have recently demonstrated that silencing or inhibition of PIN1 impairs the maintenance of mammary CSCs of both human and mouse origin[28,31]. In order to evaluate the impact of KPT-6566 administration on breast CSCs maintenance, secondary mammosphere (M2) formation assays were performed in MDA-MB-231 cells. Cells were treated with KPT-6566 or DMSO, prepared as single-cell suspensions and grown in low-attachment conditions to form M2, as previously done[28]. KPT-6566 treatment showed a significant inhibitory effect on M2 formation compared to DMSO (Fig. 6e and Supplementary Fig. 3h). This result was further confirmed by the decrease of the $CD44^+/CD24^{-/low}/ESA^+$ breast CSC enriched population[102] and reduction of the

levels of three different stem cell markers[103,104] following KPT-6566 treatment (Supplementary Fig. 3i and Fig. 6f). To evaluate the requirement of PIN1 for these effects, we tested the M2 formation efficiency (M2FE) of MCF10AT1 cells transduced with control- or *PIN1* short hairpin RNA (shRNA) expressing vectors, and treated with KPT-6566, PiB, or DMSO. sh*PIN1* expressing cells showed a twofold decrease in M2FE compared to control shRNA expressing cells (Fig. 6g and Supplementary Fig. 3j,k). Treatment of control cells with PiB or KPT-6566 caused a similar decrease of M2FE. In contrast to PiB, KPT-6566 had no impact in *PIN1* silenced cells, further supporting a specific PIN1 inhibitory activity of this compound. To confirm this finding, we transduced MCF10A cells with empty- or HA-tagged PIN1-expressing vectors, and tested their M2FE. As already known, MCF10A cells *per se* have a very low M2FE, but this feature can be enhanced by PIN1 overexpression, which also induces an enrichment of the $CD44^{high}/CD24^{low}$ cell population associated with stemness traits[28,105]. This PIN1-dependent gain of function was abolished by PiB and by KPT-6566 in a dose-dependent manner (Fig. 6h, Supplementary Fig. 3l,m and Supplementary Table 6).

KPT-6566 promotes degradation of PIN1

Slowly dissociating drugs, such as high affinity or covalent binders that cause structural changes of their target, have been shown to promote target degradation[89]. Notably, we consistently observed that KPT-6566 treatment of MEFs and human cancer cells caused a decrease of endogenous PIN1 levels (Fig. 5b and 7a). *PIN1* promoter activity or *PIN1* mRNA levels were only slightly reduced following KPT-6566 treatment in MDA-MB-231 cells (Supplementary Fig. 4a,b), likely due to the disruption of the positive feed-forward loop existing between PIN1 and its transcription factors[26,27]. We thus hypothesized that the effect of KPT-6566 in reducing PIN1 levels mainly occurred through protein degradation. The observed decrease in PIN1 protein was similar to that obtained upon treatment with 20 μM all-*trans*-retinoic acid (ATRA), another PIN1 inhibitor shown to target PIN1 for degradation[51]. Instead, other PIN1 inhibitors, like Juglone or PiB, did not impact on PIN1 protein levels (Fig. 7a), as already observed by us and by others[27,28,106]. Moreover, upon KPT-6566 treatment, same effects were observed on endogenous PIN1 in cancer cell lines of different origins (Fig. 7b), and on HA-tagged PIN1 protein ectopically expressed in *PIN1* knockout MDA-MB-231 cells (Fig. 7c). KPT-6566 exerted these effects in a dose- and time-dependent manner (Fig. 7d,e), and by promoting PIN1 proteasomal degradation, since addition of MG132, a proteasome inhibitor, rescued the levels of both overexpressed and endogenous PIN1 (Fig. 7f and Supplementary Fig. 4c). This indicates that the covalent modification of PIN1 induced by KPT-6566 elicits structural changes leading to PIN1 degradation.

KPT-6566 elicits cellular responses to oxidative stress

Mass Spectrometry data suggest the transfer of the sulfanyl-acetate moiety of KPT-6566 to PIN1 C113 as a specific mode of action of this compound. Hence, besides irreversibly blocking the PIN1 active site, a remnant chemical species originates from KPT-6566 as a result of the KPT-6566-PIN1 interaction. This species can be released in the cellular compartment and interact with different cellular molecules. We hypothesized that this byproduct is 4-*tert*-butyl-N-(4-oxonaphthalen-1(4H)-ylidene)benzene-1-sulfonamide (hereinafter referred to as KPT-6566-B (**2)**). Containing a quinone-mimic substructure with the potential to generate reactive oxygen species, both KPT-6566 and KPT-6566-B may generate H_2O_2 in cells and induce oxidative stress[107]. In addition, KPT-6566-B has also features of a highly reactive electrophile that can engage different nucleophilic species in the cell and form DNA adducts[108] (Supplementary Fig. 5a).

To expand our observations regarding the action of KPT-6566 in cells, we compared the gene expression profiles of MDA-MB-231 cells treated with KPT-6566 or with *PIN1* RNAi, using an Illumina microarray platform. Treatments with DMSO and with control RNAi respectively were carried out as internal controls. Unsupervised hierarchical cluster analysis of the expression profiles of KPT-6566 and DMSO treated cells unveiled 499 significantly modulated genes. 832 were the differentially expressed genes between *PIN1*- and control RNAi treated cells. Comparison of the two lists of genes revealed similarities between KPT-6566 and *PIN1* RNAi treated cells. Indeed, 34% of all genes downregulated by KPT-6566 were also downregulated after *PIN1* silencing (Fig. 8a and Supplementary Table 7). However, KPT-6566 treatment also induced a peculiar transcriptional program, since among its up-regulated genes only 8% overlapped with those upregulated upon *PIN1* silencing (Fig. 8a and Supplementary Table 8). In order to obtain more information about the cellular processes affected by KPT-6566, we performed Gene Ontology (GO) and Ingenuity Pathway Analysis (IPA). Both analyses revealed a common enrichment for biological themes and pathways connected to cell cycle and cell proliferation, as expected for compounds targeting PIN1 in cancer cells[13], supporting the notion that part of the effect of KPT-6566 on gene transcription is mediated by PIN1 inhibition (Fig. 8b,c and Supplementary Table 9). We confirmed this result by RT-qPCR analysis of the expression of selected genes related to cell cycle (Supplementary Fig. 5b). Strikingly, IPA analysis revealed that, besides PIN1 inhibition, KPT-6566 elicits additional effects, in particular perturbing pathways related to inflammation and oxidative stress response (Fig. 8c). These pathways were predicted to be activated by KPT-6566 but not modulated by *PIN1* silencing. In line with the reactive nature of KPT-6566 and KPT-6566-B, the NRF2-mediated oxidative stress response, which physiologically represents one of the most important, intracellular, anti-oxidant mechanisms[109], emerged among others as a pathway

differentially regulated by KPT-6566. We analyzed several genes of this pathway and the expression data demonstrated a good correlation with microarray analyses (Fig. 8d). Altogether these analyses support the notion that KPT-6566 acts on one hand as a PIN1 inhibitor, and on the other as an inducer of cellular stress responses.

Given this premise and considering the induction of the NRF2-dependent antioxidant response by KPT-6566, we analyzed ROS levels by CellROX FACS analyses in MDA-MB-231 and PC3 cells upon KPT-6566 administration. This analysis showed that treatment with KPT-6566 increased endogenous ROS levels, and this effect was drastically reduced by adding N-Acetyl-Cysteine (NAC), a ROS scavenger and thiol group donor[110] (Supplementary Fig. 5c). A similar result was obtained by treating MDA-MB-231 cells with KPT-6566-B (Supplementary Fig. 5d).

In order to investigate if KPT-6566 treatment elicits ROS formation also in normal cells, we performed CellROX analyses in MCF10A cells and observed an increase also in this cell type (Supplementary Fig. 5c). However in MCF10A cells the amount of ROS was significantly lower as compared to cancer cells and KPT-6566 treatment did not alter cell viability (Fig. 5g).

KPT-6566 induces DNA damage in a PIN1-dependent manner

In addition to ROS production elicited by both KPT-6566 and KPT-6566-B, KPT-6566-B might be also involved in the formation of DNA adducts due to its unsubstituted quinone-mimic substructure. DNA adducts or ROS induced DNA damage are either repaired and/or can be converted into double strand breaks (DSBs)[108,111]. It is thus conceivable that treatment with KPT-6566, once converted to KPT-6566-B, could induce DNA damage thus evoking a DNA damage response (DDR)[112]. To test this hypothesis, we analyzed histone H2AX Ser139 phosphorylation (γH2AX), a marker of DNA damage[112], in MDA-MB-231 cells treated with KPT-6566 or KPT-6566-B. Both compounds, indeed, elicited a dose-dependent increase of H2AX phosphorylation (Fig. 9a and Supplementary Fig. 6a).

KPT-6566 treatment caused H2AX phosphorylation also in other cancer cell lines, while normal immortalized MCF10A breast cells did not show signs of DDR. Treatment with Bleomycin, a radiomimetic known to induce DSBs, caused H2AX phosphorylation in all cell lines, indicating that the DDR mechanisms were intact (Fig. 9b and Supplementary Fig. 6b).

We next asked whether KPT-6566 treatment caused DNA damage in a PIN1 dependent manner. As shown in Figures 9c-e and Supplementary Figure 6c, PIN1 was required for the DNA damaging activity of KPT-6566, but not of KPT-6566-B. In fact, KPT-6566 treatment in MDA-MB-231 cells caused H2AX phosphorylation and γ-H2AX-positive foci formation in the majority of cells. However, while KPT-6566 effect was almost undetectable in *PIN1* silenced cells (Figs. 9c-e), KPT-

6566-B DNA damaging activity was independent from PIN1, since the compound elicited H2AX phosphorylation to a same extent in control and *PIN1* silenced MDA-MB-231 cells (Supplementary Fig. 6c). Accordingly, KPT-6566-B did not cause any decrease in PIN1 levels in MDA-MB-231 cells (Supplementary Figs. 6a,c).

Notably, other PIN1 inhibitors, such as ATRA, PiB or Juglone, were not able to induce H2AX phosphorylation at the concentrations generally used to inhibit PIN1 (Fig. 6f). These results indicate that the presence of PIN1 is required for the DNA damaging activity of KPT-6566, and demonstrate that KPT-6566 treatment elicits a PIN1-mediated intracellular release of KPT-6566-B, causing DNA damage. This effect was partially rescued by treatment with the highly efficient ROS scavenger melatonin[113] (Supplementary Fig. 6d), suggesting that besides ROS production, the release of KPT-6566-B might contribute to DNA damage through formation of DNA adducts.

KPT-6566 induces cell death in cancer cells

Upon KPT-6566 administration, we observed DNA damage and killing effects preferentially in cancer cells (Fig. 5e,g and 9b). Tumor cells are sensitive to DNA damage and depletion of antioxidant reservoirs and, over a certain threshold, stress overload may lead to cancer cell death[4,114]. Hence, we hypothesized that, upon KPT-6566 treatment, the observed acute increase of ROS and DNA damage along with the effects of PIN1 inhibition, would represent the *coup de grâce* leading to proliferation arrest and cell death. To assess whether KPT-6566 treatment impaired cancer cells viability by inducing both proliferation arrest and cell death, we performed a Trypan blue assay in control- or *PIN1* silenced MDA-MB-231 cells treated with DMSO or KPT-6566 (Supplementary Fig. 7a). As expected, *PIN1*-silencing caused growth arrest[27], but not cell death. KPT-6566 treatment caused both a decrease in cell number and an increase of the number of dead cells, indicating that, in addition to the proliferation arrest associated with PIN1 inhibition, KPT-6566 also induced cell death. Propidium Iodide/AnnexinV FACS analyses confirmed these results, indicating that KPT-6566 induced cell death with traits of late apoptosis and necrosis (Fig. 10a and Supplementary Fig. 7b). We investigated this feature in cell lines from breast, prostate, lung and pancreatic tumors by evaluating the presence of cell death markers (PARP cleavage, cleaved Caspase-3, secreted HMGB1)[115] by western blot analysis (Fig. 10b and Supplementary Fig. 7c). In line with the previous observations, all tested cell lines showed markers of both apoptotic and necrotic cell death, supporting a widespread killing activity of KPT-6566 towards cancer cells.

Finally we evaluated the effect of KPT-6566 *in vivo* and as a first step we tested its general toxicity in nude mice. At high doses of the compound (60 or 90 mg kg^{-1} injected intravenously) a strong phlebitis was observed at the site of injection. Chronic intraperitoneal (i.p.) administrations of 30

and 45 mg kg^{-1} of KPT-6566 were better tolerated, causing only local, non life-threatening toxicity at the site of inoculation, where granulation and fibrotic thickening of the peritoneal wall were observed (personal observations). Based on this result, we tested the effect of a daily administration of 5 mg kg^{-1} i.p. of KPT-6566 in a lung colonization assay. To this aim, we performed tail vein injection of MDA-MB-231 cells in nude mice (15 animals). The day after cancer cell injection, mice were randomized in two groups to be treated with either KPT-6566 or the vehicle. 27 days after cancer cell inoculation, control mice began to show signs of distress, as determined by body weight loss (Supplementary Fig. 7d). Mice were sacrificed and lungs were extracted and analyzed for metastatic growth by both metastatic area determination and organ weight. The metastatic growth in KPT-6566 treated animals was significantly reduced compared to controls (Fig. 10c, and Supplementary Fig. 7e). Interestingly, *post mortem* morphologic analyses of vital organs did not reveal any sign of local or systemic/organ toxicity.

Discussion

The prolyl-isomerase PIN1 represents a critical player in several signaling circuitries characterizing both CSCs and non-CSC tumor cells. As a consequence of this function, PIN1 inhibition causes the collapse of numerous oncogenic pathways at the same time, making this isomerase an attractive drug target for the development of treatments against aggressive and drug-resistant cancers. Despite considerable efforts, however, poor success has been reached so far: the available PIN1 inhibitors either lack the required specificity and/or potency, or cannot efficiently enter cells to inhibit PIN1 function *in vivo*.

Through a mechanism-based screening we have identified a novel PIN1 small molecule inhibitor (KPT-6566). KPT-6566 is characterized by a unique mechanism of action, combining PIN1 inhibition with the release of a cytotoxic molecule. KPT-6566 blocks PIN1 catalytic activity by covalent interaction and elicits PIN1 proteasome-dependent degradation. Moreover it represents a selective inhibitor of PIN1, as it does not interact with other thiol-containing PPIases.

Several PIN1 inhibitors have been identified so far with both covalent and non covalent mechanisms of action[9,15]. Among them, ATRA, Juglone, and PiB, have shown activity in cells and in mouse models[51,116,117]. Our study indicates that KPT-6566 has a number of advantages over these PIN1 inhibitors. As KPT-6566, Juglone covalently interacts with PIN1 catalytic domain. However, Juglone has a relatively simple structure that affects its specificity. Indeed, Juglone has several off-targets and manifests PIN1 independent activities[15,82]. Unlike Juglone or PiB, which exerts its effects also through Parvulin 14 inhibition, KPT-6566 is highly specific towards PIN1 and mainly ineffective in cells deprived of PIN1. Like KPT-6566, also ATRA promotes PIN1 degradation. Despite this and the advantage of being an FDA approved drug, ATRA showed less potency towards PIN1 than KPT-6566, likely due to its non-covalent mechanism of action and its very short half-life[51].

Most of all, however, KPT-6566 represents a one of a kind PIN1 inhibitor because it associates a highly specific PIN1 inhibitory activity with the release of a reactive quinone-mimicking byproduct that generates DNA damage and elicits cancer cell death. Indeed, as a PIN1 inhibitor and a ROS producing and DNA damaging agent, KPT-6566 exerts both cytostatic and cytotoxic effects (Fig. 10d). As a consequence of PIN1 inhibition and degradation, KPT-6566 reduces levels and/or activity of several PIN1 client proteins, such as Cyclin D1, c-JUN, MCL-1, N1-ICD, and mut-p53. Although the effects on single client proteins are only moderate, the simultaneous impairment of multiple PIN1 targets may account for the observed strong suppression of all tested, cancer-related phenotypes depending on PIN1 function, namely proliferation, colony formation, invasion and CSC maintenance. As a consequence of the release of a DNA damaging byproduct and of ROS

generation, KPT-6566 induces a significant increase of DNA damage and cell death specifically in cancer cells, while only a slight increase of ROS levels in normal cells. Normal cells express lower levels of PIN1 than cancer cells. This may account for a slower kinetic of KPT-6566-B and DNA damage production in these cells and for their limited sensitivity to KPT-6566 treatment. Moreover, normal cells are exposed to low levels of oxidative stress. Cancer cells, instead, are characterized by increased DNA damage and oxidative stress that make them more vulnerable to agents causing further accumulation of ROS and DNA damage[4,109,114]. Indeed, upon KPT-6566 treatment, acute ROS overload along with a conspicuous increase of DNA damage due to KPT-6566-B production causes cancer cells death. Consistent with the pharmacological, biochemical and anti-cancer properties observed *in vitro*, KPT-6566 chronic administration in mice effectively reduced MDA-MB-231 lung colonization without major toxicity. Further studies are required to dissect the mechanisms involved in DNA damaging activity of KPT-6566-B, such as adducts formation.

The mechanism of action of KPT6566 meets the criteria of modern rational drug design envisaging targeted delivery of drug conjugates that release their cytotoxic counterparts specifically in cancer cells[118]. Although additional structural modifications might further improve KPT-6566 drug-likeness, its chemical features and selectivity make it already an attractive molecule to be developed for a potential use as an anti-cancer drug in humans.

Experimental procedures

Virtual screening

A library of commercial compounds was generated using a drug like collection obtained from Asienx (www.asienx.com), Maybridge (www.maybridge.com), Bionet (www.keyorganics.co.uk), Specs (www.specs.net), Chembridge (www.chembridge.com), ChemDiv (www.chemdiv.com), and Enamine (www.enamine.net). Virtual Screening of this collection was performed using a covalent docking approach suitable for large-scale virtual screening (VS) called CovDock-VS method previously described[91] on the structure of the catalytic pocket of PIN1. Briefly, compounds were prepared using the Virtual Screening Workflow (VSW) ligand preparation tab in Maestro (Maestro v9.2. (2011) Schrödinger, Inc., Portland). ''Regularize input geometries'' was applied and ionization states and tautomers were determined by the ionizer at a pH 7.4. Compounds were subsequently filtered in Canvas using the following chemical property ranges that correspond to the Lipinskis' roles of five for enhanced druglikeness: Molecular Weight 300-550, H-bond donors 0-5, H-bond acceptors 1-10, Rotatable bonds < 10, AlogP < 5.5, Total charge -1à1, PSA <140. The PIN1 structure (PDBID: 2XPB)[92] was used for structure based screening following protein preparation in Maestro (Maestro v9.2. (2011) Schrödinger, Inc., Portland). In short, this included assignment of bond orders for ligands, addition of hydrogen atoms, optimization of the hydrogen bonding network, and a restrained minimization. All default options were used.

Cytotoxicity tests

Mouse fibroblast 3T3 and human malignant melanoma A375 cells were resuspended in DMEM cell culture medium containing 10% fetal bovine serum (Gibco) and antibiotics (penicillin and streptomycin, Gibco). 100 μl/well were transferred to the assay plate (5,700 or 4,700 cells/well for 3T3 and A375 respectively) and incubated overnight in a humidified incubator at 37°C and 5% CO_2. KPT compounds were serially diluted in assay media (9 serial 1:3 dilutions) and 100 μl/well were added to the assay plate. Final assay volume of each well was 200 μl, containing KPT compounds, starting from 30 μM concentration downwards. After 70 hours of incubation 20 μl of Promega Substrate CellTiter 96® AQ$_{ueous}$ One Solution Cell Proliferation Assay Reagent were added to each well and, according to the manufacturer's procedures, after short incubation at room temperature in a humidified chamber protected from light, absorbance was read at 490 nm. Means of data collected in duplicate were plotted on a logarithmic scale and IC50 value were obtained.

Recombinant protein production and purification

Recombinant human PIN1 (Uniprot ID: Q13526), PIN1 S67E, and PIN1 C113A were cloned in frame in pNIC28-Bsa4 vector (generous gift from Opher Gileadi, SGC Oxford) by Ligase Independent Cloning (LIC) as fusion proteins with an N-terminal 6xHis tag followed by TEV cleavage site starting from pcDNA3 expressing vectors[27,28,119]. Protein expression was done in *Escherichia coli* BL21(DE3) cells using the autoinduction protocol[120] incubating cells at 37°C for 4 hours followed by 18 hours incubation at 25°C. Soluble proteins were purified from the total cellular lysate by binding to Ni-NTA Agarose (Qiagen) and eluting with 50 mM Tris pH 8.0, 500 mM NaCl, 500 mM Imidazole. Proteins were buffer exchanged in 50 mM Tris pH 8.0, 150 mM NaCl, 0.5 mM EDTA, 1 mM DTT and the 6xHis tag removed by 6xHisTEV protease (produced in house) performed during o/n dialysis at 4°C. The uncleaved proteins and the 6xHis-TEV were removed by affinity chromatography on Ni-NTA Agarose, and untagged PIN1 (wt and mutants) was collected in the flowthrough fraction and further purified on Superdex 75 10/300 size exclusion column (GE Healthcare) using 30 mM HEPES pH 7.8, 100 mM NaCl as mobile phase. Finally the proteins were dialyzed at 4°C for 18 hours in 30 mM HEPES pH 7.8 to remove trace of salt.

Human FKBP4 (Uniprot ID: Q02790) and PPIA (Uniprot ID: P62937) were cloned in frame with the pGTVL1 vector (generous gift from Opher Gileadi, SGC Oxford) by Ligase Independent Cloning (LIC) as fusion proteins with an N-terminal GST starting from pANT7_cGST FKBP4 and PPIA expressing vectors. The proteins were expressed in E. coli BL21(DE3) cells grown at 37°C in Terrific Broth medium (Fluka) supplemented with 1% (w/v) Glycerol (Sigma) and induced with 1 mM isopropyl thio-β-galactoside (Sigma) at midlog growth phase. The cell cultures were collected by centrifugation after 3 h growth at 37°C. Soluble GST-FKBP4 and GST-PPIA were affinity purified from the total cellular lysate on Protino® Glutathione Agarose 4B (Macherey-Nagel) and eluted with 20 mM reduced glutathione (Sigma) in 20 mM Tris pH 8.0, 10 mM DTT. GST fusion proteins were further purified by size exclusion chromatography on HiLoad 16/60 Superdex 200 column (GE Healthcare) in 30 mM HEPES pH 7.8, 100 mM NaCl, 2 mM DTT. Finally the recombinant proteins were buffer exchanged (in 30 mM HEPES pH 7.8, 10 % Glycerol) and concentrated on AMICON15 devices (Millipore), using 50 kDa MWCO for GST-FKBP4 and 10 kDa MWCO for GST-PPIA.


Protease coupled isomerization assay

0.5 nM recombinant PIN1 protein was incubated in a 96-multi-well plate for 3 hours at 0°C in 80 μL HEPES buffer pH=7.8 in presence of 30 μM KPT compounds, or DMSO. In parallel, 0.5 nM bovine serum albumin (PanReac Applichem) or PIN1 S67E were incubated with DMSO as above. Immediately before measurement 15 μL of Trypsin 50 mg/mL (Sigma) and 5 μL of Suc-AEPF-

MCA peptide 100 μg ml^{-1} (ChemDiv) in TFE LiCl 480mM were added and the solutions mixed. Hydrolysis of the substrate was monitored by measuring the fluorescence of the released MCA exciting at 370 nm and detecting at 440 nm every 5 seconds for 5 minutes using an EnSpire® Perkin Elmer multiplate reader. Normalized fluorescence data were converted in Suc-AEPF-MCA concentration values that were used to calculate the PPIase activity K following the method described in Küllertz et al[121]. using the value of BSA (k_0) as reference of an uncatalyzed reaction. The same procedure was followed for GST-FKBP4 and GST-PPIA PPIase assays using Suc-ALPF-MCA and Suc-AAPF-MCA peptides (Bachem), respectively. Proteins were incubated with Cyclosporin (Calbiochem #A239835), FK-506 (Calbiochem #342500), or KPT-6566.

Synthesis of compounds 1 – 3

Compound **1** was obtained through a modified procedure previously described for similar structures[5]. Briefly, intermediate **3** was synthetized in 62 % yield via regioselective coupling reaction between 2-chloro-1,4-naphthoquinone and 4-*tert*-butylbenzene-1-sulfonamide using titanium (IV) chloride tetrahydrofuran complex and trimethylamine (TEA). The same conditions were applied also for the preparation of the compound **2**. Starting from naphthalene-1,4-dione, the procedure afforded, besides the title compound **2** (yield 23 %), also the chloro derivative **3** as sideproduct. This fact underlines the electrophile nature of compound **2**, being reasonably able to react with chlorine ions released from TiCl$_4$. In the following step, the intermediate **3** was then subjected to nucleophilic substitution by thioglycolic acid in the presence of dry pyridine to afford the desired acid **1** in 64 % yield.

R = Cl, H

2 R = H
3 R = Cl
1 R = SCH$_2$COOH
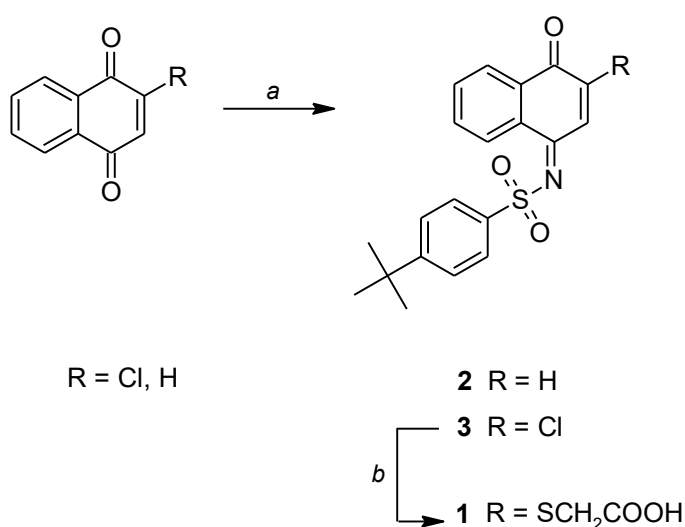
Scheme 1. (**a**) 4-*tert*-butylbenzene-1-sulfonamide, TiCl$_4$·2THF, TEA, dry THF, reflux; (**b**) HSCH$_2$COOH, dry pyridine, dry THF, rt.

General methods: All chemical reagents were obtained from commercial sources (Sigma Aldrich, Alfa Aesar) and used without further purification. Thin-layer chromatography (TLC) was carried out to monitor the process of reactions. Analytical grade solvents (diisopropyl ether, dichloromethane [DCM], ethyl acetate, methanol [MeOH], petroleum ether b.p. 40 - 60°C [petroleum ether], hexane) were used without further purification. Tetrahydrofuran (THF) was distilled immediately prior to use from Na and benzophenone under N_2. Purification of compounds was achieved with flash column chromatography on silica gel (Merck Kieselgel 60, 230-400 mesh ASTM) using the eluents indicated. The biological experiments were conducted on compounds with a purity of at least 95%. Purity was determined by HPLC analyses, performed on a Waters HPLC system composed by: Waters 1525EF binary pump, Waters 717 plus autosampler and Waters 2996 PDA detector. The analytical column was Waters XTerra Phenyl (4.6x150, 5um) column, flow 1 ml/min; compounds were dissolved in CH_3CN or MeOH. The mobile phase consisted of MeOH (or CH_3CN)/water with 0.1% trifluoroacetic acid; two gradient profiles of mobile phase were used to assay the purity of each compound.

Melting points (m.p.) were measured on a capillary apparatus (Büchi 540). The final m.p. determination was achieved by placing the sample at a temperature 10° C below the m.p. and applying a heating rate of 2° C min^{-1}. MS spectra of compound **3** was performed on Waters Micromass ZQ equipped with ESCi source for electrospray ionization. ^{1}H- and ^{13}C-NMR spectra for all described compounds were performed on a Bruker Avance 300 instrument. For coupling patterns, the following abbreviations are used: br = broad, s = singlet, d = doublet, dd = doublet of doublets, t = triplet, q = quartet, m = multiplet. Chemical shifts (δ) are given in parts per million (ppm). For compounds **1** and **2**, HRMS spectra were recorded on an LTQ Orbitrap mass spectrometer (Thermo Scientific, Bremen, Germany) equipped with an atmospheric pressure interface and an ESI ion source instrument.

4-*tert*-Butyl-*N*-(3-chloro-4-oxonaphthalen-1(4*H*)-ylidene)benzene-1-sulfonamide (3). TiCl$_4$ ·2THF (520 mg, 1.56 mmol) and TEA (0.476 mL, 3.43 mmol) were added to a solution of 2-chloro-1,4-naphthoquinone (300 mg, 1.56 mmol) and 4-*tert*-butylbenzene-1-sulfonamide (333 mg, 1.56 mmol) in dry THF (15 mL) at 0 °C. The mixture was retrieved to room temperature, then heated at reflux for 3h. The cooled black mixture was poured into ethyl acetate (100 mL) and the resulting suspension was filtered through a pad of Celite. The filtrate was concentrated, the residue obtained was suspended in DCM (100 mL). The brown insoluble particles were removed by filtration, and the filtrate was again concentrated to dryness. The residue was purified by flash chromatography (eluent: petroleum ether/ethyl acetate 95/5 v/v) to obtain a yellow solid (mp: 194.9 - 196.0°C from crystallization by DCM/hexane). Yield: 62 %; TLC (petroleum ether/ethyl acetate, 90:10 v/v): R_f =

0.43; ^{1}H NMR (300 MHz, CDCl$_3$): δ 8.69 (s, 1H), 8.20 – 8.16 (m, 2H), 8.00 (d, J = 8.5 Hz, 2H), 7.77 – 7.57 (m, 4H), 1.38 (s, 9H). ^{13}C NMR (75 MHz, CDCl$_3$) δ 177.14, 160.80, 157.71, 145.05, 137.29, 134.22, 133.94, 133.08, 131.46, 129.77, 127.94, 127.49, 127.02, 126.34, 35.45, 31.20. MS (m/z): [M]$^+$ 388.

2-{[4-(4-*tert*-Butylbenzenesulfonamido)-1-oxo1,4-dihydronaphthalen-2-yl]sulfanyl}acetic acid (1). Compound **3** (150 mg, 0.39 mmol) was dissolved in THF (10 mL) and mercaptoglycolic acid (0.27 mL, 0.39 mmol) and dry pyridine (0.31 mL, 0.39 mmol) were added to the resulting solution. The mixture was stirred at room temperature for 30 min, then concentrated under reduced pressure. The orange residue was dissolved in ethyl acetate, the resulting solution was washed with 0.5 N HCl, water and brine, dried over Na$_2$SO$_4$ and concentrated under reduced pressure. The crude material was purified by flash chromatography (eluent: DCM/ethyl acetate/HCOOH 80:20:0.1 v/v/v) to give a yellow solid. Yellow solid (mp: 184.3-187.4 °C from trituration with diisopropyl ether). Yield 64 %. TLC (DCM/MeOH/HCOOH, 95:5:0.1 v/v/v): R_f = 0.22; ^{1}H NMR (300 MHz, DMSO-d_6): δ 13.38 (br s, 1H), 8.13 - 8.02 (m, 2H), 7.98 (d, J = 8.4 Hz, 2H), 7.88 – 7.77 (m, 3H), 7.71 (d, J = 8.4 Hz, 2H), 3.97 (s, 2H), 1.33 (s, 9H). ^{13}C NMR (75 MHz, CDCl$_3$) δ 180.42, 175.36, 168.48, 159.80, 156.75, 153.47, 137.71, 134.72, 133.78, 132.89, 131.25, 126.90, 126.82, 126.45, 119.75, 35.03, 33.32, 30.75. HRMS (m/z): [M]$^+$ calcd. for C$_{22}$H$_{21}$NO$_5$S$_2$, 444.0939; found, 444.0934.

4-*tert*-Butyl-*N*-(4-oxonaphthalen-1(4*H*)-ylidene)benzene-1-sulfonamide (2). This compound was prepared using the procedure described for compound **1** except for using naphthalene-1,4-dione (247 mg, 1.56 mmol) as starting material. After filtration, the crude material was purified by two subsequent flash chromatography steps (eluents: petroleum ether/ethyl acetate 95/5 v/v and petroleum ether/DCM 50:50 v/v) to obtain a yellow solid (mp: 183.9-185.0°C; from trituration with diisopropyl ether). Yield: 23 %. TLC (petroleum ether/DCM 50:50 v/v): R_f = 0.25; ^{1}H NMR (300 MHz, CDCl$_3$): δ 8.44 (d, J = 10.5 Hz, 1H), 8.18 (d, J = 7.5 Hz, 1H), 8.12 (d, J = 7.7 Hz, 1H), 8.00 (d, J = 8.5 Hz, 2H), 7.79 - 7.64 (m, 2H), 7.61 (d, J = 8.5 Hz, 2H), 6.89 (d, J = 10.5 Hz, 1H), 1.37 (s, 9H). ^{13}C NMR (75 MHz, CDCl$_3$) δ 184.00, 163.08, 157.50, 137.61, 136.96, 133.81, 133.66, 133.26, 132.44, 131.91, 127.42, 126.85, 126.76, 126.27, 35.43, 31.22. HRMS (m/z): [M]$^+$ calcd. for C$_{20}$H$_{19}$NO$_3$S, 354.1158; found, 354.1162.

Determination of IC50 and inactivation constants in PPIase assays

For IC50 determination, human recombinant PIN1 was preincubated with different concentrations of KPT-6566 and PPIase activity was measured after 180 minutes. K values of PPIase activity were plotted against inhibitor concentration in a semi-logarithmic plot. IC50 values were calculated using

log (inhibitor) vs. normalized response function of GraphPad Prism software (GraphPad Software, La Jolla, CA). For inactivation constants determination, human recombinant PIN1 was preincubated with different concentrations of KPT-6566 and PPIase activity was measured after 0, 60, 120 or 180 minutes. The logarithm of the percentage of the remaining isomerization activity was plotted against preincubation time, yielding a semi-logarithmic plot. The observed rate constant for inhibition, k_{obs}, at each concentration was determined from the slope of the semi-logarithmic plot of inhibition versus time. The k_{obs} values were re-plotted against inhibitor concentration, and fitted to a hyperbolic equation (One site binding-hyperbola; GraphPad Software), according to the equation $k_{obs} = k_{inact}[I]/(K_i + [I])$, to obtain values for K_i and k_{inact}. k_2 is the rate constant that defines the maximal rate of inactive enzyme formation, I is the initial concentration of the inhibitor, and K_i is the inhibitor concentration when $k_{obs} = k_{inact}/2$. The k_{inact}/K_i ratio represents the second-order rate constant for the reaction of the inhibitor with the target.

LC/MS analysis

For LC-MS analyses KPT-6566 was dissolved in DMSO at a concentration of 10 mM. PIN1 samples were prepared in 30 mM HEPES buffer pH 7.9. 10 μg of PIN1 protein at a concentration of 9 μM were incubated with 3 fold excess compound KPT-6566, in 100 mM HEPES buffer pH 7.9 for 1 h in ice. The reaction was stopped by adding 1 μL of 10% v/v TFA and the samples were injected in the HPLC/MS instrument. WT PIN1 or the cysteine mutant C113A, incubated with KPT-6566 or in 2.7% DMSO were analyzed for full molecular weight determination by liquid chromatography/electrospray ionization mass spectrometry (LC/ESI-MS) using a 1100 HPLC apparatus coupled through an API-ESI source to a 1946 MSD single quadrupole MS detector, both from Agilent (Palo Alto, CA, USA). A RP Poroshell 300SB-C3 column (2.1 mm ID x 75 mm 5mm) was used and proteins were eluted applying a 0.05% TFA/acetonitrile gradient. Acquired MS spectra were deconvoluted using the ChemStation deconvolution software package (Agilent).

Protein digestion and MALDI-ToF-ToF MS and MS/MS analysis

PIN1 protein was digested adding ProteaseMAX™ Surfactant Trypsin Enhancer (Promega Corporation) (0.01% v/v final concentration) and 1 mg of TPCK Trypsin to the reaction solution. The mixture was incubated for 30 minutes at 37°C. 0.3 μl of the samples were mixed with 0.3 μl of alpha-cyano-4-hydroxycinnamic acid (HCCA) matrix (20 mg in 1 ml of 50% acetonitrile, 0.1% TFA) loaded on the MALDI plate and analyzed by 4800 MALDI ToF/ToF (ABI Sciex) in reflector conditions using optimized parameters. Peptides at m/z possibly containing modified cysteine were

submitted to MS/MS analysis. Obtained spectra were manually inspected to reconstruct the sequence.

Molecular-docking study

Computational studies were carried out using Schrodinger suit running on a Linux based customized work station with CentOS platform. Grid-Based Ligand Docking with Energetics (Glide) program was used to analyze the binding conformations of KPT-6566 and PIN1[96]. Three dimensional structures of PIN1 (PDBID: 2XPB)[92] were retrieved from the Protein Data Bank (PDB) (www.rcsb.org). The protein structures were organized using the Protein Preparation Wizard, whereas the 3D structure of the ligand was optimized using LigPrep module and the partial charges were ascribed using Optimized Potentials for Liquid Simulations (OPLS3) force-field[122]. Hydrogen atoms were added to the protein structure to pH 7.0 considering the appropriate ionization states for both the acidic and basic amino acid residues. The binding pocket of PIN1 was defined by a $10 \times 10 \times 10$ Å box centered on the central position of C113. "Extra-Precision" (XP) mode of Glide application of Schrodinger suite helped to measure the binding affinity of proteins to ligand docking. The protocol facilitates flexible ligand docking within the rigid receptor and the best ligand pose with reference to the protein was chosen based on the grading obtained by Glide Score[98].

Cell lines and treatments

Unless otherwise stated, all cell lines were purchased from ATCC or obtained from other laboratories cooperating on the project. Human cell lines were subjected to STR genotyping with PowerPlex 18D System and their identity confirmed comparing the results to reference ATCC database. They were also routinely tested for absence of Mycoplasma infection by PCR/Immunofluorescence. HMEC are normal hTERT immortalized epithelial breast cells[123]. MCF10A are normal immortalized epithelial breast cells, MCF10AT1 are xenograft-passaged T24 H-Ras transformed MCF10A cells[100]. MDA-MB-231 and MDA-MB-468 are breast carcinoma cell lines, H1299 is a lung carcinoma cell line, PC3 is a prostatic carcinoma cell line, LNCaP is a prostatic carcinoma cell line derived from metastatic site, PANC1 is a pancreatic carcinoma cell line, SKOV3 is a ovarian carcinoma cell line, HeLa is a human cervical carcinoma cell line. *PIN1* knockout MDA-MB-231 cells were generated by CRISPR/Cas9 genome engineering technology. Immortalized *Pin1*$^{-/-}$ mouse fibroblasts were obtained by spontaneous immortalization from MEFs of C57BL6/129Sv mixed background and were already described[28]. MDA-MB-231, MDA-MB-468, PANC1, SKOV3, HeLa and MEFs were cultured in DMEM (BioWhittaker) supplemented

with 10% fetal bovine serum (Gibco), 100 U ml^{-1} penicillin and 100 μg ml^{-1} streptomycin (Euroclone). H1299, PC3, LNCaP cells were grown in RPMI (BioWhittaker) supplemented with 10% fetal bovine serum and penicillin/streptomycin. MCF10A and MCF10AT1 cells were maintained in DMEM:F12 Ham's (1:2) (BioWhittaker), supplemented with 5% horse serum (Gibco), 10 μg ml^{-1} insulin (Sigma), 0.5 μg ml^{-1} hydrocortisone (Sigma) and 20 ng ml^{-1} EGF (Cell Guidance System). HMEC cells were maintained in MEBM (BioWhittaker), supplemented with 0.4% Bovine Pituitary Extract (Life Technologies), 5 μg ml^{-1} insulin, 0.5 μg ml^{-1}, hydrocortisone and 10 ng ml^{-1} EGF. Transient transfections were performed using standard procedures as already described[27,28]. For creation of stable clones, a selection corresponding to the expressed vectors was applied for 2 weeks to transfected or infected cells at concentrations of 2 μg ml^{-1} for puromycin (Sigma) and 5 μg ml^{-1} for blasticidin (InvivoGen). 10 mM KPT-6566 or 5 mM KPT-6566-B dissolved in DMSO were used for cell treatments at the indicated concentrations. Control cells received DMSO at the same concentrations ranging from 0.05-0.01%. PPIase-Parvulin Inhibitor PiB (Calbiochem #529627), Juglone (Calbiochem #420120), ATRA (all-trans retinoic acid, Sigma R2625), MG-132 (Calbiochem #474790), NAC (N-Acetyl-L-Cysteine, Sigma A7250), Melatonin (Sigma M5250), and Bleomycin (EURO Nippon Kayaku GmbH, Sanofi Aventis), were resuspended as indicated in the respective datasheets.

Immunoblotting and immunofluorescence

For immunoblotting analyses protein lysates were loaded and separated in SDSPAGE, followed by Western blotting on Nitrocellulose membranes (Amersham). For β-mercaptoethanol stripping of the primary antibody membranes were shortly boiled in 0.1 mM β-mercaptoethanol, 1% SDS, 50 mM Tris/HCl pH 6.9, then washed by shaking at RT with PBS, followed by blocking in Blotto-tween (PBS, 0.2% Tween-20, not fat dry milk 5%) or with TBST (0.2% Tween-20, Tris/HCl 25 mM pH7.5) plus 5% BSA (PanReac Applichem) depending on the antibody. For immunofluorescence, after 48 hours of treatment with the compounds, cells were fixed in 4% paraformaldehyde for 20 minutes, washed in PBS, permeabilized with Triton 0.1% for 5 min and blocked in PBS + BSA 1% for 30 min. Antigen recognition was done by incubating primary antibody for 1 h at 37°C and with Goat anti-mouse Alexa Fluor 568 (Life Technologies) as secondary antibody for 30 min at 37°C. Nuclei were counterstained with Hoechst 33342 (Life Technologies). Representative fluorescence images were taken with a 630X magnification on a Leica DM4000B microscope equipped with a LEICA DFC420C camera (Leica Microsystems S.r.l. Milan, Italy) and acquired with Leica Application Suite 2.5.0 R1 (Leica Microsystems).

Quantitative Real Time PCR (qRT-PCR) analysis

Total RNA from cell lines was extracted with QIAzol Lysis Reagent (Qiagen) and cDNA was transcribed with QuantiTect (Qiagen) in accordance with manufacturer's protocols. cDNA was then amplified on a CFX96 Touch Real-Time PCR Detection System with SsoAdvanced SYBR Green Supermix (Biorad) and analyzed with Biorad CFX Manager software. Expression levels are always given relative to histone *H3*.

Proliferation assays

For proliferation curve, mouse embryo fibroblasts were seeded at a density of 5.000 cells per well in a 6-well plate and incubated for 24 hours in 10% FBS-supplemented DMEM culture medium. Cells were then treated with KPT-6566 or DMSO every second day. The number of cells was counted every second day with by hemocytometer counting after trypsin digestion.

For Trypan blue staining, cells were seeded at a density of 250.000 cells per well in a 6-well plate and incubated for 24 hours in 10% FBS-supplemented DMEM culture medium. Cells were then treated with KPT-6566 or DMSO. After 24 hours the number of cells was counted after trypsin digestion and staining with 0.2% Trypan Blue (Sigma).

Viability assays

For WST assay, MCF10A and MCF10AT1 cells were seeded in 96-multi-well plate at a concentration of 4000 cells/well. 24 hours after seeding, cells were treated with the compound or DMSO as a negative control. 48 hours after compounds administration, growing medium was removed and WST-1 was added to the cells (Promega). Absorbance was read in an EnSpire® Perkin Elmer multiplate reader. For ATP LITE assay, cells were seeded in 96-multi-well view-plate at a concentration of 4000 cells/well. 24 hours after seeding, cells were treated with the compound or DMSO as a negative control. 48 hours after compound administration, growing medium was removed and cells were lysed with 50 μL of ATPlite 1step substrate solution (Perkin Elmer). Luminescence was read in an EnSpire® Perkin Elmer multiplate reader. IC50 values were calculated using variable slope log (inhibitor) vs. normalized response function of GraphPad Prism software.

Colony formation assay

Cells were seeded at a density of 5.000 (MDA-MB-231) or 7.500 cells (PC3) per 6 cm diameter plate and incubated for 24 hours in 10% FBS-supplemented DMEM culture medium. Cells were then treated with KPT-6566, PiB or DMSO. After 10 days, cells were fixed in 4% formaldehyde

and stained with Giemsa (Sigma) diluted solution 1:10 in water for 2 hours. Colonies ≥ 50 pixels were counted using ImageJ[124] software after background subtraction.

Invasion assay

Invasion assays were performed by seeding cells at a density of 5.000 cells per well in 24-well PET inserts (8.0 mm pore size, Falcon) with matrigel-coated filters. Cells were treated for 20 hours with KPT-6566 or DMSO and then invading cells were fixed, stained with 0.5% Crystal Violet (Sigma) and counted with a 20X objective on CK30 Olympus optical microscope (Olympus Italia Srl, Milan, Italy).

Mammosphere cultures

To obtain mammospheres, cells from monolayer cultures were enzymatically disaggregated (0.05% trypsin–EDTA, Gibco) to a single cell suspension, passed though a 40 lm cell strainer (BD Falcon), plated at clonogenic density (2.500 cells/cm^2), and grown in non-adherent culture conditions, as described[28]. In detail, cells were grown for 7–10 days in DMEM:F12 (1:2) supplemented with B27 (Invitrogen Corporation, Carlsbad, CA, USA), 20 ng/ml EGF (PROSPEC, East Brunswick, NJ, USA), 20 ng/ml bFGF (BD Biosciences, San Jose, CA, USA), 4 g/ml heparin (StemCell Technologies Inc.), 0.5 µg/ml hydrocortisone (Sigma) and 5 µg/ml Insulin (Sigma) in low attachment 24- or 96-well plates (Corning) in a humified incubator at 37°C, 5% CO_2. Primary mammospheres ($\geq$200 µm) were obtained, collected, counted and again enzymatically disaggregated as above to re-plate cells at clonogenic densities to obtain secondary mammospheres. Percentages of mammosphere forming efficiencies (%MFE) were calculated as number of mammospheres ($\geq$200 µm) divided by the plated cell number and multiplied by a hundred. Mammospheres were counted with a 20X objective on an Olympus CK30 microscope (Olympus Italia Srl, Milan, Italy).

Flow cytometric analyses

FACS analyses of CD44/CD24/EpCAM surface markers were performed as described[28,102]. Non confluent cell cultures were trypsinized into single cell suspension, counted, washed with phosphate-buffered saline (PBS), and blocked in PBS + BSA 1% + EDTA 2 mM. Staining with antibodies was performed for 30 minutes at 4°C and cells were analyzed by BD FACSCelesta™ Cell Analyzer (BD Biosciences). For CellROX analysis, cells were treated with KPT-6566, NAC or DMSO. After 48 hours, CellROX® Green Reagent (Thermo Fisher Scientific) was added at a final concentration of 5 µM for 30 minutes. Cells were then washed, trypsinized and analyzed by FACS.

Mean fluorescence intensity (MFI) was derived from each sample and the baseline fluorescence was calculated from the sample that was not incubated with CellROX reagent. For Annexin V/Propidium Iodide analysis, Alexa Fluor® 488 Annexin V/Dead Cell Apoptosis Kit (Invitrogen) was used following the manufacturer's protocols. Analyses were performed on a FACSCalibur cell sorter (Becton Dickinson) and data were analyzed with FlowJo software for Mac (FlowJo, LLC 2013-2016).

Microarray hybridization and low level analysis

For gene expression profiling in MDA-MB-231 cell lines, we used the Illumina HumanHT-12-v4-BeadChip (Illumina). Total RNA isolated from the cell lines with control siRNA or *PIN1* siRNA or treated with DMSO or KPT-6566 for 48 hours were reverse transcribed and amplified according to standard protocols and in vitro transcription was then carried out to generate cRNA. cRNA was hybridized onto each array (three biological replicates for the KPT-6566 condition and two for PIN1 siRNA condition) and then labeled with Cy3-streptavidin (Amersham Biosciences). The array was then scanned using a BeadStation 500 system (Illumina). The probe intensities were calculated and normalized using GenomeStudio Data Analysis Software's Gene Expression Module (GSGX) Version 1.9 (Illumina). Further data processing was performed in the R computing environment version 3.2 (http://www.r-project.org/), with BioConductor packages (http://www.bioconductor.org/).

Gene signatures, functional annotation and pathway enrichment analysis

Full transcriptomic expression datasets (GEO database record GSE84909) have been imported to Ingenuity Pathway Analysis (IPA) software (Qiagen, www.ingenuity.com). *p* value and log fold-change cutoffs were applied in IPA as reported in the text and figures. Pathway analysis module of IPA was further used to associate analyzed gene lists with molecular pathways (Fig. 8c). An independent, parallel method for analyzing the signatures was the pathway-related gene ontology term enrichment analysis, using DAVID/EASE web tool with default parameters and procedures (Fig. 8b and Supplementary Table 9).

Plasmids, retroviral vectors

Retroviral pLPC-HA-PIN1, pMSCV-HA-PIN1 and pSR shRNA *PIN1* (corresponding to the siRNA sequence #1) were already described[28,53].

Oligonucleotides

All oligonucleotides were supplied by MWG.

Oligonucleotides for quantitative real time PCR of human genes

Gene symbol	Forward 5'-3'	Reverse 5'-3'
BUB1	ATTCAAGCCACAGAGTGGAGCAG	AGAACTTGTGTTGGCAACCTTATGTG
DEPDC1	ATCAGATGACCTCCCTCACTGGGT	GGTTGCAGCAAGCCCAAAATGTT
HEY2	AGGGGGTAAAGGCTACTTTGA	TGGCGCAAGTGCTGAGATG
BIRC5	GCCCAGTGTTTCTTCTGCTT	CCGGACGAATGCTTTTTATG
PIN1	CTGGAGCTGATCAACGGCTACATCC	GCAGCGCAAACGAGGCGTCT
CCNA2	AGCAGCCTGCAAACTGCAAAGTTG	TGGTGGGTTGAGGAGAGAAACAC
CCNB2	GGCTGGTACAAGTCCACTCC	GAAGCCAAGAGCAGAGCAGT
CCND1	ACGGCCGAGAAGCTGTGCATC	CCTCCGCCTCTGGCATTTTGGAG
CCNE2	TGAGCCGAGCGGTAGCTGGT	GGGCTGGGGCTGCTGCTTAG
CDC25C	GTATCTGGGAGGACACATCCAGGG	CAAGTTGGTAGCCTGTTGGTTTG
P21	TACCCTTGTGCCTCGCTCAG	GAGAAGATCAGCCGGCGTTT
BCL2	GCGACTCCTGATTCATTGG	GTCTACTTCCTCTGTGATGTTG
GADD45	GTGGTGTTGTGCCTGCTG	AGGATGTTGATGTCGTTCTCG
cFOS	GGGGCAAGGTGGAACAGTTA	AGTTGGTCTGTCTCCGCTTG
HO1	AAGACTGCGTTCCTGCTCAA	GGGGGCAGAATCTTGCACTT
NQO1	TGAAAGGCTGGTTTGAGCGA	CTGCCTTCTTACTCCGGAAGG
TXNRD1	CTTTTTCATTCCTGCTACTCTACC	CTCTCTCCTTTTCCCTTTTCC
DNAJB9	TAGTCGGAGGGTGCAGGATA	CGCTCTGATGCCGATTTTGG
H3	GTGAAGAAACCTCATCGTTACAGGCCTGGT	CTGCAAAGCACCAATAGCTGCACTCTGGAA

Oligonucleotides for cloning

Original vector	Forward 5'-3'	Reverse 5'-3'
pcDNA3HA PIN1; pcDNA3HA PIN1 S67E; pcDNA3HA PIN1 C113A	TACTTCCAATCCATGGCGGACGAGGAGAAGCTGCC	TATCCACCTTTACTGTCATCACTCAGTGCGGAGGATGATGTG
pANT7_cGST FKBP4	CATCATAGATCTATGACAGCCGAGGAGATGAAG	CATCATCTCGAGCTATGCTTCTGTCTCCACCTG
pANT7_cGST PPIA	CATCATGGATCCATGGTCAACCCCACCGTGTTC	CATCATCTCGAGTTATTCGAGTTGTCCACAGTC

siRNA sequences

siRNA	Sequence 5'-3'	Reference
si*PIN1*#1	CGGGAGAGGAGGACUUUGA	[53]
si*PIN1*#2	GCCAUUUGAAGACGCCUCG	[53]
siCtrl	Allstar NEGATIVE control, Qiagen	

Antibodies for western blot, immunofluorescence, and flow cytometric analysis

The following antibodies were used: rabbit polyclonal anti-PIN1 (home-made)[27], mouse anti-pRB (554164, BD Pharmigen), rabbit polyclonal anti-p-pRB pS807/811 (9308, Cell Signaling), rabbit polyclonal anti-Cyclin D1 (2922, Cell Signaling), mouse monoclonal anti-Cyclin D1 (2926, Cell Signaling), rabbit polyclonal anti-Actin (A2066, Sigma), rabbit polyclonal anti-H-RAS C-20 (sc-520, Santa Cruz), rabbit polyclonal anti-Cleaved Notch1 Val1744 (4147, Cell Signaling), rabbit polyclonal anti-NF-κB p65 C-20 (sc-372, Santa Cruz), rabbit polyclonal anti-c-JUN 60A8 (9165, Cell Signaling), rabbit polyclonal MCL-1 S-19 (sc-819, Santa Cruz), rabbit polyclonal anti-Oct4 (2750, Cell Signaling), rat anti-HA (Roche), rabbit monoclonal anti-Slug C19G7 (9585, Cell Signaling), rabbit polyclonal anti-Sox-9 H-90 (20095, Santa Cruz), mouse monoclonal anti-γH2AX Ser139 clone JBW301 (05-636, Millipore), rabbit polyclonal anti-HMGB1 (ab18256, abcam), rabbit monoclonal anti-Cleaved Caspase-3 Asp175 5A1E (9664, Cell Signaling), rabbit polyclonal anti-Cleaved PARP p85 Fragment (G7341, Promega). Flow cytometric analysis was performed with mouse anti-human PE conjugated anti-CD44, FITC conjugated anti-CD24 antibodies (BD) and APC conjugated anti-EpCAM CD326 (Miltenyi Biotec).

Animal studies

Experiments were performed with 6-week-old female Hsd:Athymic Nude-*Foxn1[nu]* mice obtained from Envigo (Udine, Italy). Mice were maintained under specific-pathogen-free conditions with constant temperature and humidity, according to institutional guidelines. Animal experimentation was conducted in conformance with the following laws, regulations, and policies governing the care and use of laboratory animals: Italian Governing Law (D.lgs 26/2014; Authorization n.19/2008-A issued March 6, 2008 by the Ministry of Health). Mario Negri Institutional Regulations and Policies providing internal authorizations for persons conducting animal experiments (Quality Management System Certificate – UNI EN ISO 9001:2008 – Reg. N° 6121); the NIH Guide for the Care and Use of Laboratory Animals (2011 edition) and EU directives and guidelines (EEC Council Directive 2010/63/UE), and in line with guidelines for the welfare and use of animals in cancer research[125]. Animal experimental protocols were reviewed and approved by the IRFMN Animal Care and Use Committee (IACUC), which includes "*ad hoc*" members for ethical issues. Animals were housed in the Institute's Animal Care Facilities, which meet international standards; they were checked regularly by a certified veterinarian responsible for health monitoring, animal welfare supervision, revision of experimental protocols and procedures. For toxicity experiments mice (3 for each group) were treated i) i.v. with vehicle (8% DMSO, 8% TWEEN80, 84% PBS) or 60 mg/kg and 90 mg/kg of KPT-6566 every two days for three times; ii) i.p. with vehicle or 30 and 45 mg/kg of KPT-6566

every two days for two weeks. For lung colonization experiments athymic nude mice were injected i.v. with 1 million of MDA-MB-231Luc[53] cells. After one day, mice were randomized in two experimental groups (at least 7 mice for each group) and treated i.p. with vehicle (4% DMSO, 4% TWEEN80, 92% PBS) or KPT-6566 5 mg/kg, every day until sacrifice (26 days of treatments). The investigators were not blinded to group allocation during experiments and outcome. During the study they were monitored for parameters including appearance and body weight. Mice were sacrificed when they became moribund. Lungs and other organs were collected, weighted and formalin fixed for histological analysis.

Histology and metastatic area determination

For lung metastases histology, 3 μm sections were cut from the lung lobes and stained with haematoxylin and eosin (H&E). For computer-aided assessment of lung tissue, the area occupied by metastatic foci, identifiable in sections of lung lobes, were calculated using a Leica Aperio Digital Pathology Slide Scanner and the software Leica Aperio Image Scope, summed, and total value was finally compared to the whole area of the lung lobe.

Statistical analyses

The sample size was chosen to include at least three biological replicates. No statistical method was used to predetermine the sample size for animal studies. Experiments for which we showed representative images were performed successfully at least 3 independent times. No samples or animals were excluded from the analysis. Standard laboratory practice randomization procedure was used for cell line groups and animals of the same age and sex. The investigators were not blinded to allocation during experiments and outcome.

Statistical tests were appropriately chosen for each experiment. For differentially expressed genes from microarray experiments statistical analysis was performed with limma and P values were adjusted for multiple testing using Benjamini and Hochsberg's method to control the false discovery rate. In the lung colonization assay P value was determined using two-tailed Mann-Whitney tests and statistical significance was set at $p<0.05$. For all other experiments P values were determined using two-tailed Student's t-test and statistical significance was set at $P<0.05$. An estimation of the variation within each group of data was indicated by s.d., std. error, s.e.m., or c.i.. The variance was similar between groups that we compared.

References

1. Webster, R. M. Combination therapies in oncology. *Nat Rev Drug Discov* **15,** 81–82 (2016).

2. Aggarwal, S. Targeted cancer therapies. *Nat. Rev. Drug Discov.* **9,** 427–428 (2010).

3. Dobbelstein, M. & Moll, U. Targeting tumour-supportive cellular machineries in anticancer drug development. *Nat. Rev. Drug Discov.* **13,** 179–96 (2014).

4. Luo, J., Solimini, N. L. & Elledge, S. J. Principles of Cancer Therapy: Oncogene and Non-oncogene Addiction. *Cell* **136,** 823–837 (2009).

5. Magee, J. A., Piskounova, E. & Morrison, S. J. Cancer Stem Cells: Impact, Heterogeneity, and Uncertainty. *Cancer Cell* **21,** 283–296 (2012).

6. Kreso, A. & Dick, J. E. Evolution of the cancer stem cell model. *Cell Stem Cell* **14,** 275–291 (2014).

7. Meacham, C. E. & Morrison, S. J. Tumour heterogeneity and cancer cell plasticity. *Nature* **501,** 328–37 (2013).

8. Patel, M. N., Halling-Brown, M. D., Tym, J. E., Workman, P. & Al-Lazikani, B. Objective assessment of cancer genes for drug discovery. *Nat. Rev. Drug Discov.* **12,** 35–50 (2013).

9. Zhou, X. Z. & Lu, K. P. The isomerase PIN1 controls numerous cancer-driving pathways and is a unique drug target. *Nat Rev Cancer* **16,** 463–478 (2016).

10. Lu, K. P. & Zhou, X. Z. The prolyl isomerase PIN1: a pivotal new twist in phosphorylation signalling and disease. *Nat Rev Mol Cell Biol* **8,** 904–916 (2007).

11. Lee, T. H., Pastorino, L. & Lu, K. P. Peptidyl-prolyl cis-trans isomerase Pin1 in ageing, cancer and Alzheimer disease. *Expert Rev Mol Med* **13,** e21 (2011).

12. Mantovani, F., Zannini, A., Rustighi, A. & Del Sal, G. Interaction of p53 with prolyl isomerases: Healthy and unhealthy relationships. *Biochim. Biophys. Acta - Gen. Subj.* **1850,** 2048–2060 (2015).

13. Lu, Z. & Hunter, T. Prolyl isomerase Pin1 in cancer. *Cell Res* **24,** 1033–1049 (2014).

14. Lu, K. P., Hanes, S. D. & Hunter, T. A human peptidyl-prolyl isomerase essential for regulation of mitosis. *Nature* **380,** 544–547 (1996).

15. Moore, J. D. & Potter, A. Pin1 inhibitors: Pitfalls, progress and cellular pharmacology. *Bioorg Med Chem Lett* **23,** 4283–4291 (2013).

16. Rustighi, A. *et al.* PIN1 in breast development and cancer: a clinical perspective. *Cell Death Differ.* 1–12 (2016). doi:10.1038/cdd.2016.122

17. Hanes, S. D. Prolyl isomerases in gene transcription. *Biochim. Biophys. Acta - Gen. Subj.* **1850,** 2017–2034 (2015).

18. Ranganathan, R., Lu, K. P., Hunter, T. & Noel, J. P. Structural and functional analysis of the

mitotic rotamase Pin1 suggests substrate recognition is phosphorylation dependent. *Cell* **89,** 875–886 (1997).

19. Liou, Y.-C. C. *et al.* Loss of Pin1 function in the mouse causes phenotypes resembling cyclin D1-null phenotypes. *Proc Natl Acad Sci U S A* **99,** 1335–1340 (2002).

20. Atchison, F. W. & Means, A. R. Spermatogonial depletion in adult Pin1-deficient mice. *Biol Reprod* **69,** 1989–1997 (2003).

21. Atchison, F. W. & Means, A. R. A role for Pin1 in mammalian germ cell development and spermatogenesis. *Front Biosci* **9,** 3248–3256 (2004).

22. Fujimori, F., Takahashi, K., Uchida, C. & Uchida, T. Mice lacking Pin1 develop normally, but are defective in entering cell cycle from G(0) arrest. *Biochem Biophys Res Commun* **265,** 658–663 (1999).

23. Hsu, T., McRackan, D., Vincent, T. S. & Gert de Couet, H. Drosophila Pin1 prolyl isomerase Dodo is a MAP kinase signal responder during oogenesis. *Nat Cell Biol* **3,** 538–543 (2001).

24. Yeh, E. S. & Means, A. R. PIN1, the cell cycle and cancer. *Nat Rev Cancer* **7,** 381–388 (2007).

25. Bao, L. *et al.* Prevalent overexpression of prolyl isomerase Pin1 in human cancers. *Am J Pathol* **164,** 1727–1737 (2004).

26. Ryo, A. *et al.* PIN1 is an E2F target gene essential for Neu/Ras-induced transformation of mammary epithelial cells. *Mol Cell Biol* **22,** 5281–5295 (2002).

27. Rustighi, A. *et al.* The prolyl-isomerase Pin1 is a Notch1 target that enhances Notch1 activation in cancer. *Nat Cell Biol* **11,** 133–142 (2009).

28. Rustighi, A. *et al.* Prolyl-isomerase Pin1 controls normal and cancer stem cells of the breast. *EMBO Mol Med* **6,** 99–119 (2014).

29. Li, Q. *et al.* The rs2233678 Polymorphism in PIN1 Promoter Region Reduced Cancer Risk: A Meta-Analysis. *PLoS One* **8,** (2013).

30. Zhang, X., Zhang, B., Gao, J., Wang, X. & Liu, Z. Regulation of the MicroRNA 200b (miRNA-200b) by transcriptional regulators PEA3 and ELK-1 protein affects expression of Pin1 protein to control anoikis. *J. Biol. Chem.* **288,** 32742–32752 (2013).

31. Luo, M. L. *et al.* Prolyl isomerase Pin1 acts downstream of miR200c to promote cancer stem-like cell traits in breast cancer. *Cancer Res* **74,** 3603–3616 (2014).

32. Lu, P. J., Zhou, X. Z., Liou, Y. C., Noel, J. P. & Lu, K. P. Critical role of WW domain phosphorylation in regulating phosphoserine binding activity and Pin1 function. *J Biol Chem* **277,** 2381–2384 (2002).

33. Eckerdt, F. *et al.* Polo-like kinase 1-mediated phosphorylation stabilizes Pin1 by inhibiting

its ubiquitination in human cells. *J Biol Chem* **280,** 36575–36583 (2005).

34. Lee, T. H. *et al.* Death-associated protein kinase 1 phosphorylates Pin1 and inhibits its prolyl isomerase activity and cellular function. *Mol Cell* **42,** 147–159 (2011).

35. Bialik, S. & Kimchi, A. The Death-Associated Protein Kinases: Structure, Function, and Beyond. *Annu. Rev. Biochem* **75,** 189–210 (2006).

36. Rangasamy, V. *et al.* Mixed-lineage kinase 3 phosphorylates prolyl-isomerase Pin1 to regulate its nuclear translocation and cellular function. *Proc. Natl. Acad. Sci. U. S. A.* **109,** 8149–54 (2012).

37. Chen, C. H. *et al.* SENP1 deSUMOylates and regulates pin1 protein activity and cellular function. *Cancer Res.* **73,** 3951–3962 (2013).

38. Chen, C. H. *et al.* Pin1 cysteine-113 oxidation inhibits its catalytic activity and cellular function in Alzheimer's disease. *Neurobiol. Dis.* **76,** 13–23 (2015).

39. Innes, B. T. *et al.* Peroxide-mediated oxidation and inhibition of the peptidyl-prolyl isomerase Pin1. *Biochim Biophys Acta* **1852,** 905–912 (2015).

40. Liou, Y. C., Zhou, X. Z. & Lu, K. P. Prolyl isomerase Pin1 as a molecular switch to determine the fate of phosphoproteins. *Trends Biochem Sci* **36,** 501–514 (2011).

41. Wulf, G., Garg, P., Liou, Y.-C. C., Iglehart, D. & Lu, K. P. Modeling breast cancer in vivo and ex vivo reveals an essential role of Pin1 in tumorigenesis. *EMBO J* **23,** 3397–3407 (2004).

42. Ryo, A., Nakamura, M., Wulf, G., Liou, Y. C. & Lu, K. P. Pin1 regulates turnover and subcellular localization of beta-catenin by inhibiting its interaction with APC. *Nat Cell Biol* **3,** 793–801 (2001).

43. Ryo, A. *et al.* Regulation of NF-kappaB signaling by Pin1-dependent prolyl isomerization and ubiquitin-mediated proteolysis of p65/RelA. *Mol Cell* **12,** 1413–1426 (2003).

44. Franciosa, G. *et al.* Prolyl-isomerase Pin1 controls Notch3 protein expression and regulates T-ALL progression. *Oncogene* (2016). doi:onc20165 [pii]10.1038/onc.2016.5

45. Khanal, P., Namgoong, G. M., Kang, B. S., Woo, E.-R. R. & Choi, H. S. The prolyl isomerase Pin1 enhances HER-2 expression and cellular transformation via its interaction with mitogen-activated protein kinase/extracellular signal-regulated kinase kinase 1. *Mol Cancer Ther* **9,** 606–616 (2010).

46. Park, J. E. *et al.* A critical step for JNK activation: isomerization by the prolyl isomerase Pin1. *Cell Death Differ* **19,** 153–61 (2011).

47. Luo, M. L. *et al.* The Rab2A GTPase promotes breast cancer stem cells and tumorigenesis via erk signaling activation. *Cell Rep.* **11,** 111–124 (2015).

48. Rajbhandari, P. *et al.* Regulation of Estrogen Receptor N-Terminus Conformation and Function by Peptidyl Prolyl Isomerase Pin1. *Mol. Cell. Biol.* **32,** 445–457 (2012).

49. Rajbhandari, P., Ozers, M. S., Solodin, N. M., Warren, C. L. & Alarid, E. T. Peptidylprolyl Isomerase Pin1 Directly Enhances the DNA Binding Functions of Estrogen Receptor alpha. *J Biol Chem* **290,** 13749–13762 (2015).

50. Yi, P. *et al.* Peptidyl-prolyl isomerase 1 (Pin1) serves as a coactivator of steroid receptor by regulating the activity of phosphorylated steroid receptor coactivator 3 (SRC-3/AIB1). *Mol Cell Biol* **25,** 9687–9699 (2005).

51. Wei, S. *et al.* Active Pin1 is a key target of all-trans retinoic acid in acute promyelocytic leukemia and breast cancer. *Nat Med* **21,** 457–466 (2015).

52. Rivlin, N., Brosh, R., Oren, M. & Rotter, V. Mutations in the p53 tumor suppressor gene: Important milestones at the various steps of tumorigenesis. *Genes Cancer* **2,** 466–474 (2011).

53. Girardini, J. E. *et al.* A Pin1/mutant p53 axis promotes aggressiveness in breast cancer. *Cancer Cell* **20,** 79–91 (2011).

54. Takahashi, K. *et al.* Ablation of a peptidyl prolyl isomerase Pin1 from p53-null mice accelerated thymic hyperplasia by increasing the level of the intracellular form of Notch1. *Oncogene* **26,** 3835–3845 (2007).

55. Hanahan, D. & Weinberg, R. A. Hallmarks of cancer: the next generation. *Cell* **144,** 646–674 (2011).

56. Shen, M., Stukenberg, P. T., Kirschner, M. W. & Lu, K. P. The essential mitotic peptidyl-prolyl isomerase Pin1 binds and regulates mitosis-specific phosphoproteins. *Genes Dev* **12,** 706–720 (1998).

57. Rizzolio, F. *et al.* Retinoblastoma tumor-suppressor protein phosphorylation and inactivation depend on direct interaction with Pin1. *Cell Death Differ.* **19,** 1152–61 (2012).

58. Suizu, F., Ryo, A., Wulf, G., Lim, J. & Lu, K. P. Pin1 regulates centrosome duplication, and its overexpression induces centrosome amplification, chromosome instability, and oncogenesis. *Mol Cell Biol* **26,** 1463–1479 (2006).

59. Xu, Y. X. & Manley, J. L. Pin1 modulates RNA polymerase II activity during the transcription cycle. *Genes Dev* **21,** 2950–2962 (2007).

60. Bernis, C. *et al.* Pin1 stabilizes Emi1 during G2 phase by preventing its association with SCF(betatrcp). *EMBO Rep* **8,** 91–98 (2007).

61. Okamoto, K. & Sagata, N. Mechanism for inactivation of the mitotic inhibitory kinase Wee1 at M phase. *Proc. Natl. Acad. Sci. USA* **104,** 3753–3758 (2007).

62. Stukenberg, P. T. & Kirschner, M. W. Pin1 acts catalytically to promote a conformational

change in Cdc25. *Mol Cell* **7,** 1071–1083 (2001).

63. Xu, Y. X. & Manley, J. L. New insights into mitotic chromosome condensation: a role for the prolyl isomerase Pin1. *Cell Cycle* **6,** 2896–2901 (2007).

64. Liao, Y. *et al.* Peptidyl-prolyl cis/trans isomerase Pin1 is critical for the regulation of PKB/Akt stability and activation phosphorylation. *Oncogene* **28,** 2436–2445 (2009).

65. Ding, Q. *et al.* Down-regulation of myeloid cell leukemia-1 through inhibiting Erk/Pin 1 pathway by sorafenib facilitates chemosensitization in breast cancer. *Cancer Res* **68,** 6109–6117 (2008).

66. Wulf, G. M. *et al.* Pin1 is overexpressed in breast cancer and cooperates with Ras signaling in increasing the transcriptional activity of c-Jun towards cyclin D1. *EMBO J* **20,** 3459–3472 (2001).

67. Ayala, G. *et al.* The prolyl isomerase Pin1 is a novel prognostic marker in human prostate cancer. *Cancer Res* **63,** 6244–6251 (2003).

68. Zheng, Y. *et al.* Ras-induced and extracellular signal-regulated kinase 1 and 2 phosphorylation-dependent isomerization of protein tyrosine phosphatase (PTP)-PEST by PIN1 promotes FAK dephosphorylation by PTP-PEST. *Mol Cell Biol* **31,** 4258–4269 (2011).

69. Rajbhandari, P. *et al.* Pin1 modulates ERα levels in breast cancer through inhibition of phosphorylation-dependent ubiquitination and degradation. *Oncogene* **33,** 1438–47 (2014).

70. Ryo, A., Wulf, G., Lee, T. H. & Lu, K. P. Pinning down HER2-ER crosstalk in SMRT regulation. *Trends in Biochemical Sciences* **34,** 162–165 (2009).

71. Lam, P. B. *et al.* Prolyl isomerase Pin1 is highly expressed in Her2-positive breast cancer and regulates erbB2 protein stability. *Mol Cancer* **7,** 91 (2008).

72. Tan, X. *et al.* Pin1 expression contributes to lung cancer: Prognosis and carcinogenesis. *Cancer Biol Ther* **9,** 111–119 (2010).

73. Pang, R. W. *et al.* PIN1 expression contributes to hepatic carcinogenesis. *J Pathol* **210,** 19–25 (2006).

74. Shi, M. *et al.* Pin1 is overexpressed and correlates with poor prognosis in gastric cancer. *Cell Biochem Biophys* **71,** 857–864 (2015).

75. Murphy, L. & Watson, R. W. Patented prostate cancer biomarkers. *Nat. Rev. Urol.* **9,** 464–72 (2012).

76. Wang, J. Z., Liu, B. G. & Zhang, Y. Pin1-based diagnostic and therapeutic strategies for breast cancer. *Pharmacol Res* **93,** 28–35 (2015).

77. Liou, Y. C. *et al.* Role of the prolyl isomerase Pin1 in protecting against age-dependent neurodegeneration. *Nature* **424,** 556–561 (2003).

78. Pastorino, L. *et al.* The prolyl isomerase Pin1 regulates amyloid precursor protein processing and amyloid-beta production. *Nature* **440,** 528–534 (2006).

79. Nakamura, K. *et al.* Prolyl isomerase Pin1 regulates neuronal differentiation via beta-catenin. *Mol Cell Biol* **32,** 2966–2978 (2012).

80. Shen, Z.-J. *et al.* Pin1 null mice exhibit low bone mass and attenuation of BMP signaling. *PLoS One* **8,** e63565 (2013).

81. Hennig, L. *et al.* Selective inactivation of parvulin-like peptidyl-prolyl cis/trans isomerases by juglone. *Biochemistry* **37,** 5953–5960 (1998).

82. Fila, C., Metz, C. & Van Der Sluijs, P. Juglone inactivates cysteine-rich proteins required for progression through mitosis. *J. Biol. Chem.* **283,** 21714–21724 (2008).

83. Kiran Aithal, B., Sunil Kumar, M. R., Nageshwar Rao, B., Udupa, N. & Satish Rao, B. S. Juglone, a naphthoquinone from walnut, exerts cytotoxic and genotoxic effects against cultured melanoma tumor cells. *Cell Biol. Int.* **33,** 1039–1049 (2009).

84. Uchida, T. *et al.* Pin1 and Par14 peptidyl prolyl isomerase inhibitors block cell proliferation. *Chem Biol* **10,** 15–24 (2003).

85. Tatara, Y., Lin, Y. C., Bamba, Y., Mori, T. & Uchida, T. Dipentamethylene thiuram monosulfide is a novel inhibitor of Pin1. *Biochem. Biophys. Res. Commun.* **384,** 394–398 (2009).

86. Urusova, D. V *et al.* Epigallocatechin-gallate suppresses tumorigenesis by directly targeting Pin1. *Cancer Prev Res* **4,** 1366–1377 (2011).

87. Nam, S., Smith, D. M. & Dou, Q. P. Ester Bond-containing Tea Polyphenols Potently Inhibit Proteasome Activity in Vitro and in Vivo. *J. Biol. Chem.* **276,** 13322–13330 (2001).

88. Fischer, G., Bang, H. & Mech, C. [Determination of enzymatic catalysis for the cis-trans-isomerization of peptide binding in proline-containing peptides]. *Biomed Biochim Acta* **43,** 1101–1111 (1984).

89. Long, M. J. C. C., Gollapalli, D. R. & Hedstrom, L. Inhibitor Mediated Protein Degradation. *Chem. Biol.* **19,** 629–637 (2012).

90. Singh, J., Petter, R. C., Baillie, T. a & Whitty, A. The resurgence of covalent drugs. *Nat. Rev. Drug Discov.* **10,** 307–317 (2011).

91. Toledo Warshaviak, D., Golan, G., Borrelli, K. W., Zhu, K. & Kalid, O. Structure-based virtual screening approach for discovery of covalently bound ligands. *J. Chem. Inf. Model.* **54,** 1941–1950 (2014).

92. Potter, A. *et al.* Discovery of cell-active phenyl-imidazole Pin1 inhibitors by structure-guided fragment evolution. *Bioorg Med Chem Lett* **20,** 6483–6488 (2010).

93. Kofron, J. L., Kuzmic, P., Kishore, V., Colón-Bonilla, E. & Rich, D. H. Determination of kinetic constants for peptidyl prolyl cis-trans isomerases by an improved spectrophotometric assay. *Biochemistry* **30,** 6127–6134 (1991).

94. Yaffe, M. B. *et al.* Sequence-Specific and Phosphorylation-Dependent Proline Isomerization: A Potential Mitotic Regulatory Mechanism. *Science (80-.).* **278,** 1957–1960 (1997).

95. Zhou, X. Z. *et al.* Pin1-dependent prolyl isomerization regulates dephosphorylation of Cdc25C and tau proteins. *Mol Cell* **6,** 873–883 (2000).

96. Friesner, R. A. *et al.* Glide: A New Approach for Rapid, Accurate Docking and Scoring. 1. Method and Assessment of Docking Accuracy. *J. Med. Chem.* **47,** 1739–1749 (2004).

97. Halgren, T. A. *et al.* Glide: A New Approach for Rapid, Accurate Docking and Scoring. 2. Enrichment Factors in Database Screening. *J. Med. Chem.* **47,** 1750–1759 (2004).

98. Friesner, R. A. *et al.* Extra precision glide: Docking and scoring incorporating a model of hydrophobic enclosure for protein-ligand complexes. *J. Med. Chem.* **49,** 6177–6196 (2006).

99. Fanghänel, J. & Fischer, G. Insights into the catalytic mechanism of peptidyl prolyl cis/trans isomerases. *Front. Biosci.* **9,** 3453–78 (2004).

100. Cordenonsi, M. *et al.* The Hippo transducer TAZ confers cancer stem cell-related traits on breast cancer cells. *Cell* **147,** 759–772 (2011).

101. Chen, H.-Z. Z. *et al.* Prolyl isomerase Pin1 stabilizes and activates orphan nuclear receptor TR3 to promote mitogenesis. *Oncogene* **31,** 2876–2887 (2012).

102. Fillmore, C. M. & Kuperwasser, C. Human breast cancer cell lines contain stem-like cells that self-renew, give rise to phenotypically diverse progeny and survive chemotherapy. *Breast Cancer Res.* **10,** R25 (2008).

103. Guo, W. *et al.* Slug and Sox9 cooperatively determine the mammary stem cell state. *Cell* **148,** 1015–1028 (2012).

104. Ben-Porath, I. *et al.* An embryonic stem cell–like gene expression signature in poorly differentiated aggressive human tumors. *Nat. Genet.* **40,** 499–507 (2008).

105. Mani, S. A. *et al.* The epithelial-mesenchymal transition generates cells with properties of stem cells. *Cell* **133,** 704–715 (2008).

106. Boussetta, T. *et al.* The prolyl isomerase Pin1 acts as a novel molecular switch for TNF-alpha-induced priming of the NADPH oxidase in human neutrophils. *Blood* **116,** 5795–5802 (2010).

107. Kilgore, J. A. *et al.* Identification of DNMT1 selective antagonists using a novel scintillation proximity assay. *J. Biol. Chem.* **288,** 19673–19684 (2013).

108. Munoz, B. & Albores, A. *DNA Damage Caused By Polycyclic Aromatic Hydrocarbons:*

Mechanisms and Markers, Selected Topics in DNA Repair. InTech (2011).

109. Gorrini, C., Harris, I. S. & Mak, T. W. Modulation of oxidative stress as an anticancer strategy. *Nat. Rev. Drug Discov.* **12,** 931–47 (2013).

110. Zafarullah, M., Li, W. Q., Sylvester, J. & Ahmad, M. Molecular mechanisms of N-acetylcysteine actions. *Cellular and Molecular Life Sciences* **60,** 6–20 (2003).

111. Jena, N. R. DNA damage by reactive species: Mechanisms, mutation and repair. in *Journal of Biosciences* **37,** 503–507 (2012).

112. d'Adda di Fagagna, F. Living on a break: cellular senescence as a DNA-damage response. *Nat. Rev. Cancer* **8,** 512–522 (2008).

113. Reiter, R. J., Paredes, S. D., Korkmaz, A., Jou, M.-J. & Tan, D.-X. Melatonin combats molecular terrorism at the mitochondrial level. *Interdiscip. Toxicol.* **1,** 137–49 (2008).

114. Trachootham, D., Alexandre, J. & Huang, P. Targeting cancer cells by ROS-mediated mechanisms: a radical therapeutic approach? *Nat. Rev. Drug Discov.* **8,** 579–591 (2009).

115. Kepp, O., Galluzzi, L., Lipinski, M., Yuan, J. & Kroemer, G. Cell death assays for drug discovery. *Nat. Rev. Drug Discov.* **10,** 221–237 (2011).

116. Chiasson, V. L., Munshi, N., Chatterjee, P., Young, K. J. & Mitchell, B. M. Pin1 deficiency causes endothelial dysfunction and hypertension. *Hypertension* **58,** 431–438 (2011).

117. Farrell, A. S. *et al.* Pin1 regulates the dynamics of c-Myc DNA binding to facilitate target gene regulation and oncogenesis. *Mol Cell Biol* **33,** 2930–2949 (2013).

118. Giang, I., Boland, E. L. & Poon, G. M. K. Prodrug applications for targeted cancer therapy. *AAPS J.* **16,** 899–913 (2014).

119. Zacchi, P. *et al.* The prolyl isomerase Pin1 reveals a mechanism to control p53 functions after genotoxic insults. *Nature* **419,** 853–857 (2002).

120. Studier, F. W. Protein production by auto-induction in high-density shaking cultures. *Protein Expr. Purif.* **41,** 207–234 (2005).

121. Küllertz, G., Lüthe, S. & Fischer, G. Semiautomated microtiter plate assay for monitoring peptidylprolyl *cis/trans* isomerase activity in normal and pathological human sera. *Clin. Chem.* **44,** 502–508 (1998).

122. Harder, E. *et al.* OPLS3: A Force Field Providing Broad Coverage of Drug-like Small Molecules and Proteins. *J. Chem. Theory Comput.* **12,** 281–296 (2016).

123. Fabris, L. *et al.* Radiotherapy-induced miR-223 prevents relapse of breast cancer by targeting the EGF pathway. *Oncogene* 1–13 (2016). doi:10.1038/onc.2016.23

124. Schneider, C. a, Rasband, W. S. & Eliceiri, K. W. NIH Image to ImageJ: 25 years of image analysis. *Nat. Methods* **9,** 671–675 (2012).

125. Workman, P. *et al.* Guidelines for the welfare and use of animals in cancer research. *Br. J. Cancer* **102,** 1555–77 (2010).
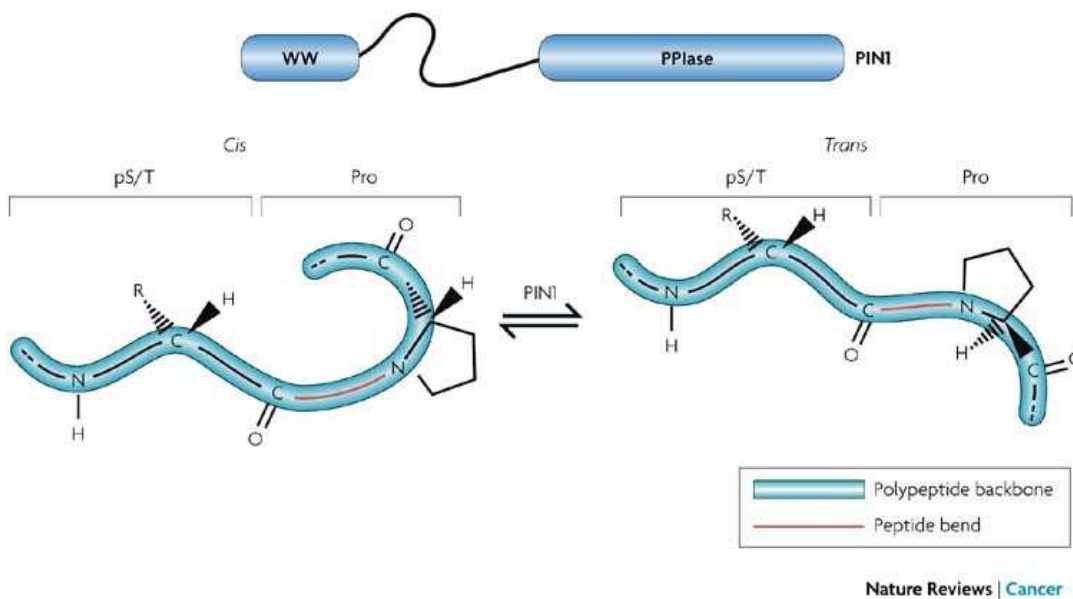
Figures

Figure 1. PIN1 domains and function.

Upper part: PIN1 consists of a WW protein interaction domain and a catalytic domain. Each domain has the capacity to bind to proteins that are phosphorylated on serines or threonines when the phosphorylated residue is immediately followed by a proline. Lower part: Prolyl isomerization can result in a substantial conformational change of the target protein leading to alterations in its function, stability and/or intracellular localization[24].
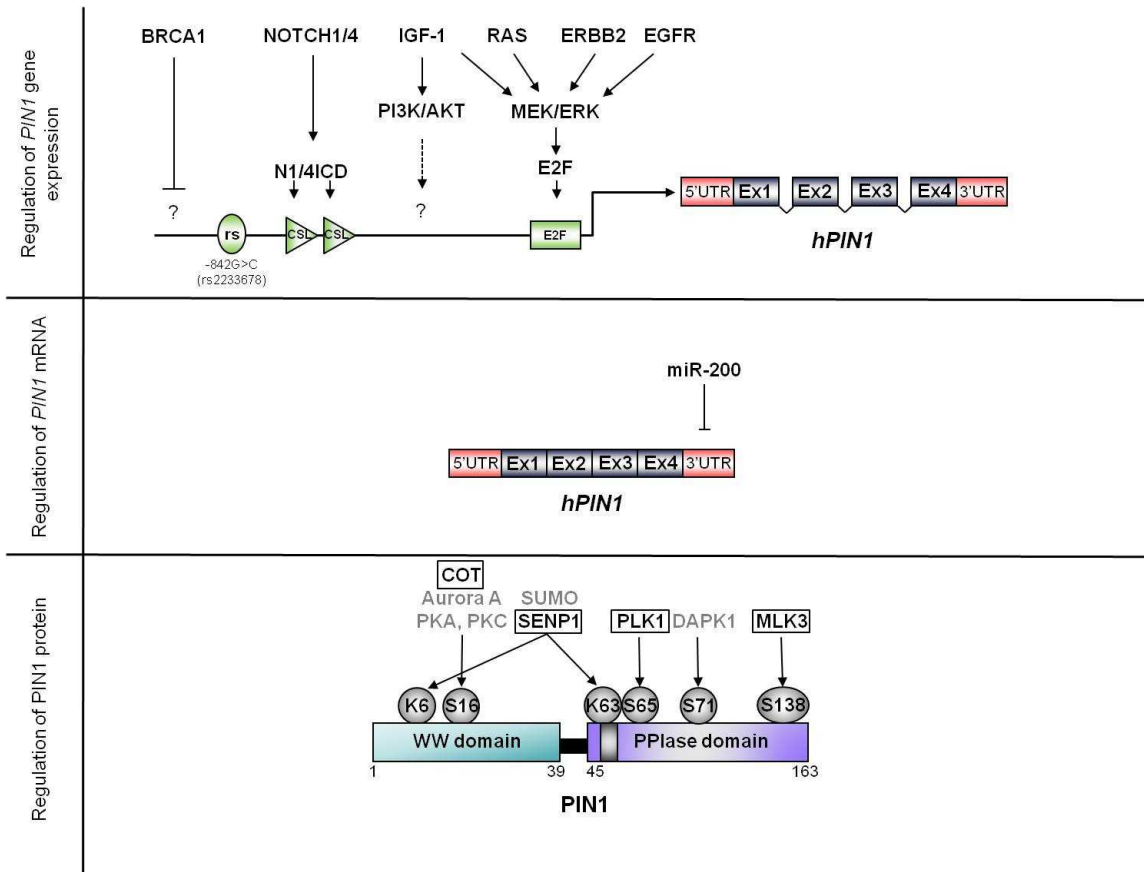
Figure 2. Regulation of PIN1 expression.

Upper part: Schematic representation of the human *PIN1* gene, encompassing the promoter sequence, the 5' and 3' untranslated regions (UTRs), and exons 1-4 (Ex). Known *cis*-elements and the upstream signals and *trans*-acting factors are indicated; CSL NOTCH-responsive element. Middle part: Scheme of the mature *PIN1* mRNA and its targeting by micro-RNA. Lower part: Schematic of the PIN1 protein structure with the sites of regulatory post-translational modifications and the responsible enzymes. The nuclear localization signal is depicted as a small gray box within the PPIase domain. Modified aminoacid residues of PIN1 are indicated with a circle, enzymes acting on the specific residue with activating or repressing function on PIN1 are indicated in black boxed or in gray letters, respectively[16].
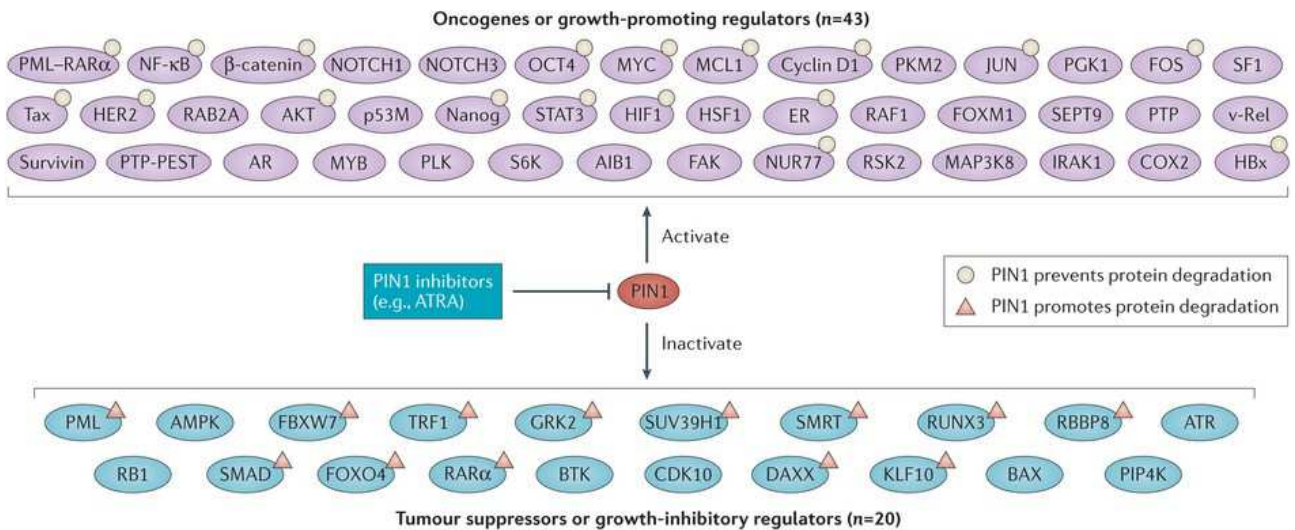
Figure 3. PIN1 sustains the activity of numerous oncogenes and inactivates tumor suppressor.

PIN1 activates more that 40 oncogenic molecules and inactivates at least 20 tumor suppressors. PIN1 inhibitors have the unique and promising property of restoring the correct balance between oncogenes and tumor suppressors[9].
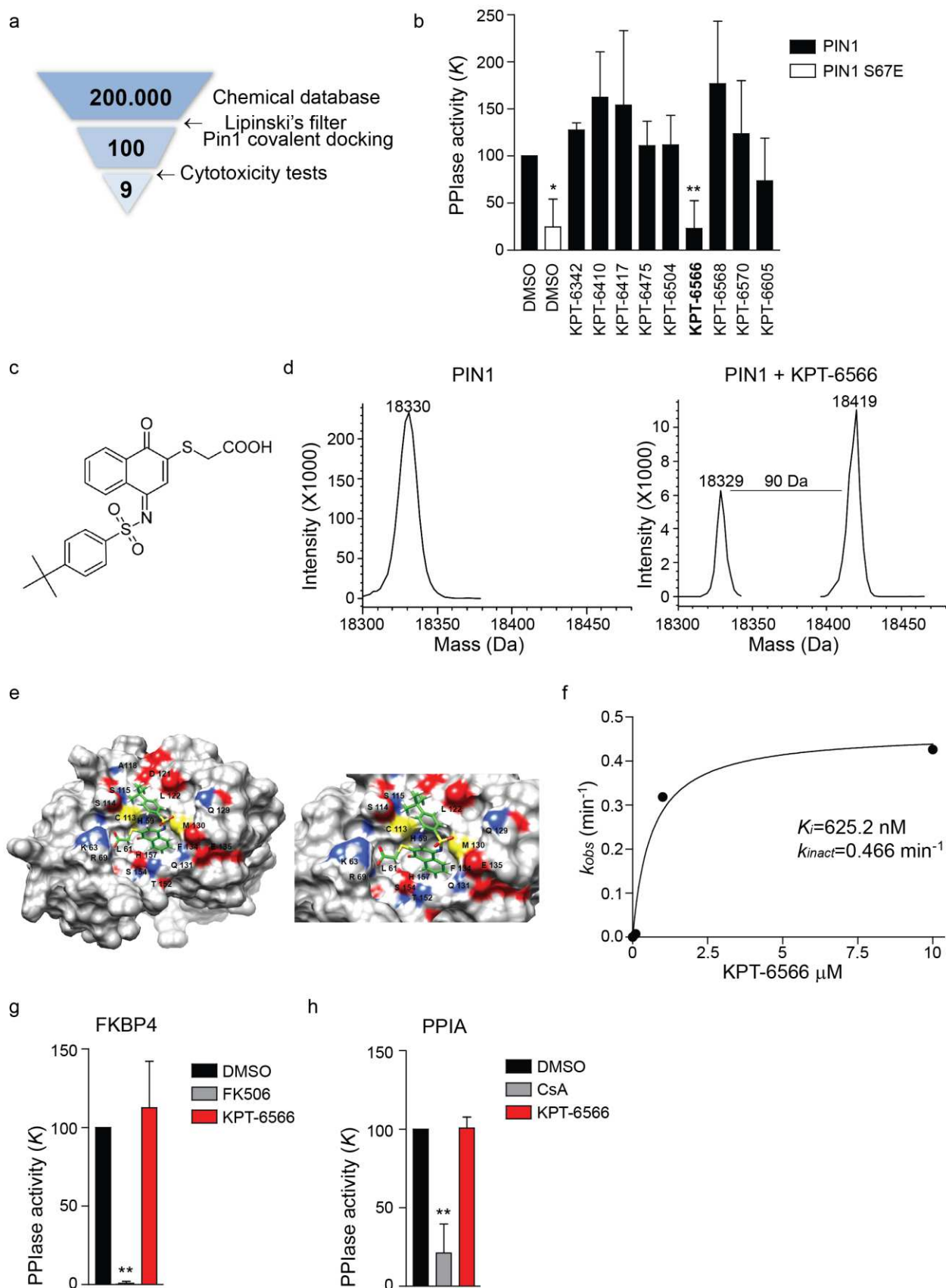
Figure 4. KPT-6566 specifically inactivates PIN1 PPIase activity *in vitro*

(**a**) Scheme representing the screening conducted with the drug like collection, indicating the stepwise approach that ends up with 9 potential covalent inhibitors of PIN1. (**b**) Bar plot indicating PPIase activity *K* of PIN1 (black), PIN1 S67E (white) and PIN1 with 30 μM of the indicated compounds. Positive hit is marked in bold. (**c**) Chemical structure

of KPT-6566 (**1**): the compound contains a polycyclic aromatic hydrocarbon bound to a sulfanyl-acetic acid group (-*S*-CH$_2$-COOH) and to a *tert*-butylphenyl group through a sulfonamide moiety (*N*-SO$_2$). (**d**) Mass spectrum deconvolution of DMSO (left) and KPT-6566 treated (right) PIN1. A molecular weight increase of 90 Da can be appreciated in the compound treated sample. (**e**) 3D image showing the docking of KPT-6566 in the catalytic pocket of PIN1. KPT-6566 is shown in green licorice representation. The surface of PIN1 is shown as solid representation and colored by heteroatom. The binding cavity is magnified in the right insert. (**f**) Plot of the observed rate constants for inhibition (k_{obs}) against inhibitor concentration of KPT-6566 from which estimations of kinetic parameters for covalent inhibition of PIN1 *in vitro* were made. The corresponding k_{inact} and K_i values are reported. (**g**) Bar plot indicating PPIase activity of GST-FKBP4 incubated with DMSO, 30 μM FK506 or 30 μM KPT-6566. (**h**) Same as in **g** for GST-PPIA incubated with DMSO, 30 μM Cyclosporin A or 30 μM KPT-6566. Data shown in **b**, **g**, **h**, are the means ± s.d. of n=3 independent experiments, *P<0.05, **P<0.01; two-tailed Student's *t*-test.

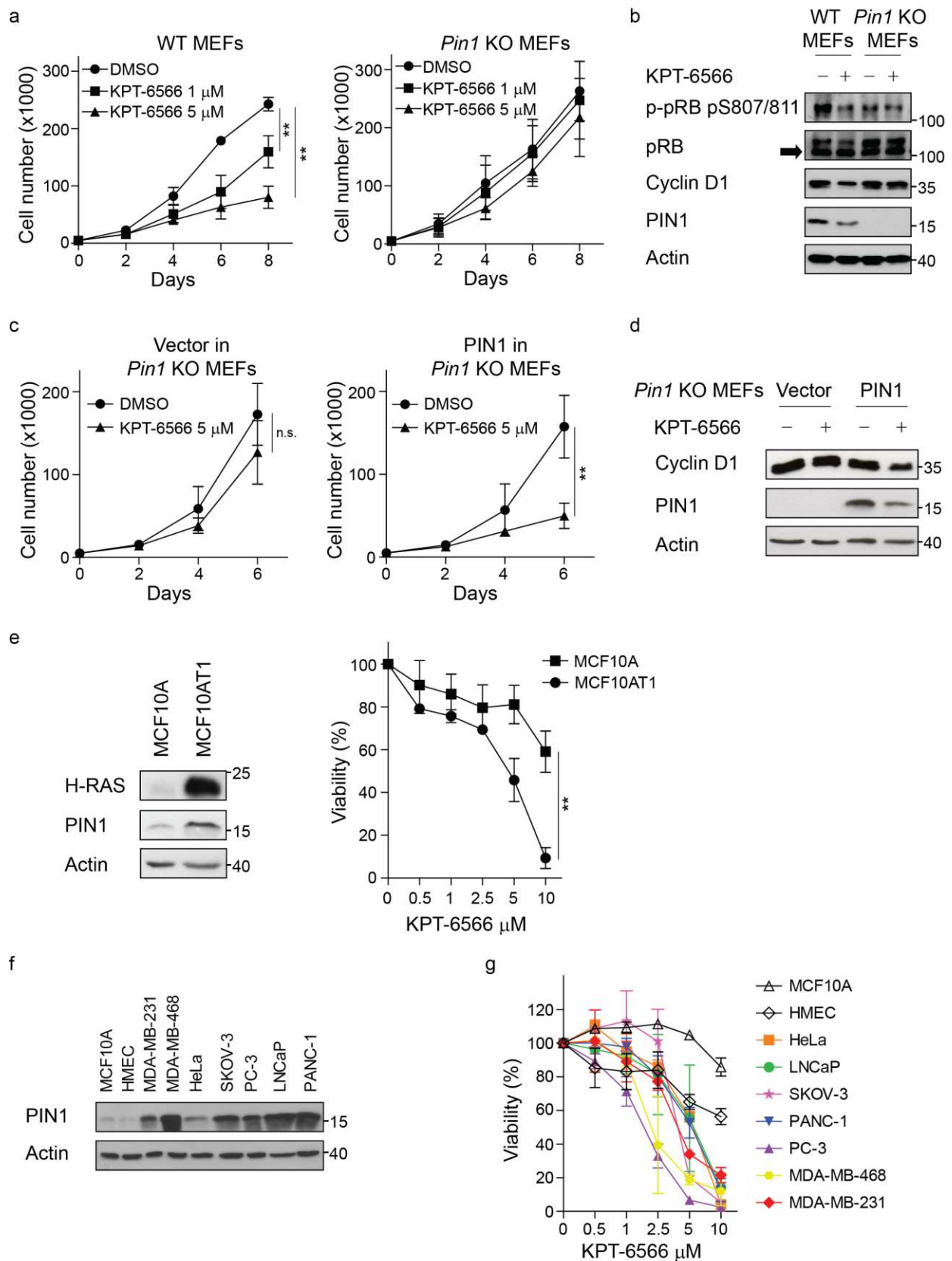**Figure 5. KPT-6566 impacts on cell proliferation and viability in a PIN1-dependent manner**

(**a**) Growth curves of WT (left) or *Pin1* KO (right) MEFs treated with the indicated concentrations of KPT-6566 or DMSO. (**b**) Immunoblotting of the indicated cell cycle-related proteins in WT or *Pin1* KO MEFs treated with 5 μM KPT-6566 (+) or DMSO (-) for 48hrs. (**c**) Growth curves in *Pin1* KO MEFs (left) or *Pin1* KO MEFs reconstituted with

HA-PIN1 (right) treated with KPT-6566 or DMSO. (**d**) Immunoblotting of the indicated proteins in *Pin1* KO MEFs or *Pin1* KO MEFs reconstituted with HA-PIN1 treated with 5 μM KPT-6566 (+) or DMSO (-) for 48hrs. (**e**) Left, immunoblotting of the indicated proteins in cell lysates from MCF10A and MCF10AT1 cells. Right, cell viability (WST) assay of MCF10A and MCF10AT1 treated with the indicated concentrations of KPT-6566 for 48hrs. (**f**) Immunoblotting of PIN1 in normal breast epithelial cells (MCF10A, HMEC) and in the indicated cancer cell lines. (**g**) Cell viability (ATPlite) assay of the same cell lines as in **f** treated with the indicated concentrations of KPT-6566 for 48hrs. **b**, **d-f** actin levels are reported as loading control; size markers are indicated. Data shown in **a**, **c**, **e**, **g** are the means ± s.d. of n=3 independent experiments, ** *P*<0.01, n.s. not significant; two-tailed Student's *t*-test.
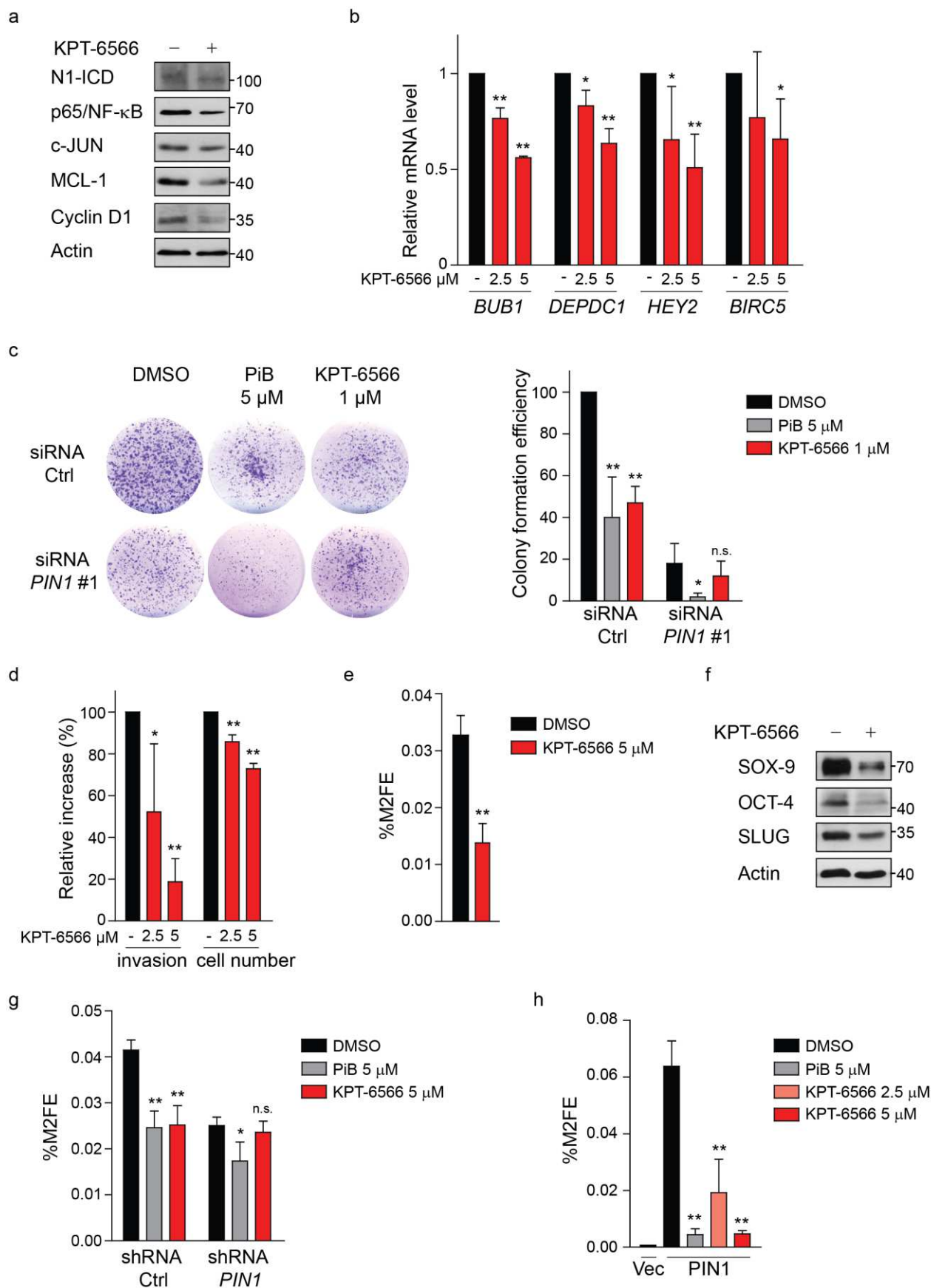
Figure 6. KPT-6566 interferes with PIN1 oncogenic functions

(**a**) Immunoblotting of PIN1 client proteins expressed in MDA-MB-231 breast cancer cells treated with 5 μM KPT-6566 (+) or DMSO (-) for 48hrs. (**b**) Quantitative RT-PCR analysis of mut-p53 and NOTCH1 target genes (*BUB1*,

DEPDC1 and *HEY2*, *BIRC5*, respectively) in MDA-MB-231 cells treated with indicated concentrations of KPT-6566 or DMSO (-) for 48hrs. (**c**) Left, representative pictures of MDA-MB-231 colonies in the indicated experimental conditions. Right, histogram showing colony formation efficiency of MDA-MB-231 cells in the indicated experimental conditions. Cells were transfected with control siRNA (siRNA Ctrl) or with *PIN1* siRNA#1. After 24hrs cells were trypsinized, plated for colony forming assay and treated with 5 μM PiB, 1 μM KPT-6566 or DMSO every two days. Colonies ≥ 50 pixels were counted 10 days after seeding using ImageJ software. (**d**) Histogram showing invasive ability and proliferation (cell number) of MDA-MB-231 breast cancer cells plated in Matrigel-coated Boyden chambers in the indicated experimental conditions for 20hrs. (**e**) Histogram showing percentage of secondary mammosphere formation efficiency (%M2FE) of MDA-MB-231 cells in the indicated experimental conditions. (**f**) Immunoblotting of the indicated proteins expressed in MDA-MB-231 breast cancer cells treated with 5 μM KPT-6566 (+) or DMSO (-) for 48hrs. (**g**) %M2FE of MCF10AT1 cells with stable control- (shRNA Ctrl) or *PIN1* silencing (shRNA *PIN1*), treated as indicated. (**h**) %M2FE of MCF10A cells transduced with empty- (Vec) or HA-PIN1-expressing vectors (PIN1), treated as indicated. **a**, **f**, actin levels are reported as loading control; size markers are indicated. Data shown in **b**-**e**, **g**, **h** are the means ± s.d. of n=3 independent experiments, * $P<0.05$, ** $P<0.01$, n.s. not significant; two-tailed Student's *t*-test.
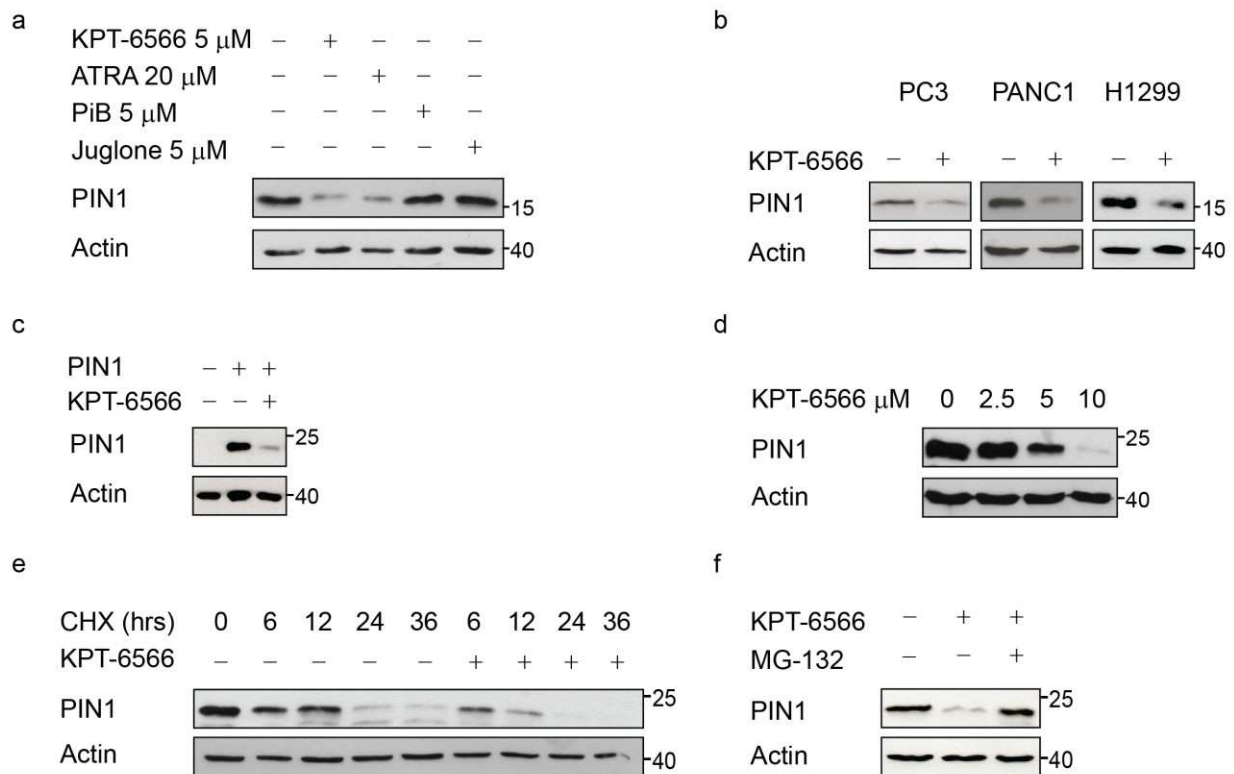
Figure 7. Interaction of KPT-6566 with PIN1 promotes its structural change and degradation

Immunoblotting of the indicated proteins in cell lysates from (**a**) MDA-MB-231 cells treated with the indicated compounds (+) or DMSO (-) for 48hrs; (**b**) PC3, PANC1, H1299 cells treated with 5 μM KPT-6566 (+) or DMSO (-) for 48hrs; (**c**) *PIN1* KO MDA-MB-231 cells transduced with empty (-) or PIN1 vectors (+) treated with 5 μM KPT-6566 (+) or DMSO (-) for 48hrs; (**d**) *PIN1* KO MDA-MB-231 cells reconstituted with HA-PIN1, treated with increasing amounts of KPT-6566 or DMSO; (**e**) *PIN1* KO MDA-MB-231 cells reconstituted with HA-PIN1, treated with 5 μM KPT-6566 (+) or DMSO (-) followed by cycloheximide (CHX) chase for the indicated hours; (**f**) *PIN1* KO MDA-MB-231 cells reconstituted with HA-PIN1, treated with 5 μM KPT-6566 (+), 10 μM MG132 (+) or DMSO (-) for 16hrs. **a-f** actin levels are reported as loading control; size markers are indicated.
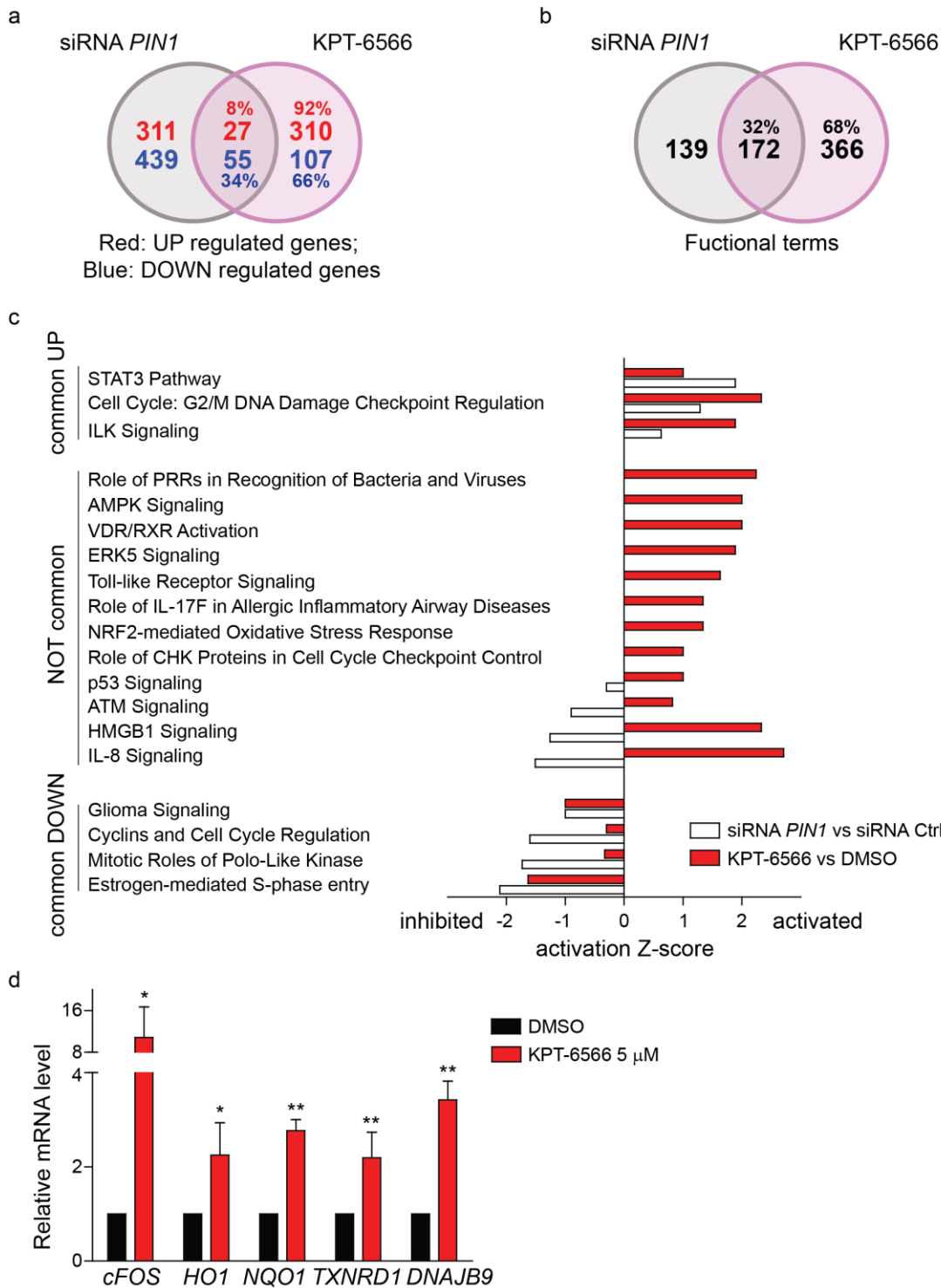
Figure 8. Global transcriptional effects of KPT-6566

(**a**) Venn diagram of the Illumina microarray analysis with common and differentially up- and down-regulated genes of MDA-MB-231 cells treated with siRNA *PIN1*#1 *vs.* KPT-6566, using a cut-off of 0.75 logFC and p-value ≤ 0.05. (**b**) Venn diagram of the Gene Ontology (GO) analysis with common and differential enrichment for functional terms of MDA-MB-231 cells treated with siRNA *PIN1 vs.* KPT-6566. (**c**) Histogram indicating comparison of IPA analysis of genes regulated by *PIN1* siRNA (white) or KPT-6566 (red) in function of their activation z-scores. (**d**) Quantitative RT-PCR analysis of NRF2 pathway members in MDA-MB-231 cells treated with the indicated compounds for 48hrs. Data are indicated as means ± s.d. of n=3 independent experiments, * *P<0.05*, ** *P<0.01*; two-tailed Student's *t*-test.
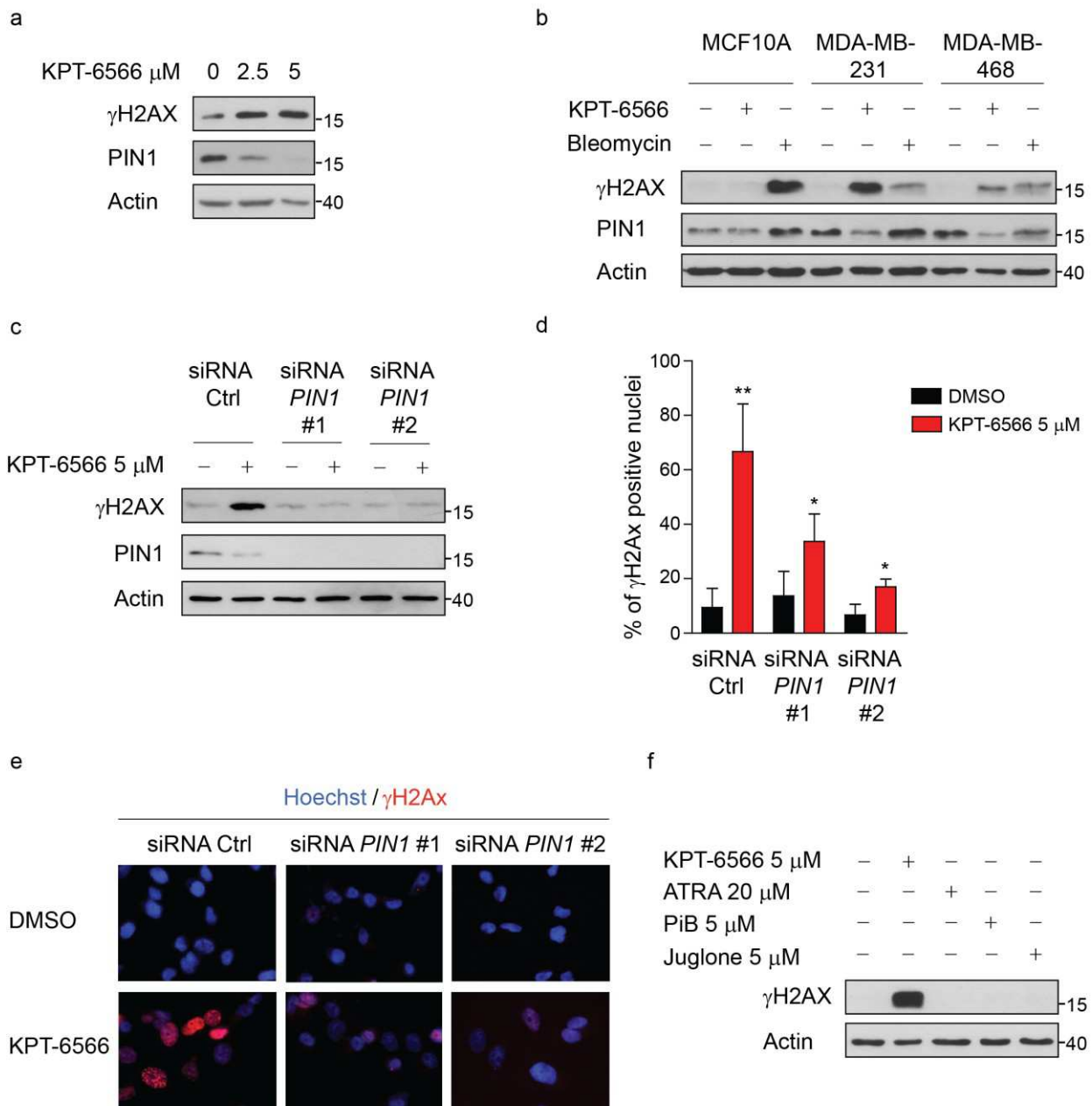
Figure 9. KPT-6566 induces DNA damage in a PIN1-dependent manner

Immunoblotting of the indicated proteins from (**a**) MDA-MB-231 cells treated with increasing amounts of KPT-6566 or DMSO for 48hrs; (**b**) MCF10A, MDA-MB-231 and MDA-MB-468 cells treated with 5 μM KPT-6566 (+), 10 μM Bleomycin (+) or DMSO (-) for 48hrs; (**c**) MDA-MB-231 cells transfected with control- (siRNA Ctrl) or two different *PIN1* siRNAs (siRNA *PIN1#1* and *PIN1#2*) and treated as indicated for 24 hours. (**d**) Histogram representing the percentage of γH2AX positive nuclei of MDA-MB-231 cells treated as in **c**. (**e**) Representative fluorescence microscope images of γH2AX (red) immunofluorescence and Hoechst (blue) staining of cells from **d**. (**f**) Immunoblotting of the indicated proteins from MDA-MB-231 cells treated with the indicated compounds (+) or DMSO (-) for 48hrs. **a-c**, **f** actin levels are reported as loading control; size markers are indicated. Data shown in **d** are the means ± s.d. of n=3 independent experiments, * $P<0.05$, ** $P<0.01$; two-tailed Student's *t*-test.
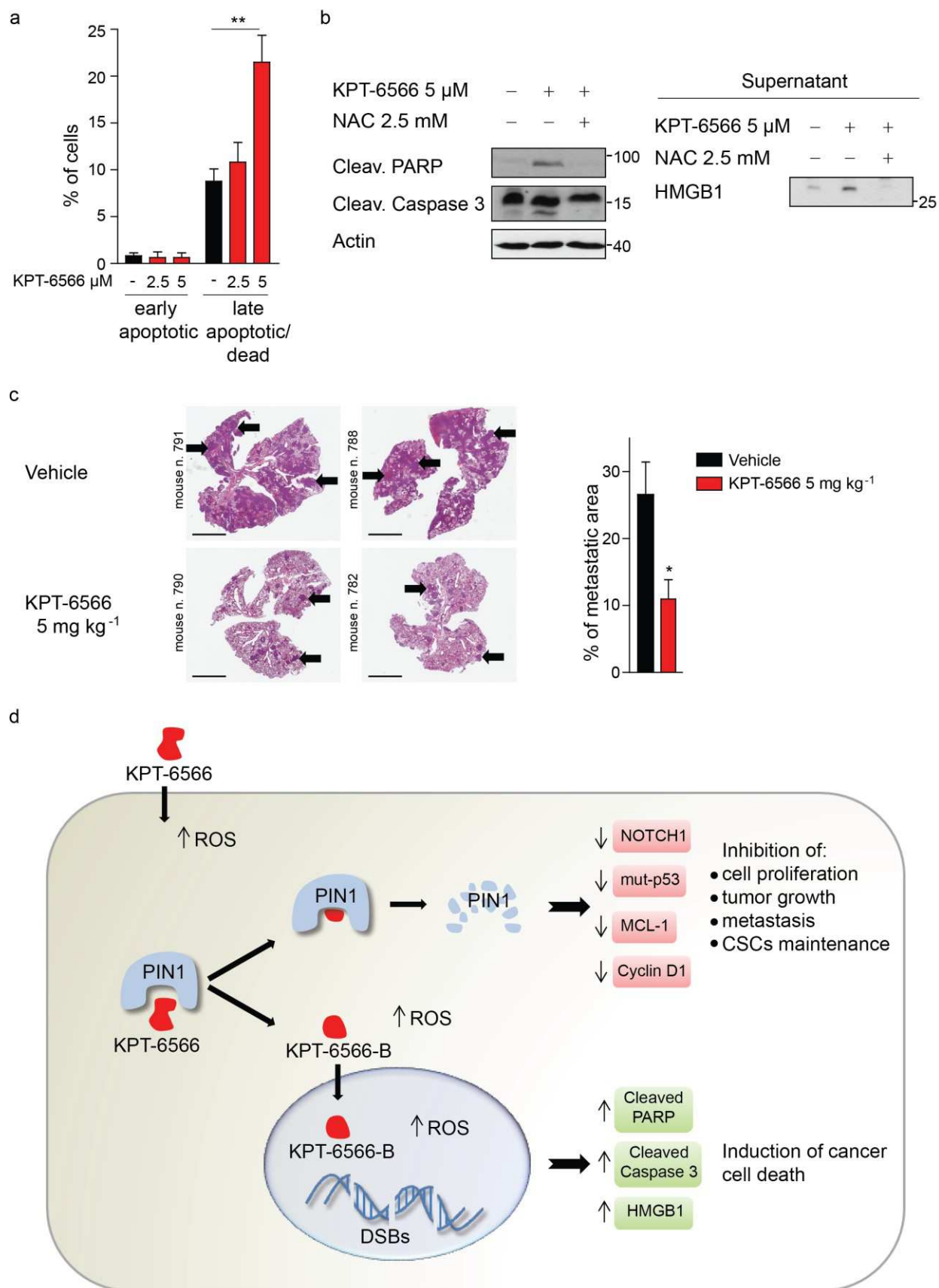
Figure 10. KPT-6566 induces cell death of cancer cells and reduces metastasis growth *in vivo*

(**a**) Histogram representing respectively the percentage of early apoptotic and late apoptotic/dead MDA-MB-231 cells in the indicated experimental conditions. Results are indicated as means ± s.d. of n=3 independent experiments, **
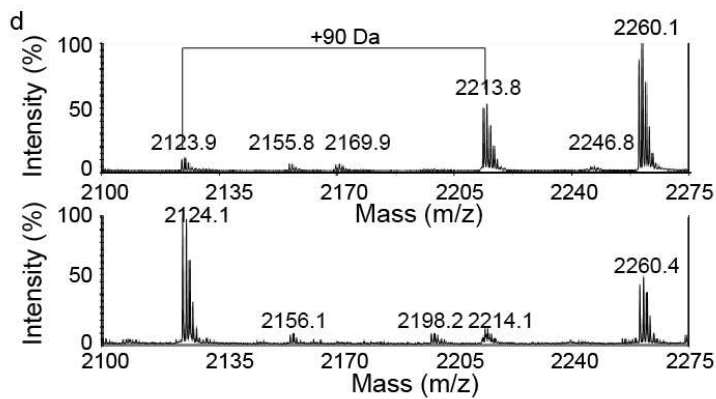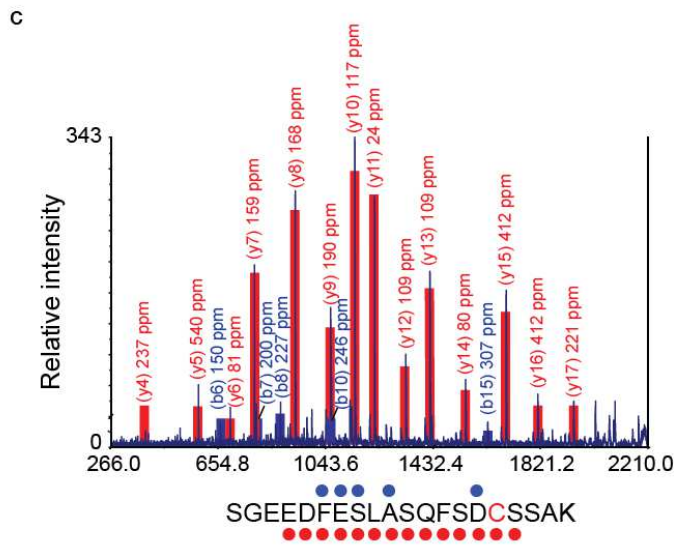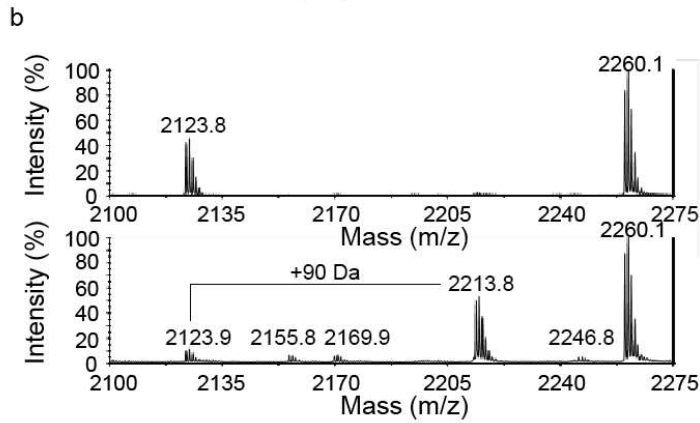
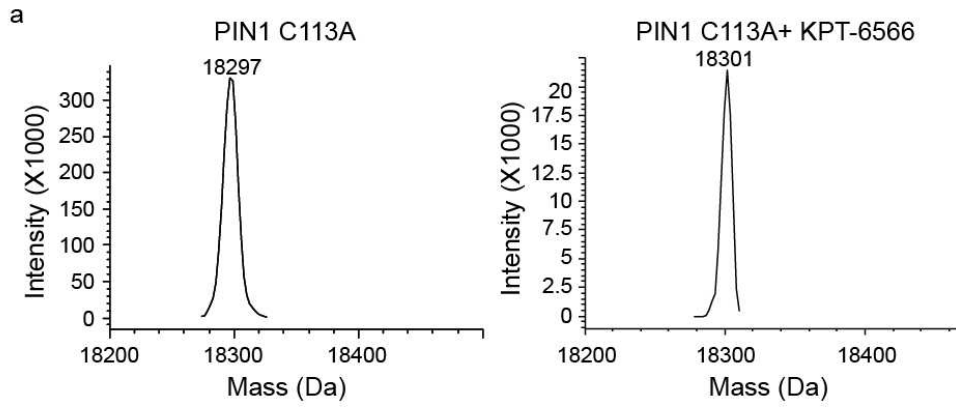*P*<0.01; two-tailed Student's *t*-test. (**b**) Left, immunoblotting of the indicated proteins of MDA-MB-231 cell lysates untreated (-) or treated (+) with the indicated compounds. Right, immunoblotting of HMGB1 from supernatant of the same cells as in the left panel; actin levels are reported as loading control; size markers are indicated. (**c**) Left, hematoxylin and eosin staining of representative sections of entire pulmonary lobes from mice inoculated with MDA-MB-231 cells and treated with vehicle (n=8) or KPT-6566 (n=7); arrows indicate representative metastases. Scale bar 3 mm. Right, computer-aided assessment of percentage of lung tissue area occupied by metastases in the indicated conditions. Data are reported in histograms as means ± s.e.m; * *P*<0.05; two-tailed Mann-Whitney test. (**d**) Proposed model of KPT-6566 mechanism of action. After entering the cell, KPT-6566 binds to PIN1 and elicits a cytostatic effect associated to covalent inhibition and degradation of PIN1 with consequent decrease of oncogenic circuitries (upper part). In addition, KPT-6566 might induce intracellular ROS production. After reaction with PIN1, KPT-6566 has a simultaneous cytotoxic effect releasing KPT-6566-B, which generates further ROS, induces DNA damage and cancer cell death (lower part).
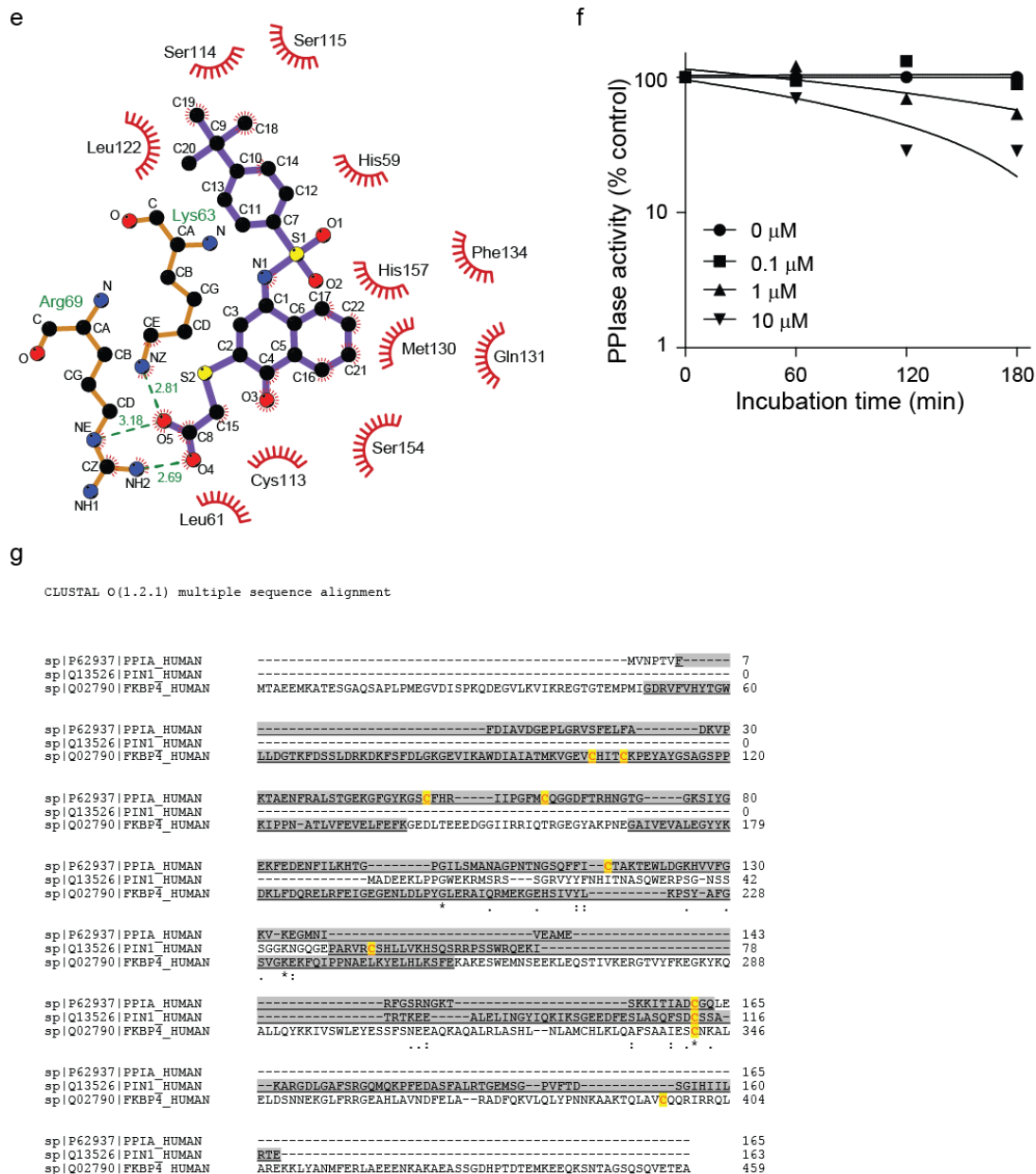
Inhibitor	Mechanism of action Potency	Known targets
Juglone	• Competitive irreversible inhibitor • Low µM range	PIN1 BUB1R Tubulin
PiB	• Competitive reversible inhibitor • Low µM range	PIN1 PAR14
***cis*-locked Alkene peptidomimetics**	• Competitive reversible inhibitors • Low µM range	PIN1
D-peptide inhibitors	• Competitive reversible inhibitors • Low nM range	PIN1
DTM	• Competitive inhibitor • Low µM range	PIN1
ECGC	• Competitive and reversible inhibitor • Low µM range	PIN1 FAS proteasome
ATRA	• Competitive and reversible inhibitor • Low µM range	PIN1 RAR

**Table 1. Major examples of PIN1 inhibitors**[9,16]

Supplementary Materials

Supplementary Figures

a

PIN1 C113A

18297

PIN1 C113A+ KPT-6566

18301

b

2123.8

2260.1

+90 Da

2123.9 2155.8 2169.9   2213.8   2246.8   2260.1

c

(y4) 237 ppm
(y5) 540 ppm
(b6) 150 ppm
(y6) 81 ppm
(b7) 200 ppm
(b8) 227 ppm
(y7) 159 ppm
(y8) 168 ppm
(y9) 190 ppm
(b10) 246 ppm
(y9) 109 ppm
(y10) 117 ppm
(y11) 24 ppm
(y12) 109 ppm
(y13) 109 ppm
(y14) 80 ppm
(b15) 307 ppm
(y15) 412 ppm
(y16) 412 ppm
(y17) 221 ppm

SGEEDFESLASQFSDCSSAK

d

+90 Da

2123.9   2155.8 2169.9   2213.8   2246.8   2260.1

2124.1

2156.1   2198.2 2214.1   2260.4

67

e

Ser114 Ser115

Leu122

C19
C9 C18
C20
C10 C14
C13
C11 C12
C Lys63 C7 O1
O CA N S1
CB N1
CG C1 C17 O2
Arg69 C3 C6 C22
N C CE CD C2 C5
CA NZ C4 C16 C21
O CB S2
CG 2.81
CD O5 C15
NE 3.18 C8
CZ O4
NH2 2.69
NH1

His59
His157 Phe134
Met130 Gln131
Ser154
Cys113
Leu61

f

Semi-logarithmic plot, PPIase activity (% control) vs Incubation time (min)
- 0 µM
- 0.1 µM
- 1 µM
- 10 µM

g

CLUSTAL O(1.2.1) multiple sequence alignment

```
sp|P62937|PPIA_HUMAN    ------------------------------------------------MVNPTVF------  7
sp|Q13526|PIN1_HUMAN    ------------------------------------------------------------  0
sp|Q02790|FKBP4_HUMAN   MTAEEMKATESGAQSAPLPMEGVDISPKQDEGVLKVIKREGTGTEMPMIGDRVFVHYTGW  60

sp|P62937|PPIA_HUMAN    ----------------------------FDIAVDGEPLGRVSFELFA--------DKVP  30
sp|Q13526|PIN1_HUMAN    ------------------------------------------------------------  0
sp|Q02790|FKBP4_HUMAN   LLDGTKFDSSLDRKDKFSFDLGKGEVIKAWDIAIATMKVGEVCHITCKPEYAYGSAGSPP  120

sp|P62937|PPIA_HUMAN    KTAENFRALSTGEKGFGYKGSCFHR-----IIPGFMCQGGDFTRHNGTG-----GKSIYG  80
sp|Q13526|PIN1_HUMAN    ------------------------------------------------------------  0
sp|Q02790|FKBP4_HUMAN   KIPPN-ATLVFEVELFEFKGEDLTEEEDGGIIRRIQTRGEGYAKPNEGAIVEVALEGYYK  179

sp|P62937|PPIA_HUMAN    EKFEDENFILKHTG---------PGILSMANAGPNTNGSQFFI--CTAKTEWLDGKHVVFG  130
sp|Q13526|PIN1_HUMAN    --------------MADEEKLPPGWEKRMSRS---SGRVYYFNHITNASQWERPSG-NSS  42
sp|Q02790|FKBP4_HUMAN   DKLFDQRELRFEIGEGENLDLPYGLERAIQRMEKGEHSIVYL----------KPSY-AFG  228
                                      *    .   .  ::      .   .  .

sp|P62937|PPIA_HUMAN    KV-KEGMNI------------------------VEAME-----------------  143
sp|Q13526|PIN1_HUMAN    SGGKNGQGEPARVRCSHLLVKHSQSRRPSSWRQEKI------------------  78
sp|Q02790|FKBP4_HUMAN   SVGKEKFQIPPNAELKYELHLKSFEKAKESWEMNSEEKLEQSTIVKERGTVYFKEGKYKQ  288
                          .  *:

sp|P62937|PPIA_HUMAN    ----------------RFGSRNGKT-----------------SKKITIADCGQLE  165
sp|Q13526|PIN1_HUMAN    ----------------TRTKEE-----ALELINGYIQKIKSGEEDFESLASQFSDCSSA-  116
sp|Q02790|FKBP4_HUMAN   ALLQYKKIVSWLEYESSFSNEEAQKAQALRLASHL--NLAMCHLKLQAFSAAIESCNKAL  346
                                        ..:                :   : .*  .

sp|P62937|PPIA_HUMAN    ------------------------------------------------------  165
sp|Q13526|PIN1_HUMAN    --KARGDLGAFSRGQMQKPFEDASFALRTGEMSG--PVFTD------------SGIHIIL  160
sp|Q02790|FKBP4_HUMAN   ELDSNNEKGLFRRGEAHLAVNDFELA--RADFQKVLQLYPNNKAAKTQLAVCQQRIRRQL  404

sp|P62937|PPIA_HUMAN    ------------------------------------------------------  165
sp|Q13526|PIN1_HUMAN    RTE---------------------------------------------------  163
sp|Q02790|FKBP4_HUMAN   AREKKLYANMFERLAEEENKAKAEASSGDHPTDTEMKEEQKSNTAGSQSQVETEA  459
```
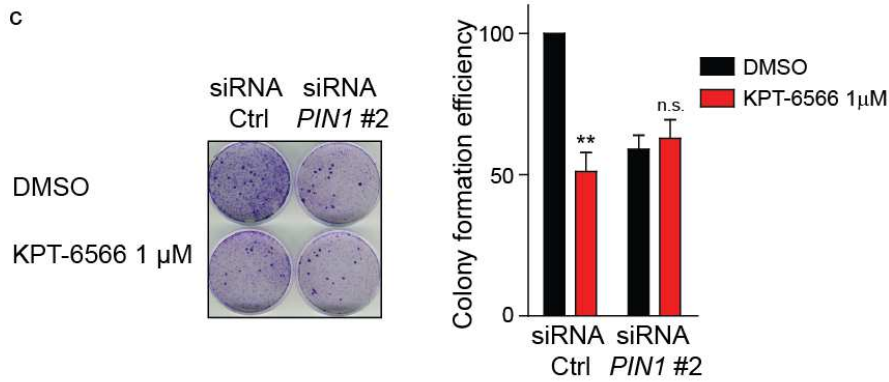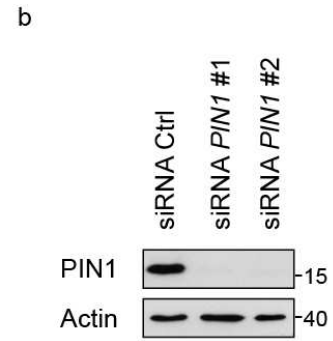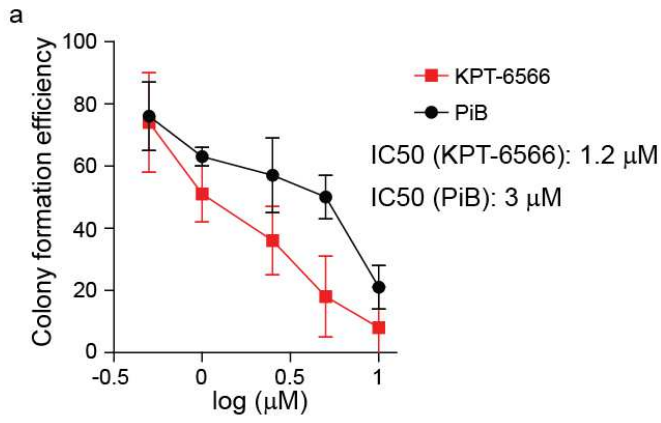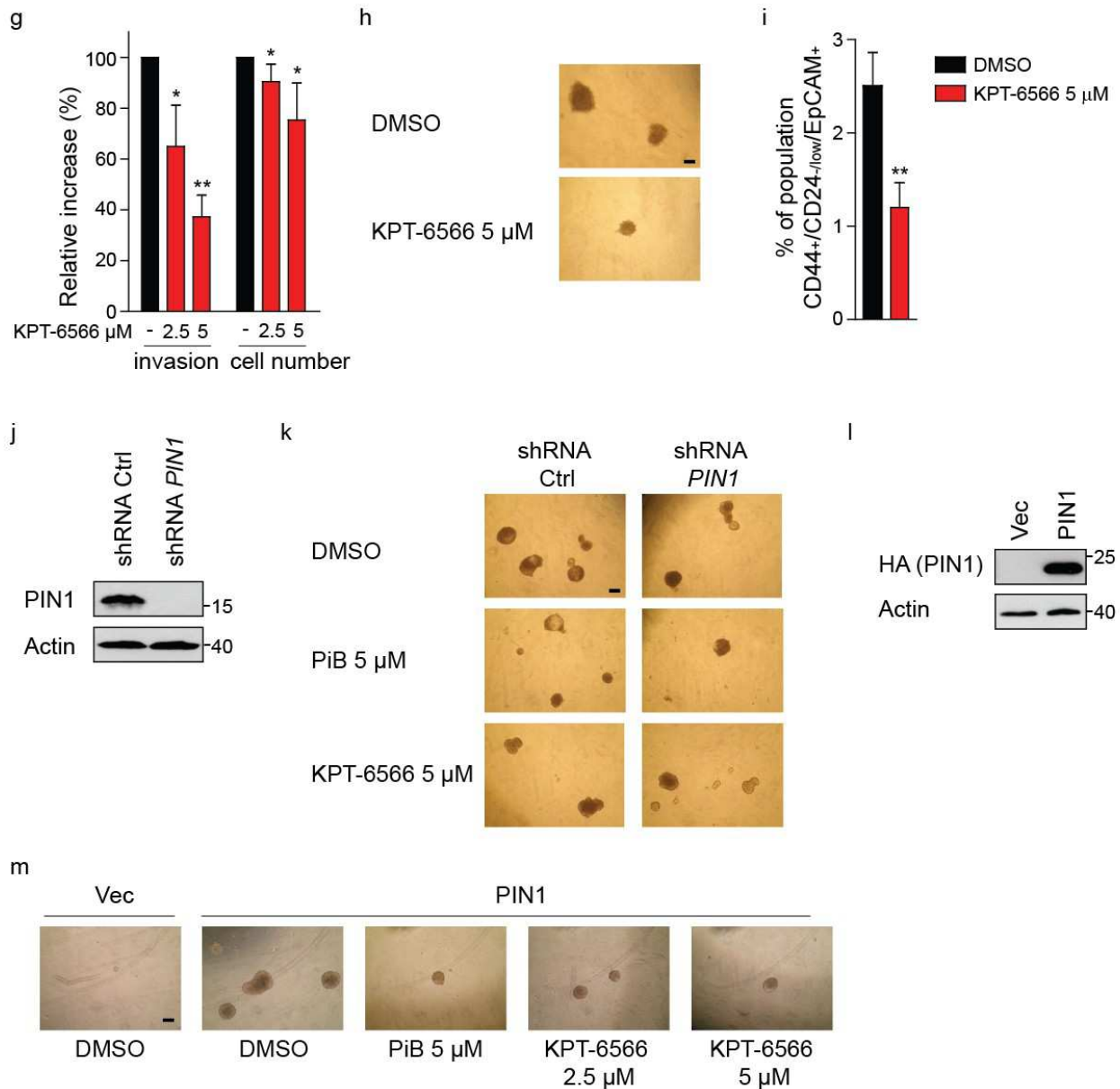
Supplementary Figure 1

(**a**) Mass spectrum deconvolution of DMSO treated (left) and KPT-6566 treated (right) PIN1 mutant C113A. (**b**) Mass spectra of trypsin digested DMSO (top) and KPT-6566 treated PIN1 (bottom) in the region 2100-2276 m/z. A clear shift of 90 Da was observed in the peptide 2123.9 Da corresponding to SGEEDFESLASQFSDCSSAK peptide and containing C113. (**c**) MS/MS spectrum of the 2213 m/z peak. Sequence is correctly assigned to the peptide SGEEDFESLASQFSDCSSAK bearing modified C113 (highlighted in red). Fragment ions containing the peptide C-terminus (y-type) or N-terminus (b-type), along with the associated mass errors are shown in red and blue, respectively. (**d**) Mass spectra of trypsin digested KPT-6566 (top) and KPT-6566 + DTT treated PIN1 (bottom) in the region 2100-2276 m/z. The 90 Da shift observed in the peptide 2123.9 Da upon KPT-6566 treatment (top) is absent in DTT co-treated sample (bottom). (**e**) 2D image showing hydrophobic contacts between KPT-6566 and PIN1. (**f**) Semi-logarithmic plot of PIN1 PPIase activity in presence of increasing concentrations of KPT-6566 at different incubation times, obtained in PPIase assays. Results are indicated as means of three independent experiments. (**g**) Protein sequence alignment obtained with CLUSTALW. PPIase domains are highlighted in grey. Cysteine residues (red) are highlighted in yellow.
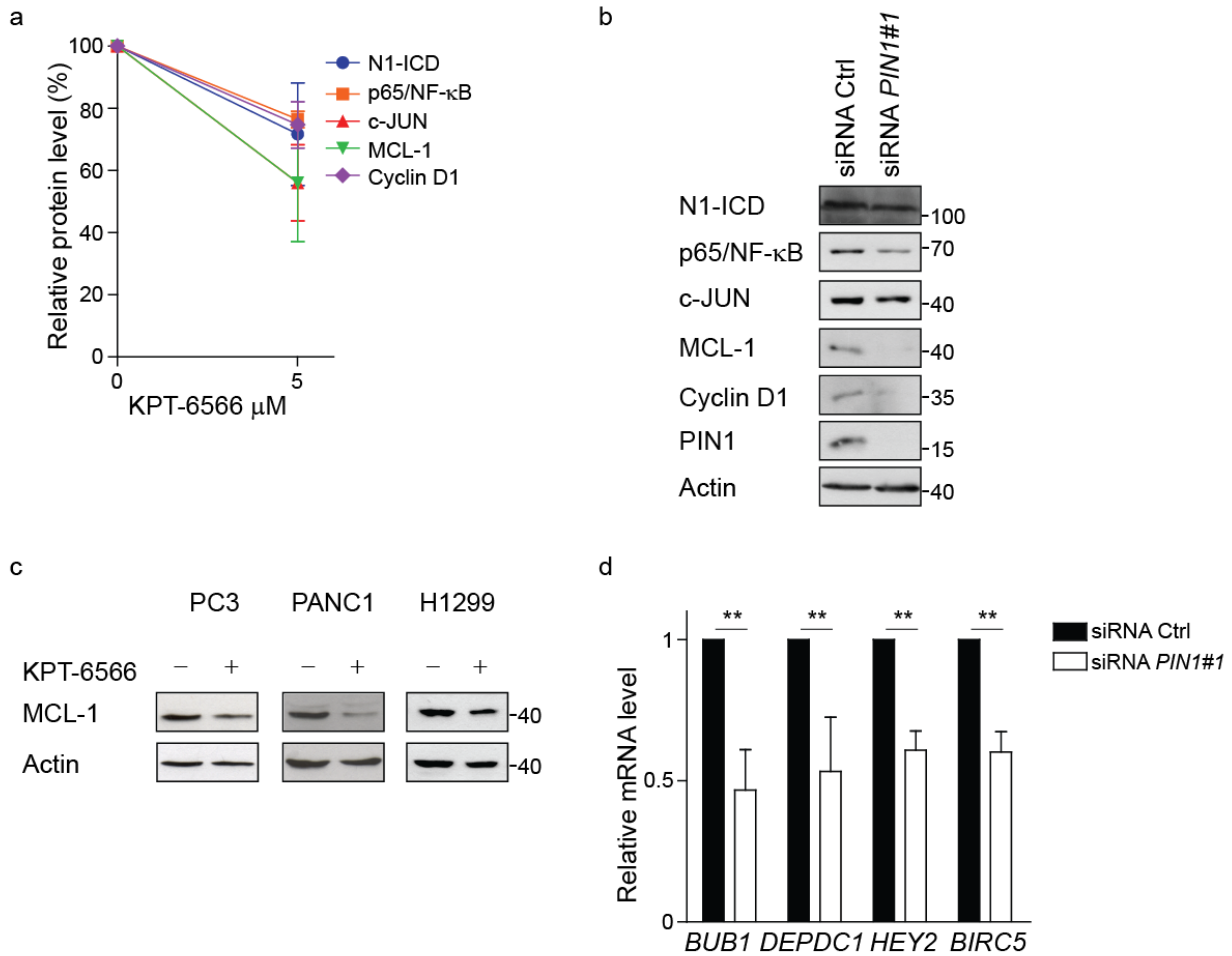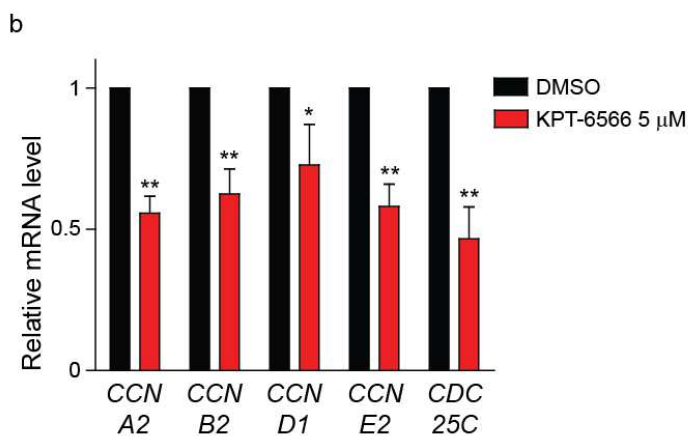
Supplementary Figure 2

(**a**) Graph showing protein quantification of immunoblotting of different PIN1 client proteins in MDA-MB-231 cells treated with KPT-6566 or DMSO for 48hrs. Quantification was obtained with ImageJ software. Protein levels were normalized to actin. (**b**) Immunoblotting of the indicated proteins from MDA-MB-231 cells transfected with control siRNA (siRNA Ctrl) o with *PIN1* siRNA (siRNA *PIN1#1*). (**c**) Immunoblotting of MCL-1 from PC3, PANC1, H1299 cells treated with 5 μM KPT-6566 (+) or DMSO (-) for 48hrs. (**d**) Quantitative RT-PCR analysis in control (siRNA Ctrl) or *PIN1* silenced (siRNA *PIN1#1*) MDA-MB-231 cells. **b**, **c** actin levels are reported as loading control; size markers are indicated. Data shown in **a** and **d** are the means ± s.d. of n=3 independent experiments, **$P<0.01$; two-tailed Student's *t*-test.
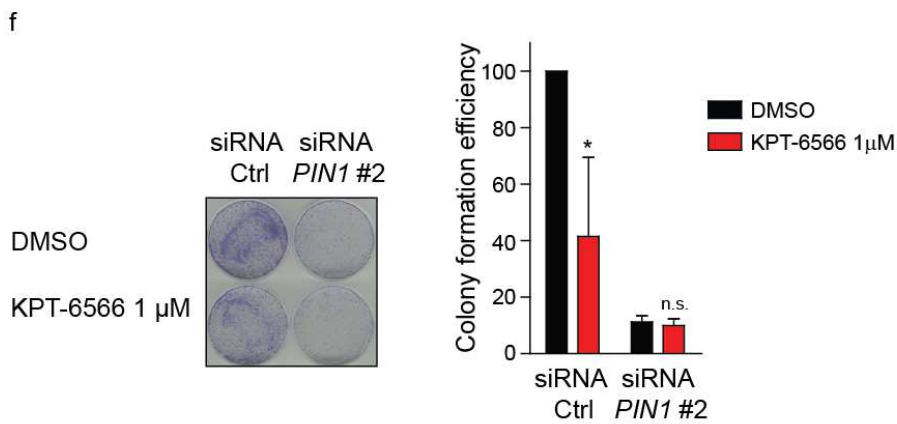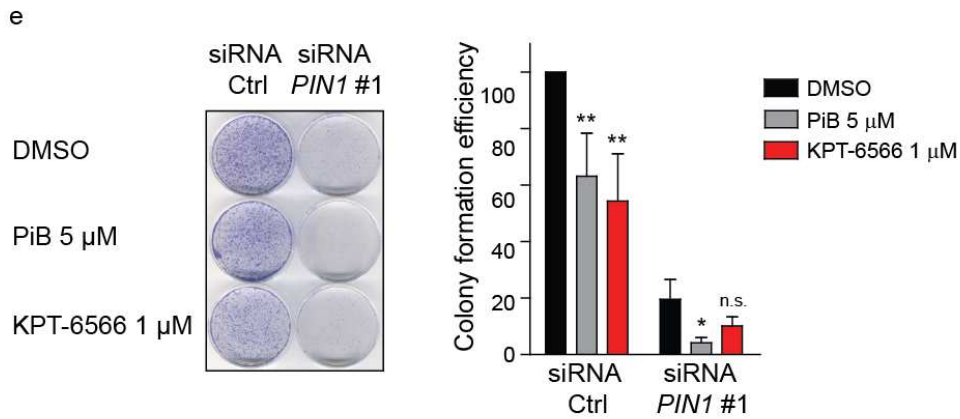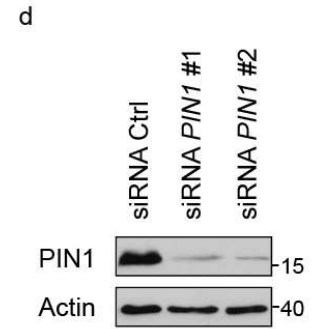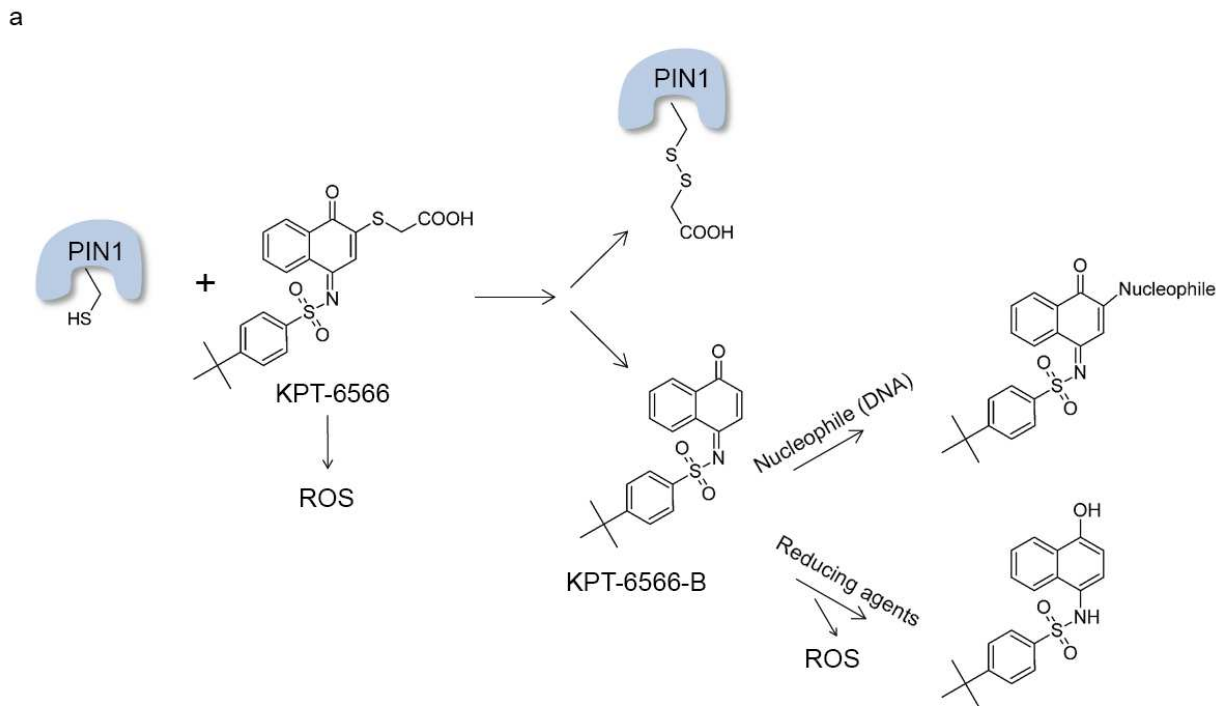
Supplementary Figure 3

(**a**) Graph showing colony formation efficiency of MDA-MB-231 cells treated with DMSO or increasing concentrations of PiB, KPT-6566. IC50 of both drugs are indicated. (**b**) Immunoblotting of the indicated proteins in cell lysates from MDA-MB-231 cells in the indicated experimental conditions. (**c**) Left, representative pictures of MDA-MB-231 colonies in the indicated experimental conditions. Right, histogram showing colony formation efficiency of MDA-MB-231 cells in the indicated experimental conditions. (**d**) Immunoblotting of the indicated proteins in cell lysates from PC3 in the indicated experimental conditions. (**e**), (**f**) as in **c** for PC3 cells. (**g**) Histogram showing invasive ability and proliferation (cell number) of PC3 cells plated in Matrigel-coated Boyden chambers in the indicated experimental conditions for 20hrs. (**h**) Representative images of secondary mammospheres obtained with MDA-MB-231 cells in the indicated experimental conditions. Scale bar (200 μm) is indicated. (**i**) Histogram showing percentage of CD44^{+}/CD24^{-/low}/EpCAM^{+} MDA-MB-231 cells in the indicated experimental conditions. (**j**) Immunoblotting of the indicated proteins from MCF10AT1 cells transduced with control- (shRNA Ctrl) or *PIN1* shRNA (shRNA *PIN1*) expressing vectors. (**k**) as in (**h**) for MCF10AT1 cells. (**l**) Immunoblotting of the indicated proteins from MCF10A cells transduced with empty- (Vec) or HA-PIN1 over-expressing vectors. (**m**) as in (**h**) for MCF10A cells. **b, d, j, l**, actin levels are reported

as loading control, size markers are indicated. Data shown in **a**, **c**, **e**, **f**, **g**, **i**, are the means ± s.d. of n=3 independent experiments, *$P<0.05$, **$P<0.01$, n.s. not significant; two-tailed Student's *t*-test.
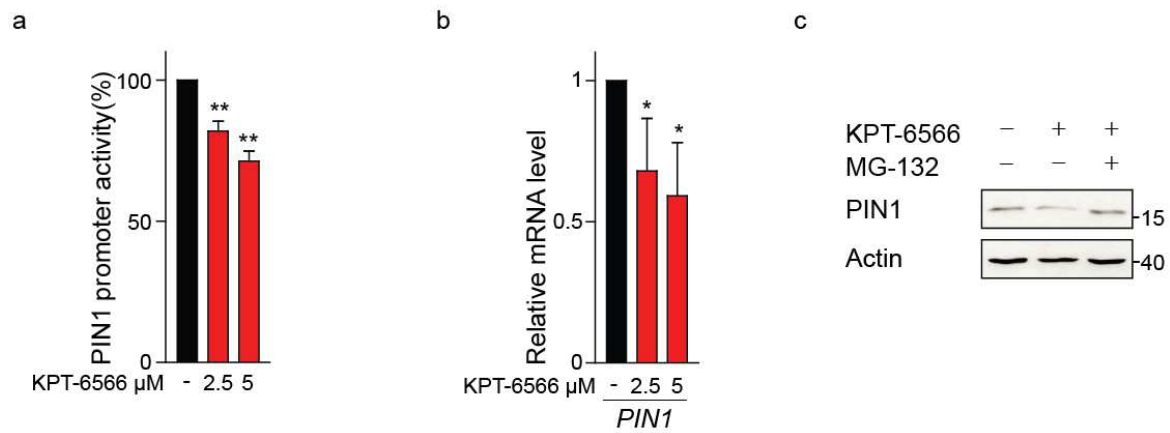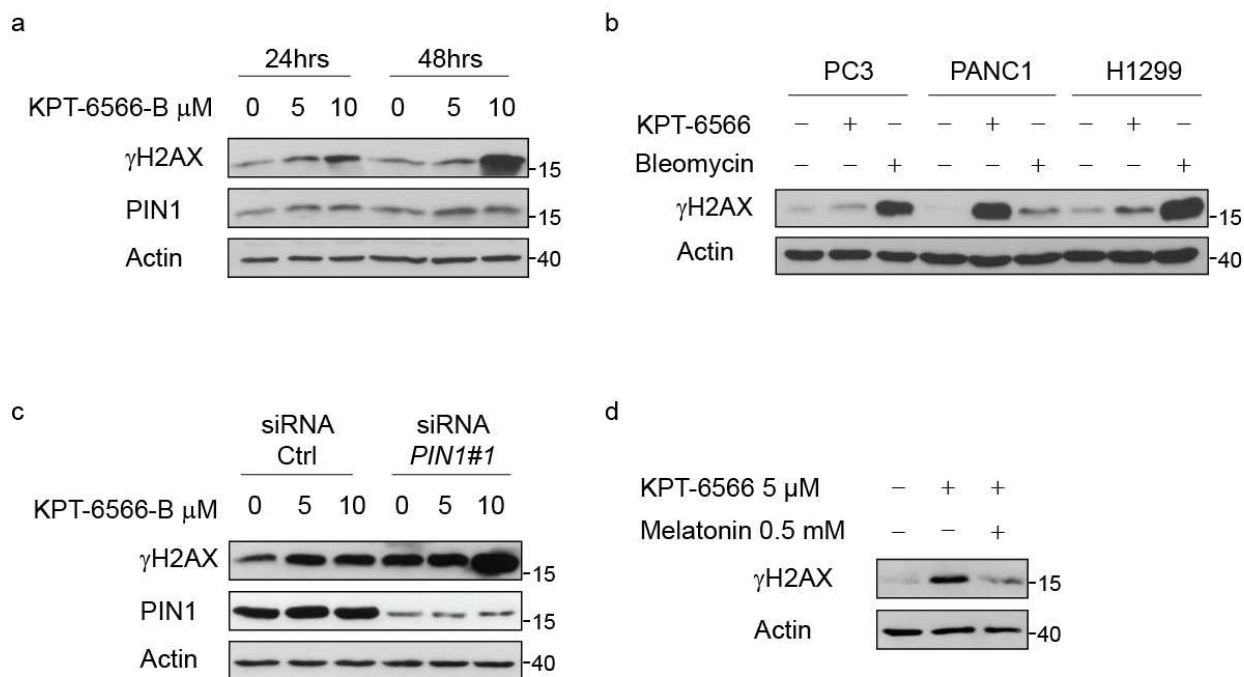
Supplementary Figure 4

(**a**) *PIN1* promoter activity in MDA-MB-231 cells treated with DMSO (-) or increasing concentrations of KPT-6566 for 48hrs. (**b**) Quantitative RT-PCR analysis in MDA-MB-231 cells treated with DMSO (-) or increasing concentrations of KPT-6566 for 48hrs. (**c**) Immunoblotting of the indicated proteins in cell lysates from MDA-MB-231 cells treated with 5 μM KPT-6566 (+), 10 μM MG132 (+) or DMSO (-) for 16hrs. Actin levels are reported as loading control, size markers are indicated. Data shown in **a**, **b** are the means ± s.d. of n=3 independent experiments, *$P<0.05$, **$P<0.01$; two-tailed Student's *t*-test.
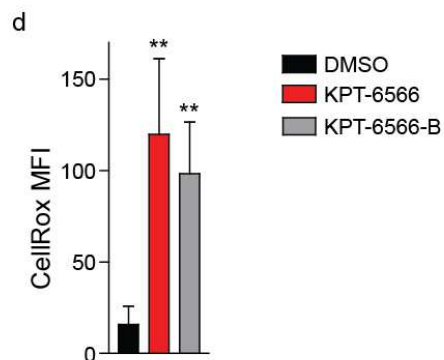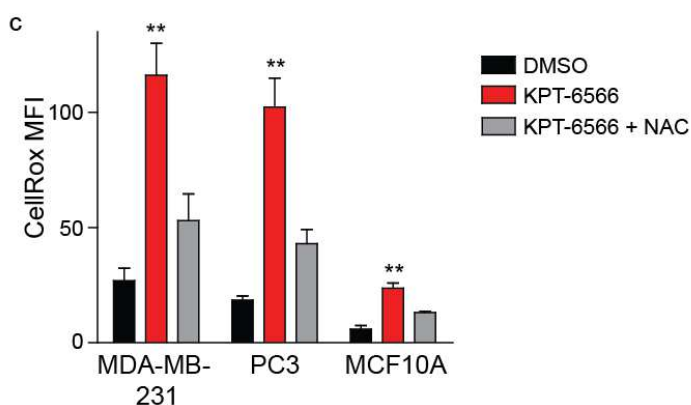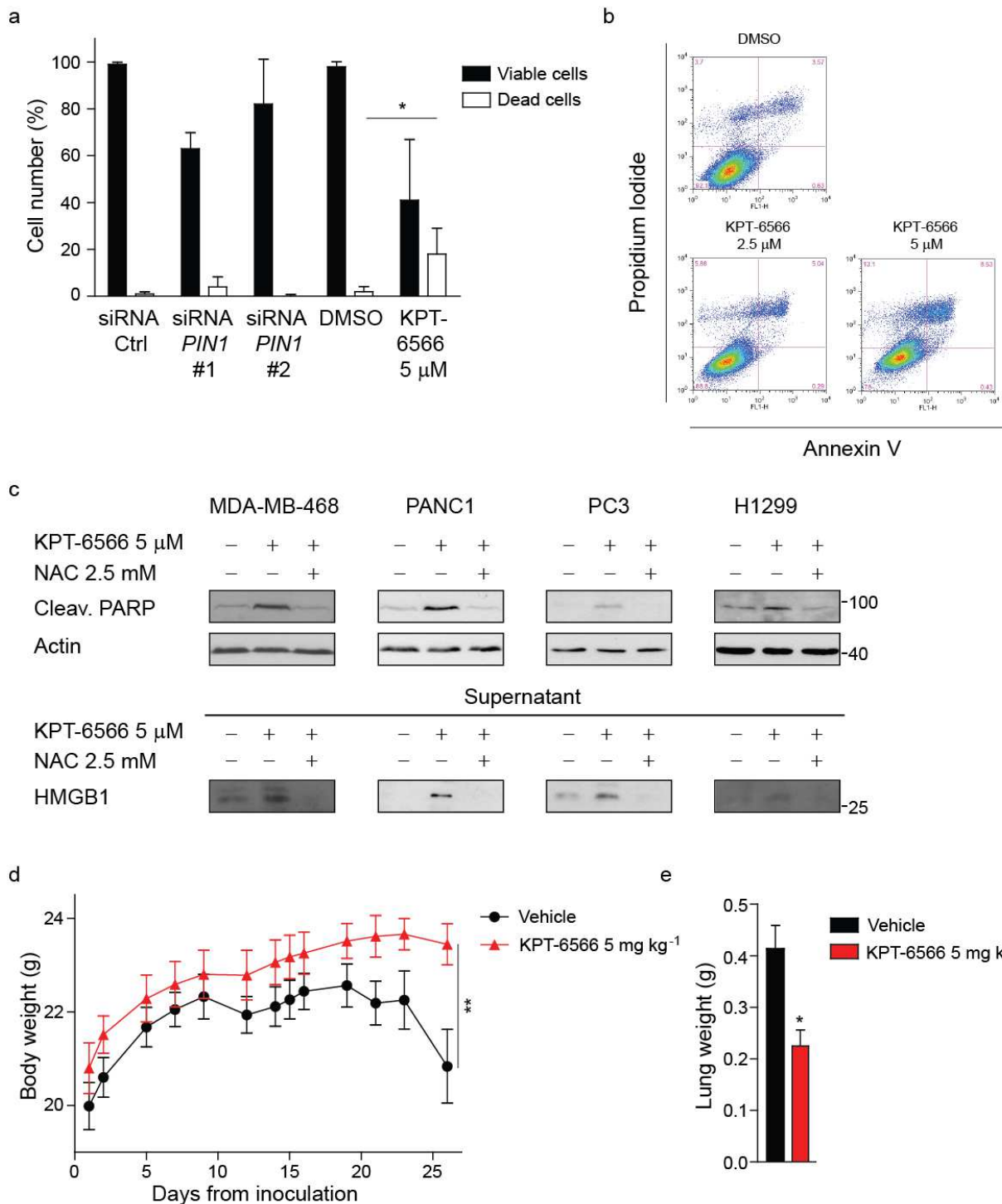
Supplementary Figure 5

(**a**) Scheme of KPT-6566 reaction with PIN1, byproduct production and possible activities of the compounds. (**b**) Quantitative RT-PCR analysis of cell cycle related genes in MDA-MB-231 cells treated with 5 μM KPT-6566 or DMSO for 48hrs. (**c**) Histogram representing CellROX mean fluorescence intensity (MFI) of MDA-MB-231, PC3 and MCF10A cells treated with 5 μM KPT-6566, 5 μM KPT-6566 plus 2.5 mM NAC or DMSO for 48hrs. (**d**) Histogram representing CellROX mean fluorescence intensity (MFI) of MDA-MB-231 cells treated with 5 μM KPT-6566, 5 μM

KPT-6566-B or DMSO for 48hrs. Data shown in **b-d** are the means ± s.d. of n=3 independent experiments, *$P<0.05$,
**$P<0.01$; two-tailed Student's *t*-test.

Supplementary Figure 6

Immunoblotting of the indicated proteins from (**a**) MDA-MB-231 cells treated with the indicated concentrations of KPT-6566-B or left untreated (0) and collected at the indicated time points; (**b**) PC3, PANC1 and H1299 cells respectively treated with 5 μM KPT-6566, 10 μM Bleomycin or DMSO for 48hrs; (**c**) MDA-MB-231 cells in the indicated experimental conditions. Cells were transfected with control siRNA (siRNA Ctrl) o with *PIN1* siRNA (siRNA *PIN1#1*). After 24hrs cells were trypsinized, plated and treated with the indicated concentrations of KPT-6566-B or left untreated (0) for 48hrs; (**d**) MDA-MB-231 cells treated with the indicated compounds for 48hrs. **a-d** Actin levels are reported as loading control, size markers are indicated.

Supplementary Figure 7

(**a**) Graph showing cell number (percentage relative to siRNA Ctrl) of MDA-MB-231 cells in the indicated experimental conditions. After 48hrs of treatment, cells were trypsinized, stained with Trypan blue and counted at the optical microscope. Results are indicated as means ± s.d. of n=3 independent experiments, *P<0.05; two-tailed Student's t-test. (**b**) Representative FACS plot of PI/AnnexinV staining of MDA-MB-231 cells treated with DMSO or increasing amounts of KPT-6566 for 48hrs. (**c**) Top, Immunoblotting of the indicated proteins of MDA-MB-468, PANC1, PC3 and H1299 cell lysates untreated (-) or treated (+) with the indicated compounds. Bottom, Immunoblotting of HMGB1 from supernatant of the same cells as in top panel. Actin levels are reported as loading control, size markers are indicated. (**d**) Graph showing body weight of KPT-6566 or vehicle treated mice during the

period of the experiment. (**e**) Graph showing lung weight of KPT-6566 or vehicle treated mice. Data shown in **d**, **e**, are the means ± s.e.m. (n=8 for vehicle treated mice; n=7 for KPT-6566 treated mice), *$P<0.05$, **$P<0.01$; two-tailed Mann-Whitney test.

Supplementary Tables

Supplementary Table 1. IC50 values of different compounds in cytotoxicity experiments performed in A375 and 3T3 cells.

	IC50 $_{A375}$ (μM)	IC50 $_{3T3}$ (μM)
KPT-6342	5.36	n.a.*
KPT-6410	8.18	20.98
KPT-6475	<0.63	6.91
KPT-6504	9.19	18.49
KPT-6517	1.75	15.67
KPT-6566	3.47	21.76
KPT-6568	n.a.	>30
KPT-6570	n.a.	>30
KPT-6605	10.28	n.a.
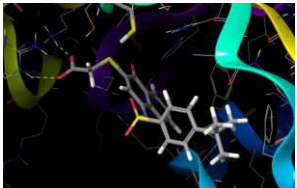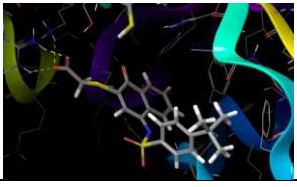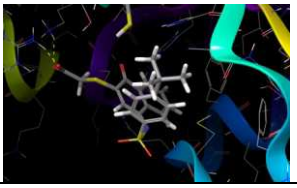
*n.a., not assessed
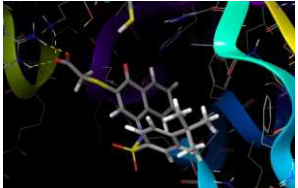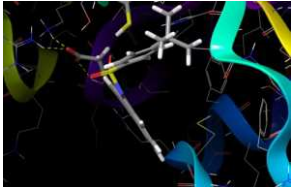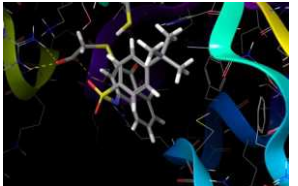
Supplementary Table 2. IC50 value of KPT-6566 for PIN1 in PPIase assay.

Inhibitor	IC50 (μM)	95% confidence intervals (μM)
KPT-6566	0.64	0.07 - 5.51

Results of n=6 independent experiments are indicated.

Supplementary Table 3. Binding poses and Glide Docking Scores of KPT-6566 docked in the PIN1 catalytic domain.

Pose	Docking Score
1	-4.280
2	-4.135
3	-4.101
4	-3.990

5	-3.642	
6	-3.299	
7	-3.536	

Supplementary Table 4. Estimated inactivation parameters of PIN1 by KPT-6566.

Enzyme	Inhibitor	k_{inact}	K_i	k_{inact}/K_i
PIN1	KPT-6566	0.466 ± 0.05781 min^{-1}	625.2 ± 324.7 nM	745.4 min^{-1} ·nM^{-1}

Curve fitting results with std.errors of n=3 independent experiments are indicated.

Supplementary Table 5. IC50 values of KPT-6566 in viability experiments performed in MCF10A and MCF10AT1 cells.

Cell line	IC50 (μM)	95% c.i. (μM)
MCF10A	14.33	8.334 - 24.65
MCF10AT1	3.4	1.699 - 6.771

Curve fitting results with c.i. of n=3 independent experiments are indicated.

Supplementary Table 6. CD44/CD24 cell distribution analysis of MCF10A cell clones.

	vector	PIN1 + DMSO	PIN1 + KPT-6566
CD44$^+$/CD24$^-$	11.53 ± 2.54	23.9 ± 0.6	3.7 ± 0.3
CD44$^+$/CD24$^+$	85.37 ± 5.62	68.97 ± 9.26	94.77 ± 1.97
CD44$^-$/CD24$^+$	0.83 ± 0.95	2.93 ± 3.54	0.13 ± 0.06
CD44$^-$/CD24$^-$	2.3 ± 2.77	4.2 ± 5.22	1.5 ± 2.17

The percentage of cells with the indicated expression of CD44/CD24 is indicated as means ± s.d. of n=3 independent biological replicates.

Supplementary Table 7. Common downregulated genes by *PIN1* siRNA and KPT-6566.

	siRNA *PIN1*		KPT-6566	
NAME	**logFC**	***p* value**	**logFC**	***p* value**
LMNB1	-1.993315205	1.60E-07	-1.390713813	0.000156902
CKAP2	-1.649824429	2.73E-06	-0.753780575	0.003598795
TOP2A	-1.602626771	0.000131038	-1.078341609	0.010420359
CENPE	-1.585619226	1.76E-06	-1.039331392	0.006439969
IFRD1	-1.527953234	2.53E-05	-0.789615487	0.001657493
C4ORF46	-1.492935571	3.13E-06	-0.75996261	0.001103998
NCAPD2	-1.422371472	6.10E-06	-1.106579457	0.00019137
ASPM	-1.322426686	0.00017389	-1.079049881	0.008428549
KIF11	-1.292576165	0.000473829	-0.797084041	0.01726246
DLGAP5	-1.284419305	0.000390296	-1.252734367	0.001500357
KIF2C	-1.273094177	2.67E-05	-0.818674427	0.002214861
HNRNPM	-1.26649729	1.87E-05	-0.783694016	0.002996742
LOC727761	-1.25243774	2.89E-05	-0.798097602	0.000726711
FAM83D	-1.230971056	2.25E-05	-1.248860947	2.17E-05
AURKA	-1.215024175	3.67E-05	-1.34676716	1.98E-05
HMGB2	-1.14477821	0.000560364	-0.788573155	0.002228307
TPX2	-1.081560493	0.000129366	-1.152835417	3.52E-05
CENPA	-1.071576604	0.000106567	-0.921716931	0.000448802
C13ORF34	-1.065797926	0.00049054	-0.854864938	0.000972674
CDCA8	-1.061286474	0.00037755	-1.292188234	6.62E-06
KIF20B	-1.056059473	0.000392444	-1.070712754	0.007440821
CCNF	-1.055952082	0.000407291	-0.947015061	0.006540934
MXD3	-1.046416767	0.000302452	-1.178858625	0.001782072
HJURP	-1.036899849	0.000139923	-0.919589512	0.000422532
KIF20A	-1.011681112	0.000190637	-1.529745689	1.03E-06
NUSAP1	-0.994421483	0.001007043	-0.845747631	0.003171494
NEIL3	-0.993173905	0.000302813	-0.928656408	0.000372391
MCM3	-0.984395764	0.000297576	-0.956936429	0.000554111
CDKN2C	-0.979586993	0.001711889	-0.794034024	0.002016578
CDCA7	-0.976233578	0.000413979	-0.912224015	0.00010797
LOC643995	-0.970129977	0.000258985	-0.766798592	0.00090016
KIF4A	-0.961539576	0.000299065	-0.837655986	0.000327823
LOC100128007	-0.960067749	0.002976062	-0.805020422	0.008296733
SYNCRIP	-0.955192593	0.00220315	-0.780805854	0.012932036
SGOL2	-0.948813369	0.000514782	-0.905695274	0.006708523
HMMR	-0.948151673	0.000633793	-1.180142451	7.55E-05
GTSE1	-0.944593639	0.001028039	-0.91930718	0.000297895
MKI67	-0.943875467	0.00058885	-1.156560495	4.85E-05
KIF23	-0.930389489	0.000679496	-1.102992023	9.99E-05

C14ORF106	-0.926309045	0.000873225	-0.94092836	0.001568464
CCNA2	-0.920340126	0.000572448	-0.928737359	0.000571694
CCNB1	-0.919049598	0.000462799	-1.233733072	9.04E-05
FEN1	-0.905229686	0.000482458	-0.883205509	0.001137971
SUPT16H	-0.882711419	0.002992406	-0.765613202	0.016517827
MLF1IP	-0.858793526	0.002829338	-0.918025183	0.013001243
NASP	-0.84545566	0.000920292	-0.952505342	8.43E-05
KIFC1	-0.842754954	0.002442351	-1.222021696	0.00017394
LOC653820	-0.841801943	0.004385814	-0.958610097	0.000267962
BIRC5	-0.827335637	0.002437142	-1.19650208	5.68E-05
ESPL1	-0.803125048	0.001339697	-0.810388086	0.007067412
KIF18A	-0.795551338	0.001973556	-1.084266901	0.001282449
CDCA3	-0.767187634	0.002589411	-1.10354153	4.28E-05
CDKN3	-0.76628107	0.00453819	-1.033036632	0.000540765
CCNB2	-0.765163113	0.00189446	-0.775948086	0.000904069
LOC731314	-0.756519109	0.003534999	-0.868921232	0.00380313

Supplementary Table 8. Common upregulated genes by *PIN1* siRNA and KPT-6566.

	siRNA *PIN1*		KPT-6566	
NAME	**logFC**	***p* value**	**logFC**	***p* value**
AHNAK2	1.127549518	6.52E-05	0.824328418	0.000689379
ANGPTL4	0.90979909	0.00236433	1.368785676	9.10E-05
ANXA10	1.241258121	0.000924395	0.780661211	0.001895984
AVPI1	0.899366798	0.001867859	1.141838128	0.005116749
C14ORF78	1.179567691	0.000118218	1.185442274	8.25E-05
CCDC85B	0.854997268	0.004862753	1.138244481	4.24E-05
CDKN1C	0.76556803	0.00418495	1.174092299	0.000149072
CYP1B1	0.971454307	0.005609335	1.723365264	0.00010894
FBXO32	0.855254752	0.000917202	1.831448046	4.12E-07
GDF15	2.845195376	9.44E-10	1.766491436	1.52E-05
IL24	0.854560753	0.003930622	2.141642086	1.24E-06
KLF9	1.042055692	0.000808668	0.90842043	0.000415111
LOC401537	0.763206127	0.003342964	0.753039859	0.006122407
LOC653506	0.787469196	0.006057272	0.940827486	0.000647647
LY96	0.998664699	0.000218698	1.071029214	0.000394229
NRP1	0.874561843	0.000796052	1.006613622	0.000104908
PLAT	1.235653185	2.79E-05	1.155336106	0.003136798
PTPRR	0.983751456	0.000532927	1.036222539	0.000111156
RASD1	1.244988195	2.84E-05	2.037272137	0.000112903
RNF44	0.908096053	0.000906069	0.778673506	0.00202333
SERPINB2	0.890693326	0.001031445	1.750849412	6.42E-07
SPRY2	0.801291706	0.001417034	1.439677097	1.20E-05
SQSTM1	1.265910641	3.45E-05	1.126794637	2.56E-05
TFPI	0.75018459	0.013166835	0.957836867	0.000429311

TXNRD1	0.771478885	0.002945497	0.935944212	0.000800093
VASN	0.758741743	0.003248575	0.887879079	0.003360611
ZNF280D	0.994482226	0.000197028	0.907139547	0.000423506

Supplementary Table 9. Commonly enriched GO terms by *PIN1* siRNA and KPT-6566.

	siRNA *PIN1 vs.* siRNA Ctrl	KPT-6566 *vs.* DMSO
Term	***P*-value**	***P*-value**
GO:0000070~mitotic sister chromatid segregation	1,88E-13	2,11E-05
GO:0000087~M phase of mitotic cell cycle	1,31E-32	4,81E-17
GO:0000278~mitotic cell cycle	6,39E-37	2,55E-20
GO:0000279~M phase	2,96E-37	1,22E-16
GO:0000280~nuclear division	4,35E-33	2,77E-17
GO:0000775~chromosome, centromeric region	1,26E-15	1,40E-05
GO:0000777~condensed chromosome kinetochore	6,86E-09	0,007923592
GO:0000779~condensed chromosome, centromeric region	8,27E-12	0,002843679
GO:0005694~chromosome	1,04E-23	4,07E-09
GO:0005819~spindle	9,88E-19	6,18E-13
GO:0006259~DNA metabolic process	1,16E-11	0,001363207
GO:0006260~DNA replication	2,06E-10	0,017600514
GO:0007049~cell cycle	3,89E-40	1,87E-22
GO:0007059~chromosome segregation	3,33E-20	5,33E-07
GO:0007067~mitosis	4,35E-33	2,77E-17
GO:0007346~regulation of mitotic cell cycle	1,09E-10	2,85E-08
GO:0010564~regulation of cell cycle process	1,16E-09	2,04E-05
GO:0015630~microtubule cytoskeleton	1,32E-15	2,47E-14
GO:0022402~cell cycle process	1,05E-38	7,34E-20
GO:0022403~cell cycle phase	1,41E-42	1,12E-20
GO:0051276~chromosome organization	6,35E-10	0,000762
GO:0051301~cell division	1,25E-25	1,44E-10
GO:0051726~regulation of cell cycle	3,22E-13	3,89E-18

Appendix

During my PhD I have been involved in the following publications and unpublished works:

- Rustighi A, Zannini A, <u>Campaner E</u>, Ciani Y, Piazza S, and Del Sal G. (2017) **PIN1 in breast development and cancer: a clinical perspective.** *Cell Death Differ*. *24*, 200–211
  Mammary gland development, various stages of mammary tumorigenesis and breast cancer progression have the peptidyl-prolyl cis/trans isomerase PIN1 at their centerpiece, in virtue of the ability of this unique enzyme to fine-tune the dynamic crosstalk between multiple molecular pathways. PIN1 exerts its action by inducing conformational and functional changes on key cellular proteins, following proline-directed phosphorylation. Through this post-phosphorylation signal transduction mechanism, PIN1 controls the extent and direction of the cellular response to a variety of inputs, in physiology and disease. This review discusses PIN1's roles in normal mammary development and cancerous progression, as well as the clinical impact of targeting this enzyme in breast cancer patients.

- <u>Campaner E</u>, Rustighi A, Zannini A, Cristiani A, Piazza S, Ciani Y, Kalid O, Golan G, Baloglu E, Shacham S, Valsasina B, Cucchi U, Pippione AC, Lolli ML, Giabbai B, Storici P, Carloni P, Rossetti G, Bello E, D'Incalci M, Cappuzzello E, Rosato A, and Del Sal G. **A new covalent PIN1 inhibitor selectively targets cancer cells by a dual mechanism of action.** *Nat Commun.* Under revision.

- Comel A, Neri C, <u>Campaner E</u>, Capaci V, Voto I, Ciani Y, Bicciato S, Carloni P, Rossetti G, Losasso V, Myers M, Edomi P, Lu H, Liao P, Sabapathy K, and Del Sal G. **Phosphorylation of Serine 249 and PIN1-induced isomerization mediate a conformational switch in mutant p53 R249S that drives tumorigenesis.** Manuscript in preparation.
  A common hallmark of tumorigenesis is the inactivation of tumour suppressor genes. In particular, about 50% of human cancers harbour a mutation in the *TP53* gene (http://www-p53.iarc.fr/). *TP53* is most frequently hit by missense mutations in its DNA binding domain, that lead to the expression of full-length p53 protein variants that lose the ability to bind wild-type p53 responsive elements on DNA but acquire novel activities, which can significantly contribute to various aspects of tumour progression, commonly described as gain of function properties. We focused on the unique association between a p53 "hot-spot" mutation, namely mutant p53 R249S, and hepatocellular carcinoma (HCC). Specifically, R249S substitution is detected in up to 90% of hepatocellular carcinomas (HCC) occurring in populations exposed to Aflatoxin B1 (AFB$_1$), a mycotoxin growing

on improperly stored grains that is metabolized by the liver to molecules forming promutagenic DNA adducts. Although the demonstration of specific mechanisms of gain-of-function activities for mutant p53 R249S is still missing, there is clear evidence of an association of R249S p53 mutation with worst prognosis in cohorts of HCC patients. Interestingly, R249S mutation is able to introduce a residue that is a putative site for phosphorylation. This is of particular interest since it is widely accepted that mutant p53 proteins become active oncogenes upon modification (particularly phosphorylation) by signaling pathways activated within tumour cells. Moreover, this phosphorylation generates a new site recognized by the prolyl-isomerase PIN1, a critical transducer of cellular signaling pathways that was previously shown to empower the oncogenic properties of different p53 mutants.

Acknowledgements